



January 2017

An Investigation Of The Thermal Degradation Of Lignin

Sara Pourjafar

Follow this and additional works at: <https://commons.und.edu/theses>

Recommended Citation

Pourjafar, Sara, "An Investigation Of The Thermal Degradation Of Lignin" (2017). *Theses and Dissertations*. 2316.
<https://commons.und.edu/theses/2316>

This Dissertation is brought to you for free and open access by the Theses, Dissertations, and Senior Projects at UND Scholarly Commons. It has been accepted for inclusion in Theses and Dissertations by an authorized administrator of UND Scholarly Commons. For more information, please contact zeinebyousif@library.und.edu.

AN INVESTIGATION OF THE THERMAL DEGRADATION OF LIGNIN

by

Sara Pourjafar

Bachelor of Science, Sahand University of Technology, 2008

Master of Science, Babol University of Technology, 2011

A Dissertation

Submitted to the Graduate Faculty

of the

University of North Dakota

In partial fulfillment of the requirements


For the degree of

Doctor of Philosophy


Grand Forks, North Dakota

August 2017

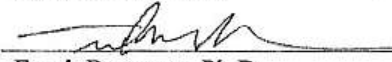
This dissertation, submitted by Sara Pourjafar in partial fulfillment of the requirements for the Degree of Doctor of Philosophy from the University of North Dakota, has been read by the Faculty Advisory Committee under whom the work has been done and is hereby approved.



Wayne Seames, Ph.D.



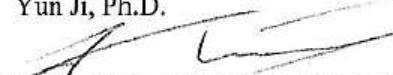
Brian Tande, Ph.D.



Frank Bowman, Ph.D.



Yun Ji, Ph.D.



Evgenii Kozliak, Ph.D.

This dissertation is being submitted by the appointed advisory committee as having met all of the requirements of the School of Graduate Studies at the University of North Dakota and is hereby approved.



Dean of the School of Graduate Studies

July 31, 2017

Date

PERMISSION

Title An Investigation of the Thermal Degradation of Lignin
Department Communication Sciences and Disorders
Degree Doctor of Philosophy

In presenting this dissertation in partial fulfillment of the requirements for a graduate degree from the University of North Dakota, I agree that the library of this University shall make it freely available for inspection. I further agree that permission for extensive copying for scholarly purposes may be granted by the professor who supervised my dissertation work or, in his absence, by the Chairperson of the department or the dean of the School of Graduate Studies. It is understood that any copying or publication or other use of this thesis dissertation or part thereof for financial gain shall not be allowed without my written permission. It is also understood that due recognition shall be given to me and to the University of North Dakota in any scholarly use which may be made of any material in my thesis dissertation

Sara Pourjafar
May 31st 2017

TABLE OF CONTENTS

LIST OF FIGURES.....	viii
LIST OF TABLES.....	x
ACKNOWLEDGEMENT.....	xii
ABSTRACT.....	xiv
CHAPTER	
I. INTRODUCTION	1
Motivation	1
Liquid Fuels from Biomass.....	2
Lignin.....	5
Introduction.....	5
Commercial Lignins.....	7
Kraft Lignin.....	8
Sulfite Lignin.....	8
Alkali Lignin.....	9
Organosolve Lignin.....	9
Lignin Decomposition.....	9
Pyrolysis.....	10
Barriers to the development of biofuel.....	11
II. THERMAL DEGRADATION OF LIGNIN USING METAL DOPED CATALYSTS.....	13
Introduction.....	13
Experimental.....	19

	Materials.....	19
	Metal doped catalyst preparation.....	19
	Experimental setup and procedure.....	20
	Characterization.....	21
	Design of experiments screening study.....	22
	Results and discussion.....	26
	Screening study results based on chemical analysis.....	26
	Temperature bounding studies.....	37
	Conclusion.....	44
..		
III.	NON-CATALYTIC DECOMPOSITION OF LIGNIN INTO CHEMICALS AND INTERMEDIATES.....	45
	Introduction.....	45
	Experimental.....	47
	Experimental set-up and procedure.....	47
	Analytical methods.....	50
	Results and discussion.....	52
	Conclusion.....	63
IV.	CONCLUSION.....	64
	APPENDIX A: CATALYST DOPING.....	66
	APPENDIX B: BATCH EXPERIMENTS SETUP.....	67
	APPENDIX C: GC-MS ANALYSIS.....	69
	APPENDIX D: ADDITIONAL CATALYTIC EXPERIMENTAL DATA.....	72

APPENDIX E: MINITAB PLOTS.....	78
APPENDIX F: CONTINUOUS FLOW REACTOR EXPERIMENTAL PROCEDURE.....	96
APPENDIX G: XRD ANALYSIS FOR ALL CATALYSTS.....	98
APPENDIX H: CONTINUOUS FLOW REACTOR SIMULATION BY MATLAB.....	
REFERENCES.....	107

LIST OF FIGURES

Figure	Page
1. The main steps in an ethanol production process from lignocellulosic biomass.	4
2. Thermochemical and chemical lignin transformation processes.	10
3. Schematic diagram of the batch reaction vessel used for all lignin decomposition experiments.....	21
4. Part of softwood lignin structure proposed by Crestini et al.....	30
5. Examples of dimeric lignin derived compounds: 1,1- diguaiacycloethane ; 1,2- diguaiacycloethane proposed by Alen et al.	31
6. XRD patterns of calcined silica-alumina, 5 wt.% Cu in SiO ₂ /Al ₂ O ₃ and 5 wt.% Mo in SiO ₂ /Al ₂ O ₃	32
7. XRD patterns of calcined γ -Alumina, 10 wt.% Cu in γ -Alumina and 10 wt.% Mo in γ -Alumina.....	32
8. a) SEM and b)EDS analysis of 5 wt.% Mo on silica-alumina	33
9. a) SEM and b) EDS analysis of 10 wt.% Mo in γ -alumina.....	34
10. SEM and EDS analysis of a) 5 wt. % Cu in SiO ₂ /Al ₂ O ₃ , b) 10 wt. % Cu in SiO ₂ /Al ₂ O ₃	36
11. Temperature bounding experimental results in terms of concentration of products per gram of lignin.....	38
12. Solid residues collected from reactor at reaction temperatures of a) 300°C b) 320°C c) 350°C.....	40
13. TG curves of reactor residues from temperature study with 5 wt.% Cu in SiO ₂ /Al ₂ O ₃ at 300, 320 and 350 °C	43
14. Schematic diagram of the continuous flow reactor	48
15. Separation and analysis steps of the experiments products.....	49
16. Identified compounds from GC-MS analysis of the DCM extracted fraction	51
17. pH analysis of collected samples at each temperature	53

18. Thermal carbon analysis profiles at six reaction temperatures	54
19. Monomer-rich fraction analysis results in terms of concentration of products per gram of lignin.....	58
20. SEM pictures of a) virgin lignin, b) sodium hydroxide treated lignin	61
21. SEM pictures of solid sample collected at a) 480 °C, b) 340 °C experimets	62
22. First step of preliminary experiments results	82
23. Second step of preliminary experiments results.....	83
24. Third step of preliminary experiments results.....	84
25. XRD analysis profiles	99

LIST OF TABLES

Table	Page
1. Content of total linkages in softwood and hardwood.....	6
2. Summary of base catalyzed lignin degradation studies.....	15
3. Summary of previous studies of heterogeneous acid catalyzed degradation of lignin	17
4. Low and high values for seven factors tested in screening study	22
5. Plackett-Burman design to screen seven factors	25
6. Concentration of compounds (wt %) obtained in the liquid phase of products from decomposition of lignin	27
7. A summary of the significance of each factor discovered in the Plackett-Burman screening study.....	28
8. Reaction condition for temperature bounding studies.....	37
9. Mass loss during TG analysis of reactor residues collected from temperature studies (wt .% loss)	43
10. Properties of sub and super critical water	46
11. Summary of parameter variations in the experiments.....	48
12. Total calculated concentration of recovered products out of initial lignin	57
13. Mass loss during TG analysis of solid residues	59
14. Catalyst support and dopants weight and types used to prepare the studied catalysts	66
15. Analyte mixtures used to prepare calibration stock solution	71
16. Analyte target ions and retention time	73
17. GC/MS analysis sequence for the first step of preliminary results	74
18. GC/MS analysis sequence for the second step of preliminary results	76
19. GC-MS analysis results of the second step of preliminary study	77
20. GC-MS analysis results of the third step of preliminary study	79

ACKNOWLEDGMENTS

This has been an amazing journey for me and hereby I would like to thank everyone who held my hand and supported me during the past four years. First, I would like to thank my beloved husband, Ghasem, who stayed by my side and encouraged me to get better every day. Then I want to wholeheartedly thank my parents for their endless love and support. This life changing experience was impossible without their tremendous sacrifices. I also want to express my deep gratitude to my advisor, Dr. Wayne Seames who was not only my academic advisor, but also a great mentor for life. I cannot ever thank him enough for everything that he taught me, which are countless.

I must thank my advisory committee for their encouragement, knowledge, resources, and opportunity to work on this challenging research. Finally, I want to thank very talented Ian Foerster for being a wonderful friend and officemate.

To my very dear Ghasem
Mom & Dad
Ali & Soosan

ABSTRACT

The goal of this research was to explore selected non-biological lignin decomposition reactions to determine if these reactions have the potential to generate fuel and chemical intermediates in a commercially feasible manner. Two different strategies were employed: 1) metal doped silica-alumina and γ -alumina catalytic decomposition reactions, and 2) base catalyzed sub- and supercritical water liquefaction.

The first strategy was built upon previous research to explore metal doped silica-alumina and γ -alumina catalytic lignin decomposition reactions in a batch reactor system. Commercially available silica-alumina and γ -alumina catalysts were individually doped with 5 and 10 wt % of molybdenum or copper via a wet impregnation method. All catalysts were characterized with SEM, XRD and EDS analyses. Twelve runs in a Plackett-Burman design were used in a screening study of the significance of seven factors: catalyst support type, catalyst dopant type, and dopant concentration, lignin concentration in water, catalyst-to-lignin ratio, reactor stirring rate, and reaction time. Aqueous products were extracted in DCM and analyzed in GC-MS. Solid residues from the reactor were analyzed via TGA and SEM. Screening study results showed that 5 wt% Cu on silica-alumina with 3 g of catalyst and 3 g of lignin in 250 ml of deionized water was the preferred condition to degrade lignin to monomers.

Next, the effect of varying the reaction temperature between 300 and 350 °C was investigated at the best reaction conditions from the screening studies. The optimum temperature was found to be around 320 °C. Lower reaction temperatures (300 °C) result in more unreacted lignin while higher temperatures (350 °C) lead to increased formation

of char and gaseous products. However, the quantity of monomers produced is still below the commercialization threshold.

The base catalyzed decomposition of lignin to monomeric compounds was studied in a novel continuous flow reactor. In these experiments, 10 wt % lignin was dissolved in a 5 wt % sodium hydroxide in water solution at either sub or supercritical conditions and then fed to a heated tubular reactor. The products from these reactions were collected as gas phase and water-soluble liquid compounds. The gas was quantified by weight difference while the water soluble compounds were acidified and extracted in DCM and analyzed with GC-FID/MS. The solid residues from the acidification treatment were filtered and analyzed with TGA. The morphology of solid residue particles was studied with SEM.

The concentration of monomers was also found to increase with increasing temperature in supercritical condition experiments (6 wt %) , all of which were higher than those from the subcritical experiments (4 wt %) where the results showed that the maximum concentration of monomers (mostly creosols) was obtained at 340 °C in subcritical water (4.7 wt%). Analysis of solid residues showed that the concentration of partially decomposed lignin was lower in residue from supercritical condition experiments and the solid residues are larger in size compared to the char that was formed at subcritical conditions.

These initial experiments did not result in monomer production at desired levels, but they were comparable to metal-doped experiments results. However, the novel reactor design substantially minimizes concerns due to tar or char formation. Future work is recommended to explore additional reaction strategies using this approach.

CHAPTER I INTRODUCTION

1.1. Motivation

Significant industrial activities have been resulted in substantial emission of greenhouse gases during the past century. The increasing concern around the globe for climate change led to an international agreement, the “Kyoto Protocol” which was adopted on December 11, 1997 in Kyoto, Japan. This protocol provided guidelines for the signing nations to reduce their greenhouse gases emissions to a certain level. In pursuit of the ultimate objective of the protocol, the nations are advised to promote sustainable developments which were defined under the second article of the protocol. Three proposed strategies to achieve this goal were included in the protocol:

- Enhancement of energy efficiency in relevant sectors of the national economy
- Promotion of sustainable forms of agriculture in light of climate change considerations
- Research on, and promotion, development and increased use of, new and renewable forms of energy, of carbon dioxide sequestration technologies and of advanced and innovative environmentally sound technologies

According to the U.S.A EPA greenhouse gas inventory data, CO₂ emissions have remained relatively constant during the years 1990 to 2014 where the most significant sources of emission are from burning coal, natural gas and fuel oil for electricity and heat. In 2008, the top carbon dioxide emitters were China and the United States with 23% and 19% of the global share of CO₂ emissions, respectively. These data not only represent the significant amount of energy consumption and industrial activities of these countries, but also shows the considerable level of energy demands. With the continued depletion of natural energy resources such as fossil fuels and natural gas, the importance of renewable sources of energy increases.

Biomass is known to be one of the most abundant source for renewable energy. Although the traditional form of converting biomass to energy is to directly burn it, advances in thermochemical technologies can introduce new and more efficient ways to generate energy from biomass.

1.2. Liquid fuels from biomass

According to the 65th edition of the BP Statistical Review of World Energy, global primary energy consumption increased by 1.0% in 2015 [1]. Renewable energy sources in power generation continued to increase in 2015, reaching 2.8% of global energy consumption, up from 0.8% a decade ago. North America has the highest share of biofuels production in the past decade. Emissions of CO₂ from energy consumption increased by only 0.1% in 2015 [1].

Bioethanol and biodiesel are two global biorenewable liquid fuels that can replace or supplement petroleum-derived transportation fuels. Bioethanol is derived from the alcoholic fermentation of simple sugars while the dominant technology for producing biodiesel is transesterification of triglycerides (TGs). Bioethanol can be produced through different pathways such as fermentation, acid hydrolysis, enzymatic hydrolysis or malting [2]. Production costs of bioethanol depends on many factors and it may vary from one country to another. For example, sugar cane is the most important substrate and input for alcohol production in South America. Ethanol-fueled cars were the initial goal of the Brazilian Alcohol Program and the sales of alcohol powered vehicles reached 96% of total sales in 1980 [3].

The other significant biofuel is biodiesel. Transesterification of TGs with chains of 16 and 22 carbon atoms in the presence of methanol will produce fatty acid methyl esters (FAME) which are the main compounds in biodiesel. Some of the advantages of biodiesel are that it is a plant-derived fuel, it does not increase the CO₂ level, and it can be domestically produced.

Despite the above mentioned advantages, there is a slight increase in NO_x emission. The overall life cycle emissions of CO₂ from 100% biodiesel fuel are 78.45% lower than those of petroleum diesel, and a blend with 20% biodiesel fuel reduces net CO₂ emissions by 15.66% [1].

Although biofuels seem to be a perfect substitute for petrochemical fuels and first generation biofuels have already found their place in the market, the sustainability of biofuel production is still the critical factor that affects the price and the future of biofuels. According to Hill et.al., if all of the corn production of the United States were used to produce bioethanol, only 12% of the nation's gasoline demand would be met [4], which makes the development of the second generation of biofuels even more essential.

Lignocellulosic feedstock is well-known as a renewable source for the production of biofuels. There are several research papers and reports that refer to lignocellulose as the most abundant renewable resource in biofuels production [5, 6]. Lignocellulose biomass is comprised of 35-50% cellulose, 20-35% hemicellulose and 15-20% lignin. The first and most challenging step to convert lignocellulose to fuel or fuel additives is to isolate cellulose from lignin and hemicellulose to reduce the crystallinity of cellulose. To achieve this goal, several chemical and biological processes were developed to pretreat lignocellulosic biomass. These processes can be classified as physical, physico-chemical and biological treatment methods [7-9].

Efficient pretreatment will facilitate the enzymatic hydrolysis of cellulose. Figure 1 summarizes the main steps of conversion of biomass to bioethanol. As can be seen, the main purpose of pretreatment step is to remove lignin and hemicellulose while maximizing sugar yield. Yet, the lignin is being treated as a waste stream.

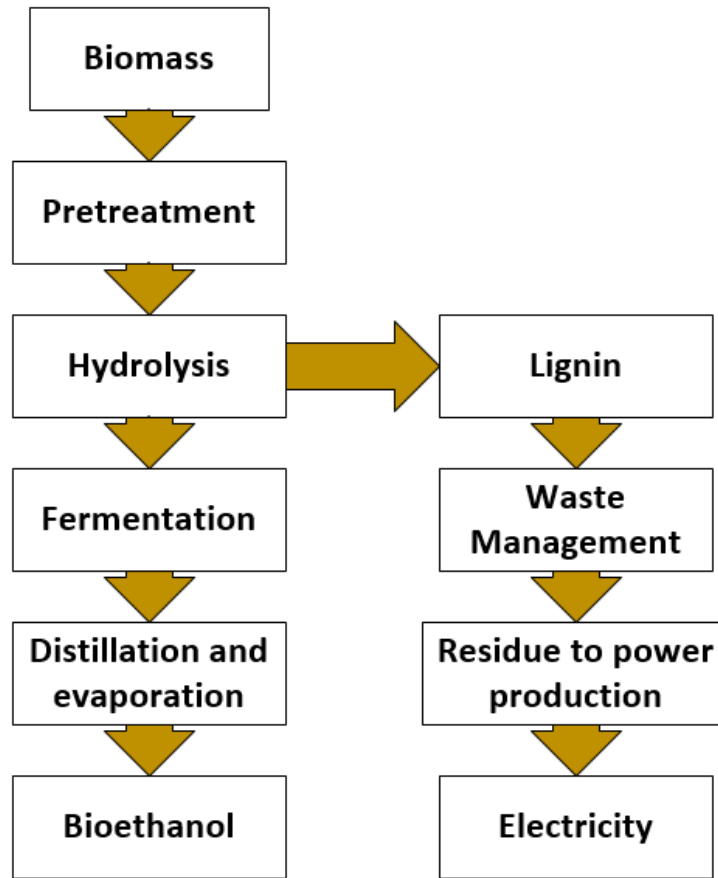


Figure 1. The main steps in an ethanol production process from lignocellulosic biomass [10]

1.3. Lignin

1.3.1. Introduction

After cellulose, lignin is the most abundant plant-derived biopolymer. Lignin is an aromatic polymer which is formed mainly by three phenolic units known as monolignols. It is present in the cellular wall of plants to give structural support, impermeability and resistance against microbial attack and oxidative stress [11]. The name lignin also refers to an unwanted by-product of the paper industry and its structure is very different from native lignin. Due to the molecular complexity and diverse structural composition, no solid definition has been established for this class of molecules.

Lignin was first described as a plant polymer that contains most of the wood methoxyl content, which are resistant to acid hydrolysis and soluble in hot alkaline [12]. It is a natural polymer with a variety of linkages between various building units. The main building units are *p*-coumaryl, coniferyl and sinapyl alcohols. Therefore, native lignin is also referred to as protolignin, that is, an immature form of lignin that can be extracted from the plant cell wall with ethanol or dioxane.

In addition to the three most abundant types of the building units in the lignin structure, there are other less abundant alcoholic units that bond variously during the biosynthesis process of lignin to form a 3D polymer that doesn't have a regular macromolecular structure. Cellulose, hemicellulose and lignin form a structure called microfibrils, which add stability to the plant cell wall [13].

Lignin can be classified in to three general groups based on plant taxonomy:

- Gymnosperm lignins (Softwood)
- Angiosperm lignins (hardwood)
- Grass lignins

Gymnosperms have a significant concentration of guaiacyl groups whereas angiosperms have a mixture of syringol and guaiacyl groups. Grass lignins contain all three major groups of lignin. As a general understanding, each type of plant is able to produce a complex and yet unique type of lignin which results in a significant structural diversity of lignin. Table 1 summarizes the distribution of total linkages present in soft/hardwood lignins:

Table 1. Content of total linkages in softwood and hardwood [14]

Linkage type	Content of total linkages (%)	
	Softwood	Hardwood
β-O-4'	45-50	60
5-5'	18-25	5
β-5'	9-12	6
β-1'	7-10	7
α-O-4'	6-8	7
4-O-5'	4-8	7
β-β	3	3

Clearly, carbon-oxygen bonds are the dominant type of bond in both soft and hardwood. Therefore, breaking the β -O-4' bond will result in an efficient degradation of the lignin molecule. Many studies were performed on lignin model compounds that only target this type of bond [15-18]. These types of studies can explain a lot about the chemistry of the degradation of lignin. However, model compounds are “cleaner” molecules and do not have the complexity of lignin, so the results cannot be directly assumed to be valid for actual lignin molecules.

1.3.2. Commercial Lignins

Lignin is a significant by-product in pulp and paper industries. In these processes, lignin will be recovered from the wood chips in order to produce a suitable pulp for paper production. Around 5 million metric tons of lignin is produced annually by the paper industries [19]. Most of this lignin is burned as a fuel to produce steam. Since lignin is a significant source of carbon, the price of chemically converted lignin can go as high as 1.08 US\$/kg while its value as a direct fuel is only 0.18 US \$/kg [20].

Lignins are divided into two major groups. The first group are the lignins that have sulfur in their structure such as Kraft lignin and lignosulfonates while the second group are defined as nonsulfur groups. To isolate the lignin from wood chips, industries usually consider three criteria:

- The lignin should be isolated efficiently
- The isolated lignin should not have major contaminants
- The isolation process should be cost effective and easy to implement

1.3.2.1. Kraft Lignin

The Kraft process was first developed in Germany in the 1870s and it is based on the use of a sodium hydroxide and sodium sulfate solution to break the lignin away from cellulose fibers. During this process, 90-95% of all the lignin in the wood will be dissolved and cellulose will be separated from lignin. The liquid that is rich in lignin is called “black liquor”. Kraft lignin can be recovered from the black liquor by acid precipitation.

Although the Kraft process is widely used in the pulping industries, there is limited number of facilities that recover Kraft lignin for chemical use such as MeadWestvaco and LignoBoost.

1.3.2.2. Sulfite Lignin

The Sulfite process uses an aqueous solution of sulfurous acid and calcium bisulfate to deconstruct wood chips in a pressurized system. The liquor that forms during the separation of cellulose is rich in lignin. This type of lignin contains 4-8% sulfur and is classified as a lignosulfonate due to the presence of sulfonate groups within its structure. Lignosulfonates have both hydrophilic and hydrophobic properties. The production procedure of this type of lignin is less aggressive than Kraft lignin and the molecular weight of the final Lignin is higher than Kraft lignin. The major drawback of this method is the formation of emulsions and foams during recovery of the lignosulfonates.

The advantages of the sulfite process are high yield for a cooked pulp, low chemical cost, and easy bleachability of the pulp while the disadvantages include the highly corrosive nature of the chemicals, lower pulp strength than kraft lignin, and limited useable wood species [21]. Companies that produce lignosulfonates are Lignitech Borregaard, Tembec, La Rochette Venizel and Nippon paper chemicals.

1.3.2.3 Alkali Lignin

Alkali lignin is typically generated from non-wood fibers such as straw and sugarcane. Alkali pretreatments increase the cellulose digestibility. The yield of this process depends highly on the lignin content of the biomass. An aqueous solution of NaOH, KOH, Ca(OH)₂, and NH₄OH are used to digest the biomass. Like Kraft lignin, the lignin is recovered by decreasing the liquor's pH. The biggest producer of this type of lignin is Green Value company.

1.3.2.4 Organosolve Lignin

During the organosolve pretreatment process, organic solvents such as ethanol, methanol or acetone are employed to extract lignin from biomass which results in the production of a high quality lignin. An efficient isolation of lignin will eventually decrease the cost of the enzyme that is being used to hydrolyze cellulose. Cellulose fibers, solid lignin and liquid solution of hemicellulosic sugars are the main products of this type of pretreatment [11]. One major drawback of this method is generation of furfural, HMF and soluble phenols from lignin which will pass to the prehydrolysis step.

1.4 Lignin Decomposition

Although lignin is a significant source of carbon, an efficient method to decompose lignin into useful chemical intermediates has yet to be developed. Several strategies have been proposed to degrade lignin [22, 23]. For example, gasification of biomass will generate syngas and lower molecular weight compounds. After isolation of the smaller compounds, conventional chemical reactions can be employed to further degrade lignin into high-value compounds. Deoxygenation of functional groups in lignin will also produce simple phenolics like BTX. Currently, BTX is commercially produced through catalytic transformation of naphtha at petroleum refineries.

Lignin can also be converted to high value chemicals through a single step decomposition process using selective catalysts. The major drawback with this approach is the lack of a catalyst that can break down lignin with a high yield of useful products. Figure 2 shows thermochemical and chemical approaches proposed for the decomposition of lignin:

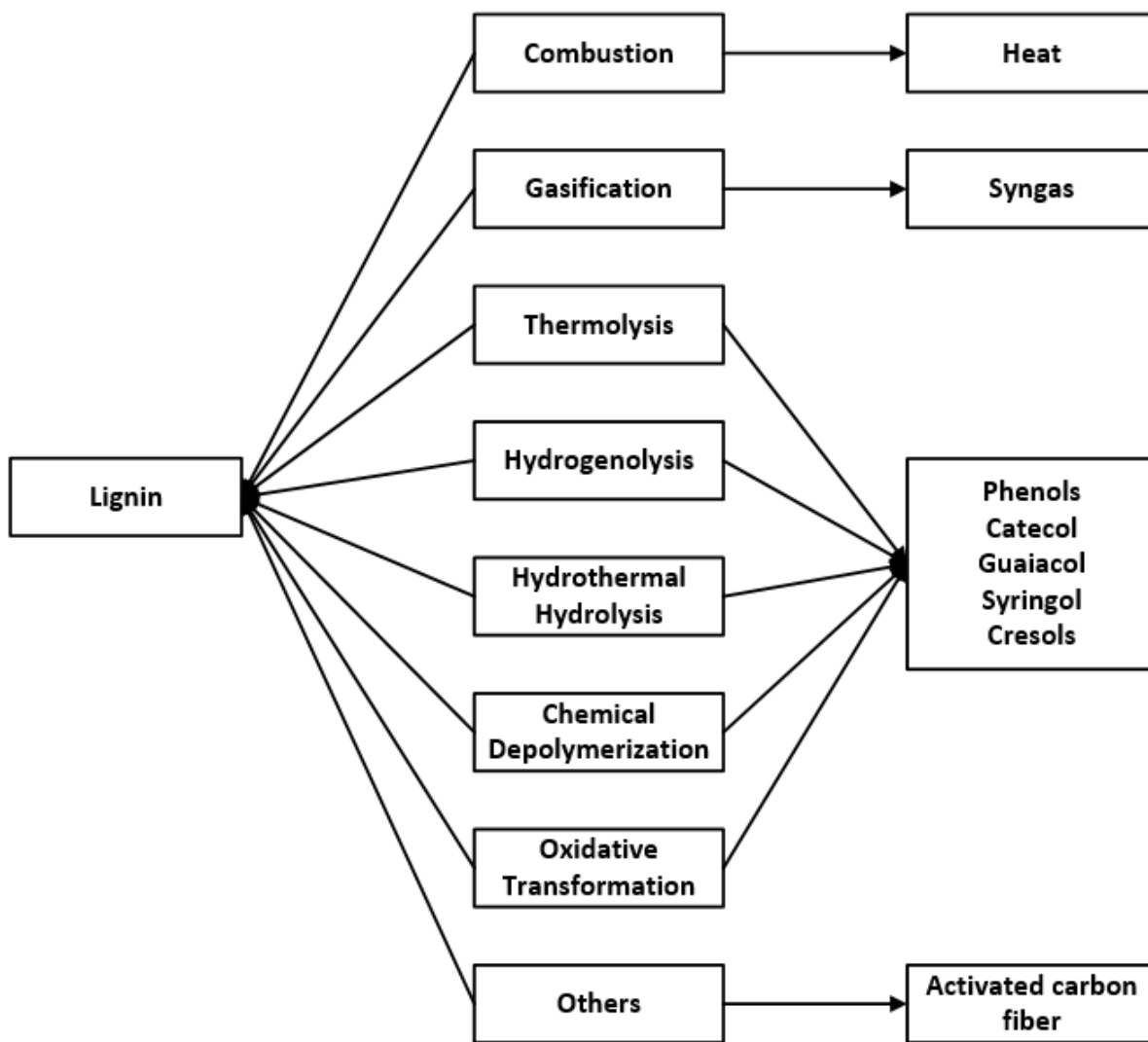


Figure 2. Thermochemical and chemical lignin transformation processes [24]

Although the type of the method has a significant effect on the final products, the composition and yield of the final products depends on lignin origin and the isolation method. Gasification, thermolysis, hydrogenolysis, hydrothermal hydrolysis and chemical

depolymerization are considered to be pyrolysis methods which is defined as thermal treatment in the absence of oxygen [25]. On the other hand, oxidative transformation is a type of thermal treatment where oxygen plays an important role in converting lignin to aldehydes [26].

1.4.1 Pyrolysis

Pyrolysis refers to a thermal decomposition which occurs in the absence of oxygen. The goal is to convert biomass into lower molecular weight oxygen-free compounds with a minimum generation of carbon dioxide. Pyrolysis processes can be categorized into two groups: slow pyrolysis and fast pyrolysis. Slow pyrolysis is more conventional than fast pyrolysis and the reaction heating rate for slow pyrolysis is 0.1-1°C/s while it is 10-200°C/s for fast pyrolysis. Fast pyrolysis is a more convenient option for lignin degradation since fast heating and rapid quenching can produce intermediate compounds that are more useful than small-chain compound gaseous products [27]. In general, there is very limited information available regarding the reaction mechanism in pyrolysis of lignin since most of the experiments that take place in lab scale setups cannot be extrapolated to larger scales [28].

1.5. Barriers to the Development of Biofuels

Second-generation biofuels (SGBs) have been produced from lignocellulosic feedstock such as cereal straw, forest residues, bagasse, and purpose grown energy crops such as vegetative grasses and short-rotation forest. The SGBs could avoid many of the concerns facing FGBs and potentially offer greater cost reduction potential in the longer term. Many of problems associated with FGBs can be addressed by the production of biofuels manufactured from agricultural and forest residues and from non-food crop feedstocks. Low-cost crop and forest biomass, wood process wastes, and the organic fraction of municipal solid wastes can all be used as lignocellulosic feedstocks.

The key points related to FGBs and SGBs are as follows:

1. Technical barriers remain for second biofuel production.
2. Production costs are uncertain and vary with the feedstock available.
3. There is no clear candidate for “best technology pathway” between the competing biochemical and thermochemical routes.
4. Even at high oil prices, SGBs will probably not become fully commercial nor enter the market for several years to come without significant additional government support.
5. Considerably more investment in research, development, demonstration and deployment is needed to ensure that future production of the various biomass feedstocks can be undertaken sustainably and that the preferred conversion technologies, including those more advanced but only at the research and development stage, are identified and proven to be viable.
6. Once proven, there will be a steady transition from FGBs (with the exception of sugarcane ethanol that will continue to be produced sustainably in several countries) to SGBs.

CHAPTER II

THERMAL DEGRADATION OF LIGNIN USING METAL DOPED CATALYSTS

2.1. Introduction

Lignocellulosic feedstock is well known as a renewable source for the production of biofuels. This resource is attractive because it does not compete with edible plant production. Lignin is defined as a complex three-dimensional polymer rich in aromatic units. It has been reported that the thermal decomposition of lignin will produce four groups of primary fractions: aqueous distillate, tar, gaseous products, and coke [29]. However, most current processes only use cellulose and hemicellulose, leaving lignin behind as a low-grade boiler fuel feedstock. Various degradation methods such as pyrolysis, acidolysis, hydrogenolysis, enzyme-based oxidation, etc., have been proposed to decompose lignin [30]. Decomposition of lignin yields various groups of products such as cresols, catechols, vanillin and guaiacols, which are difficult to obtain from a single step petrochemical process and thus have potential as valuable chemical fuel intermediates [RW.ERROR - Unable to find reference:194].

In a study by Barbier et al., the liquefaction of alkali lignin and phenolic compounds in aqueous media at 370 and 390 °C at 25 MPa was investigated. Based on the reported results, lignin was partially degraded and the product was significantly different at sub- versus supercritical pressures [31]. Kruse et al. noted that the hydrothermal conversion of lignin produces liquid bio-oils and phenols through liquefaction. According to their results, the most valuable liquid chemicals will be produced in a range of 150 to 370 °C and 10 to 22.5 MPa [32].

Lignin can also be decomposed through base- or acid-catalyzed reactions. Katahira et al. investigated the effect of NaOH as a catalyst for the degradation of Kraft lignin along with four other substrates in aqueous media at elevated temperatures. A lower concentration of sodium hydroxide at 330 °C resulted in an increased liquid fraction as well as gaseous products while the

solid residue was decreased significantly [33]. It was proposed that the base catalyst targets the weaker bonds in lignin, which occur through two reaction paths: scission of either aryl-alkyl-ether or aryl-aryl-ether bonds.

Although base-catalyzed reactions can result in partial degradation of lignin, the second and more challenging step is to recover the monomers from the liquid phase. Vigneault et al. examined the effect of five different solvents to extract monomers from the aqueous products phase obtained from the base catalyzed depolymerization (BCD) of lignin [34]. Their results showed that ethyl acetate and diethyl ether were the best solvents to extract monomers. In another study conducted by Toledano et. al., degradation of an organosolv lignin obtained from olive tree pruning was investigated using four different types of base as a catalyst. Their results showed that the base catalyst selection may significantly affect the oil yield. Potassium hydroxide tended to be the most effective catalyst for generating phenolic monomers [35].

Table 1. Summary of base catalyzed lignin degradation studies

<i>Catalyst</i>	<i>Feedstock</i>	<i>Reaction condition</i>	<i>Products</i>	<i>Ref.</i>
NaOH, KOH, LiOH, Ca(OH) ₂	Lignin extracted from olive tree pruning	300°C, 90MPa, 40 min in water	5-20% of phenolic monomers depends on the base content	[36]
Cu doped porous metal oxides (Cu-PMOs)	Lignin model compound: DMBF	300°C, 2 h, Methanol	22% 2-ethylphenol, 63% methylated 2-ethylphenol and 11% phenol	[37]
KOH, NaOH, CsOH, LiOH, Ca(OH) ₂ , Na ₂ CO ₃	Kraft and Organosolv Lignin	290°C, 5-60 min, Ethanol	Monomers with MW~180 g/mol and acetic acid	[38]
NaOH	Lignin from acetosolv pulping, formosolv pulping and from acetosolv/formosolv pulping	300°C, 80 min, Water	Formosolv lignin had 28.19% phenolic monomers	[39]
NaOH with Ru/C	Organosolv South China pine lignin	260°C, 240 min, Anhydrous methanol	92.5% conversion, 12.69% phenolic monomer and 6.12% aliphatic alcohol	[40]
NaOH, KOH, NH ₄ OH	Commercial hydrolytic lignin and commercial organosolv lignin	165-350 °C, 15 min, Water	Less than 5wt % of original lignin converted to monomers	[41]
NaOH	Kraft lignin	270-315 °C, LHSV of 1.4–4 h ⁻¹ , Water	8.4 wt % of monomers at 315 °C and 1.4 h ⁻¹	[42]
NaOH	Steam treated lignin from softwood	300-330 °C, 45 min, Water	26 products including guaiacol, catechol and vanillin as major low Mw	[43]
NaOH	Alkaline lignin	220-300°C, 0.5-4 h, Water/Ethanol	Drastic decrease in product molecular weight at 260 °C and 3 hour reaction condition with phenol as major product	[44]
NaOH	Organosolv lignin	240-340 °C, 2-16 min, water	Short residence time and lower temperature favor production of syringol.	[45]

Table 1 summarizes recent studies of the degradation of lignin using base catalysts. As can be seen, the most common catalyst in these studies was sodium hydroxide. Base catalyzed depolymerization (BCD) reactions tend to have a high activation energy which explains the fact that most low molecular weight compounds are produced at around 300 °C. Moreover, the origin of the lignin also has a significant effect on the final product distribution. For example, under similar reaction conditions, organosolv lignin degradation will result in the production of mainly syringol and catechol while for Kraft lignin pyrocatechol is considered to be the main product [19].

Since BCD reactions follow a simpler pathway, they target aryl-alkyl ether bonds which are less stable compared to the C-C bonds that connect the aromatic rings within the lignin structure. In general, BCD reactions require high temperature and high pressure. Such reaction conditions might result in decomposition of lignin into low molecular weight phenolic products but at the same time, it may result in the production of gaseous products and oligomers.

Pyrolytic decomposition of lignin at elevated temperature and in the presence of commercially available heterogeneous catalysts degrades biomass to bio-oil, gas and char. Zeolites, well-known commercially available catalysts, are able to degrade a variety of biomass into a mixture of aromatics [20]. Zeolites are mainly composed of silica and alumina tetrahedral structures. The microporous structure of the zeolites allows small reactants to diffuse into the crystal where many active acid sites are located [21].

Table 2. Summary of previous studies of heterogeneous acid catalyzed degradation of lignin

<i>Catalyst</i>	<i>Feedstock</i>	<i>Reaction condition</i>	<i>Products</i>	<i>Ref.</i>
Si-Al cat ZrO ₂ -Al ₂ O ₃ -FeO _x	Kraft lignin	200-350°C, Water-Butanol, 2 h	6.5% phenols	[46]
ZSM-5, β-zeolite, Y-zeolite	Lignin extracted from pulp mill black liquor	Fast pyrolysis, 650 °C, helium flow	Increasing the SiO ₂ /Al ₂ O ₃ ratio in zeolites structure decreased the aromatic yield	[47]
Mo ₂ N/γ-Al ₂ O ₃	Alkaline lignin	500-850°C, fast pyrolysis, helium flow	Presence of Mo ₂ N/γ-Al ₂ O ₃ decreased oxygenated volatile organics and increased aromatic hydrocarbons (mostly benzene and toluene)	[48]
HZSM-5: SiO ₂ /Al ₂ O ₃ =25- 200	Alkaline lignin	500-764°C, 3-99sec, helium flow	Aromatics increased from 0.2 to 5.2 wt.% while coke also increased from 24 to 39.7%	[49]
Formic acid, Pd/C, Nafion SAC-13	Kraft spruce	300°C, Water	Guaiacol, pyrocatechol and resorcinol as main phenols	[50]
ZrO ₂ + K ₂ CO ₃	Kraft lignin	350°C, Phenol/Water	Presence of K ₂ CO ₃ increased the formation of 1-ring aromatic products from 17% to 27%	[51]
NiMo/Al ₂ O ₃	Wheat straw soda lignin	350°C, Tetralin, 5h	Lignin was converted into gases (9 wt%) and liquids (65 wt%)	[52]
MoS ₂	Kraft lignin	400-450°C, 1h, water	Phenols (8.7% of the original lignin), cyclohexanes (5.0%), benzenes (3.8%), naphthalenes (4.0%), and phenanthrenes (1.2%) were produced	[53]

Table 2 summarizes previous studies where heterogeneous acids were used to facilitate the decomposition of lignin. One of the major drawbacks of using zeolites to degrade processed lignin is the significant amount of char that forms on or within the zeolite's structure. Char fouls the catalyst and may make the regeneration of the catalyst expensive or infeasible.

Brønsted acid sites are directly related to the activity of many catalysts in C-C cleavage reactions. H-ZSM-5 has a higher density of both Brønsted and Lewis acid sites compared to most commercially available catalysts [RW.ERROR - Unable to find reference:195]. However, this does not necessarily mean that a higher catalyst acidity will result in higher conversion of lignin to low molecular weight compounds as the small pore size limits catalytic activity to secondary reactions [RW.ERROR - Unable to find reference:196]. This consideration illustrates that another important factor for choosing a proper catalyst for lignin degradation is the pore size of the catalyst. The pore size of zeolites is usually around 2-4 nm while silica-alumina catalysts have a pore diameter of around 8 nm, which may be more appropriate for degradation of large lignin molecules.

Characterization of $\text{SiO}_2\text{-Al}_2\text{O}_3$ amorphous catalyst and other types of zeolites showed that the surface areas for the above-mentioned catalysts and some other commercially known zeolites such as HZSM-5, Y-zeolite and β -zeolite have BET surface areas ranged from 383 m^2/g to 574 m^2/g [54]. Although silica-alumina catalysts do not have the largest surface area, they feature the largest pore volume, around 0.75 mL/g .

In this study, the catalytic thermal degradation of lignin was investigated with silica-alumina and γ -alumina catalyst supports and molybdenum (Mo) and copper (Cu) metal dopants. A screening study was conducted to examine the effect of the catalysts and operating conditions on final products yield and composition. The novel chemical analysis protocols resulted in a

comprehensive characterization of the reaction product, as opposed to the mere analysis of the GC-elutable fraction extracted into an organic solvent.

2.2. Experimental

2.2.1. Materials

Indulin AT (commercialized in the kraft form), a softwood lignin, was supplied by MeadWestvaco (Glen Allen, VA). Silica-alumina was purchased from Sigma-Aldrich (St. Louis, MO) and γ -alumina with a specific surface area of 255 m²/g and a total pore volume of 1.12 cm³/g was obtained from Alfa Aesar (Haverhill, MA) as 3mm extruded granules. The γ -alumina granules were crushed and sieved to 150 μ m particles. Molybdenum(VI) oxide (MoO₃), copper (II) nitrate hemipentahydrate (Cu(NO₃)₂·2.5H₂O), and acetone (\geq 99.9% purity) were purchased from Sigma Aldrich (St. Louis, MO). Purified water was obtained from an in-house milli-Q ultrafiltration system and was used for catalyst preparation and hydrothermal experiments.

2.2.2. Metal doped catalyst preparation

Before impregnation, SiO₂-Al₂O₃ and γ -Alumina catalyst supports were calcined separately at 500°C for 6 hours in a muffle furnace for complete transformation to their protonic forms. An aqueous colloidal solution with a defined quantity of reagent (Mo and Cu) was added to a beaker containing activated SiO₂-Al₂O₃ or γ -Alumina (depend on the catalyst being made). To dope sufficient concentration of Mo on the catalyst support, the solution was oversaturated with MoO₃ reagent due to the anticipated loss of Mo in the final calcination step. Each solution was stirred at room temperature overnight. The well-dispersed mixture was placed in a furnace at 120°C for 12 hours where all the water evaporated. The solid was crushed to finer particles and

was again placed in the oven at 500°C for 4 hours to complete the calcination process. Doping was verified with XRD analysis.

2.2.3. Experimental set-up and procedure

All experiments were conducted in a 500ml batch autoclave reactor purchased from Parr Instruments Company (Parr 4575 series HP/HT). A schematic diagram of the reactor is shown in figure 1. Defined amounts of lignin, metal-doped catalyst, and purified water were mixed in a beaker. To obtain a homogeneous mixture of water/lignin/catalyst, the beaker was placed in a sonicator for 30 minutes. The mixture was then poured into the reaction vessel which was then sealed. The reaction vessel was purged three times with nitrogen in order to remove oxygen from the gas space. After purging the vessel, the reactor was charged one last time with nitrogen to the reaction starting pressure.

Depending on the desired reaction temperature, it takes around 2 to 3.5 hours for the system to reach the target temperature. After completion of reaction, the vessel was cooled using cold running water inside a coil inserted in the reactor. The system temperature returned to room temperature in around one hour. After cooling, gas was vented. Then the mixture of liquid and solid products were separated using vacuum filtration. The reaction vessel was then washed with acetone to collect remain solid residues. Solid residues on the filter paper were recovered using acetone and dried at 80 °C.

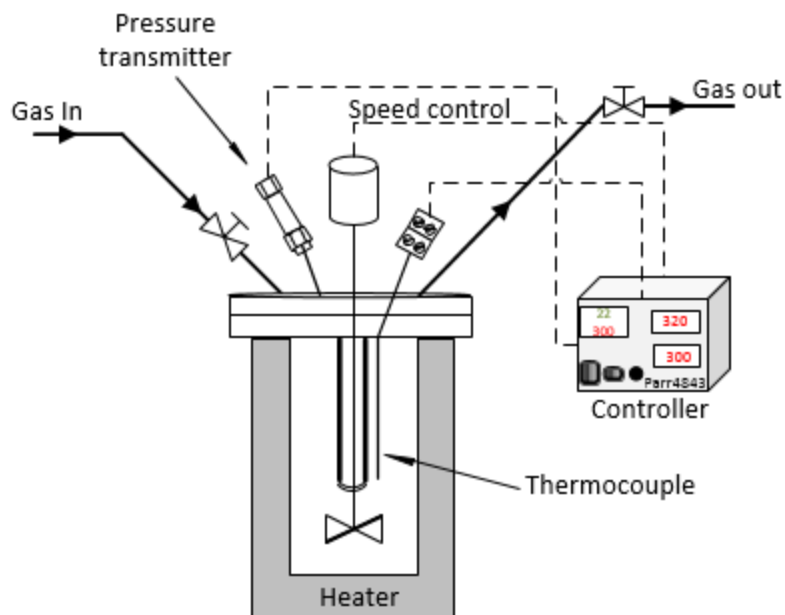


Figure 1. Schematic diagram of the batch reaction vessel used for all lignin decomposition experiments

2.3. Characterization

Analysis of lignin decomposition products were performed using a GC–FID/MS (HP 5890 gas chromatograph) equipped with an autosampler (HP 7673 injector). For the analysis, the liquid product samples (1 ml) were derivatized with dichloromethane (3ml) at room temperature. The analyses were performed in splitless mode with an injection volume of 1 μ l. The GC separation was performed using a 42 m long Agilent DB-5MS capillary column with 250 μ m I.D. and 0.25 μ m film thickness. Helium was used as a carrier gas at a constant flow rate of 1.2 mL/min. The GC column temperature program started at 50 °C for 1 min, followed by a 40 °C/min gradient to 80 °C, 25°C/min gradient to 320 °C, and a hold for 7 min. The mass spectrometer was used in the full scan mode (m/z of 33-700 amu) with the transfer line temperature of 280 °C.

Thermogravimetric analysis (TGA) of selected reactor solid residues was carried out using a TA instruments TGA-DSC Q-series (SDT-Q600). Thermal gravimetric curves were obtained under a dynamic atmosphere of argon at constant flow of 100 ml/min. The temperature program

was as follows: isothermal at room temperature for 5 minutes, ramp with a heating rate of 25 °C per minute, then isothermal for 5 minutes at 300, 400, 500, 850 and 870 °C.

Scanning electron microscopy (SEM) (Hitachi S-3400N equipped with high TOA ports for EDS, Japan) was employed to study the surface morphology of selected catalysts and reactor residues. All the samples were gold coated for forty seconds.

The XRD analysis of selected catalysts was conducted using a Rigaku Smartlab 3Kw instrument equipped with a D/teX detector using Cu K α radiation ($\lambda = 1.5302 \text{ \AA}$). The samples were scanned in the range of $10 < 2\theta < 80^\circ$.

2.4. Design of Experiments-Screening study

A twelve-run Plackett-Burman design was used to screen the importance of seven factors where three factors were associated with catalyst synthesis and four factors were introduced to optimize the reaction condition. Table 3 shows the factors selected along with their low and high levels.

Table 3. Low and high values for seven factors tested in screening study

Factor	Low (-)	High (+)
Catalyst support type	γ -Al ₂ O ₃	SiO ₂ -Al ₂ O ₃
Dopant type	Mo	Cu
Lignin concentration in water	1.2	1.7
Catalyst weight (g)	2	3
Autoclave Stirring rate	320	400
Dopant weight percent	5	10
Reaction time (min)	30	45

The first factor studied was the catalyst support type. It is believed that γ -Alumina possesses Lewis acid sites that are suitable for pre-cracking of hydrocarbon macromolecules [55]. Amorphous silica-alumina is the other catalyst support, which is a commercially available catalyst

for hydrocracking of heavy oil fractions [56]. Although the density of Brønsted acid sites in silica-alumina is not as high as zeolites, they are very efficient at breaking strong C-C bonds compared to zeolites and clay [57] and their microporous structure make them a better absorbent and desorption agent since the larger pore size in silica-alumina catalyst doesn't foul as fast as zeolites.

The second factor tested the effect of dopant type on lignin decomposition. It is known that molybdenum oxide can enhance the acidity of the catalyst supports because of the acidity of the incorporated MoO₃, which is predominantly Brønsted in nature. On the other hand, research has shown that Cu-doped catalysts not only improved the physical strength of the catalyst under hydrotreatment condition, but also deoxygenated lignin model compounds [58].

The third factor tested the lignin concentration in water. Low and high values for this factor were chosen from in-house preliminary studies. The amount of catalyst used for each experiment was the fourth factor. This factor examines the effect of acidic-site densities on the product composition.

The fifth factor was the autoclave stirring-rate. Preliminary testing showed that at stirring rates below 320 rpm, the mixing was inefficient and most of the lignin powder settled to the bottom of the vessel while at above 400 rpm a significant amount of char was generated due to the strong vortex that threw lignin powder out of the liquid phase.

Dopant concentration in the catalyst support was the sixth factor of interest. Following the reasoning behind the second factor, the sixth factor tested the effect of dopant density on product type and distribution. Since both types of dopants are supposed to increase the acidity, the sixth factor is examining the doping method and its level of success by measuring the reaction products.

Reaction time is the seventh and final factor that was tested in this set of experiments. Although very short residence time may result in incomplete degradation of lignin, long residence

times may also have negative effects such as re-polymerization and the formation of char and gaseous products. 30 and 45 minutes were chosen as reaction times which is considered as the time that passes after the vessel reaches the desired temperature.

The twelve run Plackett-Burman design was conducted in duplicate and each replicate was studied in a block. All the experiments in each replicate were randomized for screening the significant factors. Table 4 shows the design along with the run order.

Table 4. Plackett-Burman design to screen seven factors

RunOrder	Catalyst support	Dopant type	Lignin concentration (wt.%)	Catalyst weight(g)	Stirrer rate (rpm)	Dopant weight%	Reaction time (min)
1	Al ₂ O ₃	Mo	1.7%	3	320	10	45
2	Al ₂ O ₃	Mo	1.2%	2	320	10	45
3	Al ₂ O ₃	Cu	1.7%	3	400	5	45
4	Al ₂ O ₃	Cu	1.2%	3	400	10	30
5	Al ₂ O ₃	Mo	1.7%	2	400	5	30
6	SiO ₂ /Al ₂ O ₃	Cu	1.2%	2	400	10	45
7	SiO ₂ /Al ₂ O ₃	Cu	1.7%	3	320	10	30
8	Al ₂ O ₃	Cu	1.2%	2	320	5	30
9	SiO ₂ /Al ₂ O ₃	Cu	1.7%	2	320	5	45
10	SiO ₂ /Al ₂ O ₃	Mo	1.2%	3	400	5	45
11	SiO ₂ /Al ₂ O ₃	Mo	1.7%	2	400	10	30
12	SiO ₂ /Al ₂ O ₃	Mo	1.2%	3	320	5	30
13	SiO ₂ /Al ₂ O ₃	Mo	1.2%	3	400	5	45
14	Al ₂ O ₃	Mo	1.2%	2	320	10	45
15	SiO ₂ /Al ₂ O ₃	Cu	1.7%	2	320	5	45
16	Al ₂ O ₃	Mo	1.7%	2	400	5	30
17	Al ₂ O ₃	Cu	1.2%	2	320	5	30
18	Al ₂ O ₃	Cu	1.2%	3	400	10	30
19	Al ₂ O ₃	Mo	1.7%	3	320	10	45
20	SiO ₂ /Al ₂ O ₃	Cu	1.2%	2	400	10	45
21	SiO ₂ /Al ₂ O ₃	Mo	1.7%	2	400	10	30
22	SiO ₂ /Al ₂ O ₃	Cu	1.7%	3	320	10	30
23	SiO ₂ /Al ₂ O ₃	Mo	1.2%	3	320	5	30
24	Al ₂ O ₃	Cu	1.7%	3	400	5	45

2.5. Results and discussion

2.5.1. Screening study results based on chemical analysis

Table 5 summarizes the results from GC-MS analysis. The identified compounds were lumped under five general categories: guaiacols, guaiacyl carbonyls, guaiacyl dimers, guaiacyl acids, and other compounds, which are mainly syringol and homovanilyl alcohol.

Table 5. Concentration of compounds (wt %) obtained in the liquid phase of products from decomposition of lignin

Run	Guaiacols	Guaiacyl carbonyls	Guaiacyl dimers	Guaiacyl acids	Other	Total
1	0.9	0.8	0.1	1.6	1.8	5.1
2	1.0	0.9	0.1	2.1	1.7	5.8
3	1.1	1.1	0.1	2.6	2.6	7.5
4	0.6	1.2	0.0	2.6	3.0	7.3
5	1.3	1.1	0.1	2.2	2.5	7.2
6	1.3	1.4	0.1	2.6	2.8	8.2
7	0.9	1.0	0.1	1.7	1.9	5.5
8	1.2	0.9	0.1	2.9	3.4	8.5
9	1.6	1.2	0.3	2.6	2.4	7.9
10	0.8	1.1	0.4	2.6	2.9	7.8
11	1.4	1.1	0.3	2.6	2.1	7.4
12	0.7	1.0	0.2	2.4	2.6	7.0
13	0.9	0.9	0.3	3.4	3.2	8.6
14	0.5	0.7	0.1	1.8	1.2	4.3
15	1.5	1.0	0.1	2.3	2.6	7.5
16	0.5	0.8	0.0	2.5	2.5	6.4
17	2.1	1.6	0.2	3.0	3.3	10.2
18	0.5	1.1	0.0	2.3	2.9	6.7
19	0.9	0.7	0.1	1.6	1.6	5.0
20	0.6	0.8	0.0	1.6	1.2	4.3
21	0.8	0.8	0.1	1.7	1.3	4.6
22	1.0	1.2	0.1	2.5	2.3	7.1
23	0.7	1.5	0.0	1.9	2.2	6.0
24	1.4	1.4	0.1	3.9	3.8	10.6

Statistical analysis of the results is summarized in table 6. As can be seen, three factors: lignin concentration in water, stirring rate, and reaction time had no significant effect on the results. On the other hand, dopant type and dopant concentration had significant effects on almost all product groups.

To obtain more guaiacols, 5 wt% of copper-doped catalyst is suggested to be more effective while guaiacyl carbonyls were obtained in the presence of copper at either 5 or 10 wt %. Production of guaiacyl dimers depends on three factors where the best achievable condition was with silica-alumina catalyst support doped with 5 wt.% Mo. The only factor with a significant effect on the production of guaiacyl acids was dopant concentration while for the production of syringol and homovanilyl alcohol, 2g of catalyst doped with 5wt.% of Cu seems to be effective.

Table 6. A summary of the significance of each factor discovered in the Plackett-Burman screening study

	Catalyst support type	Dopant type	Lignin wt.% in water	Catalyst weight (g)	stirring rate (rpm)	Dopant wt.%	Reaction time (min)
Guaiacols	*	+	*	-	*	-	*
Guaiacyl carbonyl	*	+	*	*	*	*	*
Guaiacyl dimers	+	-	*	*	*	-	*
Guaiacyl acids	*	*	*	*	*	-	*
Others	*	+	*	-	*	-	*
Total GC-elutable compounds	*	+	*	*	*	-	*

“+” indicates the significance of the factor at its high level, “-” indicates the significance of the factor at its low level, “*” indicates no effect

During these lignin decomposition reactions, a wide range of functional subunits of lignin were removed from the base lignin molecule in order to produce monomeric compounds that can be hydrogenated to alkenes or other low molecular weight chemicals. Note that a considerable concentration of guaiacols are obtained from the degradation of phenolic dimers [33] so the acidity of the catalyst support plays an important role in the products molecular weight distribution.

The intrinsic activity of the catalyst supports was low due to the limited number of Brønsted acid sites, which is the reason that, according to the screening study results, the type of the catalyst support was not as important as other investigated factors. However, in the case of guaiacyl dimers, the silica-alumina catalyst support was shown to have a significant effect. Silica-alumina targets the β -O-4 bonds but due to its low acidity, it cannot break the stronger C-C bonds, leading to the production of guaiacyl dimers. Figure 2 shows a portion of softwood lignin structure where cleavage of β -O-4 bonds may result in the formation of dimeric compounds such as diguaiacylethane, which has a highly resistant 5-5' biphenyl bond (Fig. 3). Yet, the results presented in table 5 showed that the concentration of guaiacols in the products from γ -alumina catalyst support experiments were considerably lower. Therefore, it appears that silica-alumina may be a better option as a catalyst support.

According to the screening study results, Cu dopant has a significant positive effect on the formation of almost all types of products. Mesoporous silica-alumina is known for its high surface area and narrow pore size while copper as a dopant exhibits significant levels of acidity. The combination of these characteristics makes Cu doped silica-alumina catalyst an attractive option for *in situ* catalytic pyrolysis. For lignin degradation purposes, Cu increased the

selectivity of the silica-alumina support toward monomeric compounds while Mo was most selective for production of guaiacyl dimers. The results also showed that 5 wt% Cu doped silica-alumina was the best option for formation of guaiacols and guaiacyl acids.

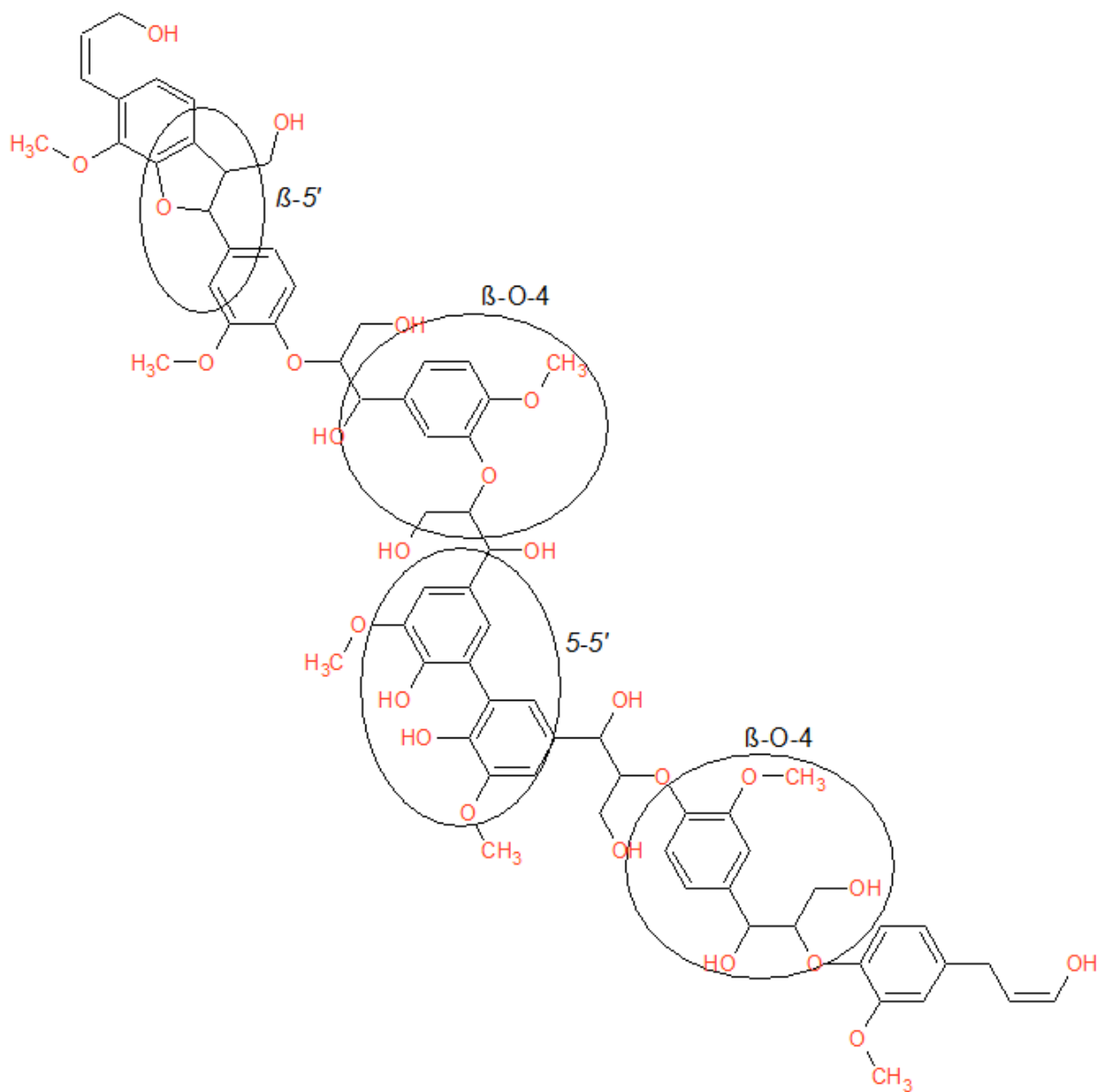


Fig 2. Part of softwood lignin structure proposed by Crestini et al. [59]

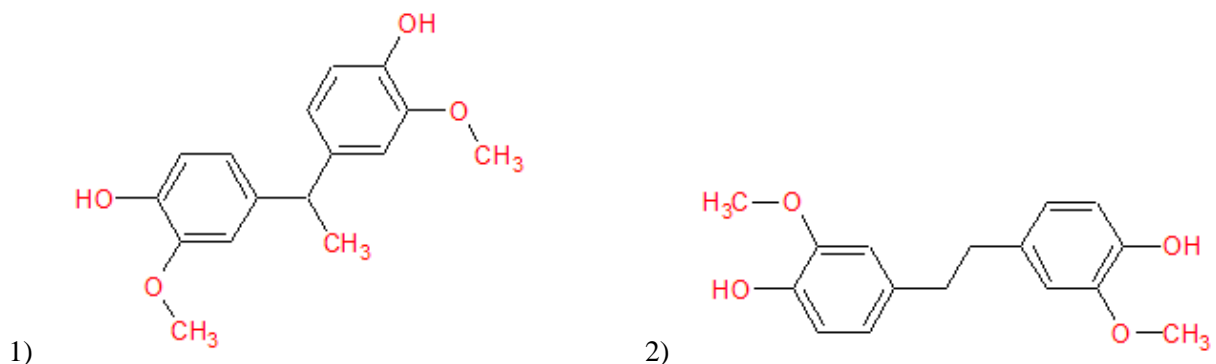


Fig 3. Examples of dimeric lignin derived compounds: 1,1- diguaiacycloethane ; 1,2- diguaiacycloethane proposed by Alen et al.[60]

XRD profiles of selected catalyst samples are presented in figures 4 and 5, respectively. As can be seen in figure 4, by comparison between un-doped silica-alumina catalyst and 5 wt. % Mo doped silica-alumina, there is no characteristic peak of Mo. The same case is true for 10 wt. % Mo in γ -alumina (fig. 5). On the other hand, characteristic peaks of copper can be seen in both silica-alumina (Fig. 4) and γ -Alumina (Fig. 5) catalyst supports.

SEM analysis was performed to further characterize the selected catalysts. EDS analysis of 5 and 10 wt. % of Mo on silica-alumina and γ -alumina (Figs. 6-7) showed the Mo characteristic peaks which suggests that the Mo concentration on the catalyst is below the XRD analysis limit of detection. This phenomenon explains the absence of a Mo peak in XRD analysis while the GC-MS analysis results show an increment in production of phenolic compounds with Mo doped catalysts.

It is worth to mention that at the catalyst preparation step, MoO_3 and catalyst support were dispersed in water and dried overnight. This step resulted in formation of a white to pale greenish molybdic acid. Since molybdic acid is volatile at temperatures above 300 °C, more of

the Mo precursors were evaporated at the final activation step at 500 °C. However, since the catalyst support/water was oversaturated with a high concentration of

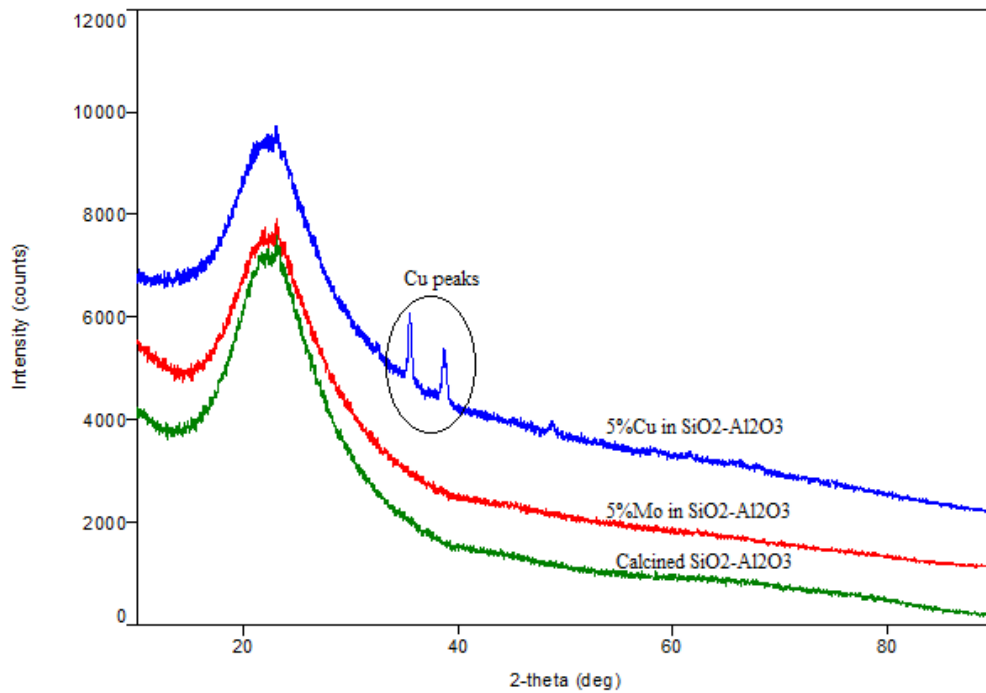


Fig 4. XRD patterns of calcined silica-alumina, 5 wt.% Cu in $\text{SiO}_2/\text{Al}_2\text{O}_3$ and 5 wt.% Mo in $\text{SiO}_2/\text{Al}_2\text{O}_3$

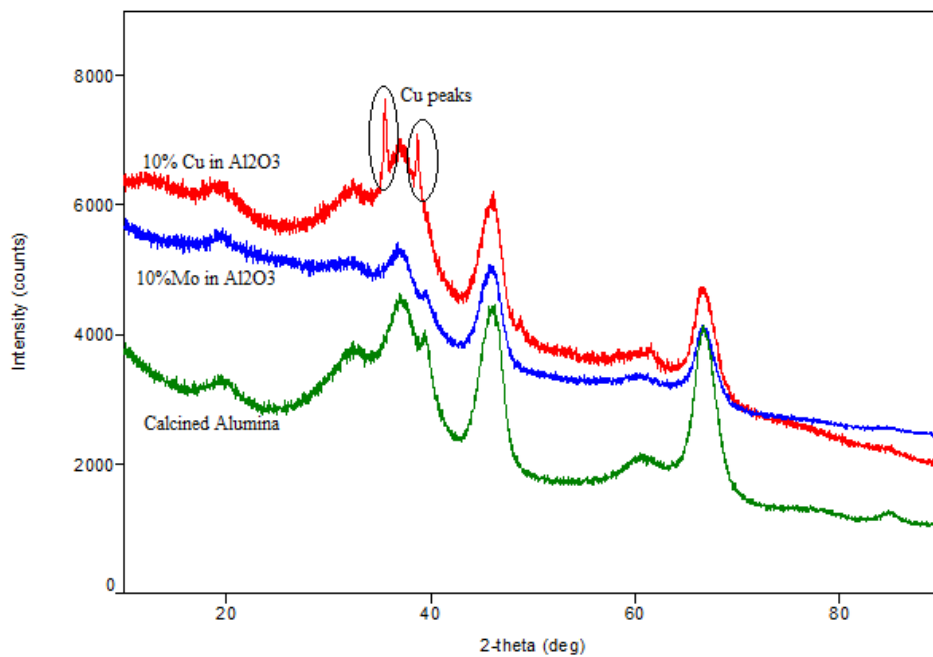
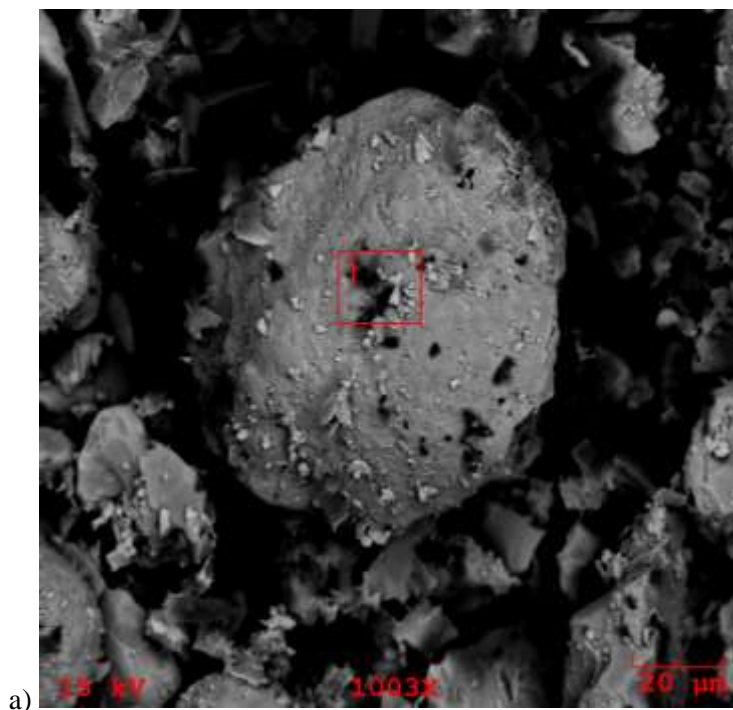
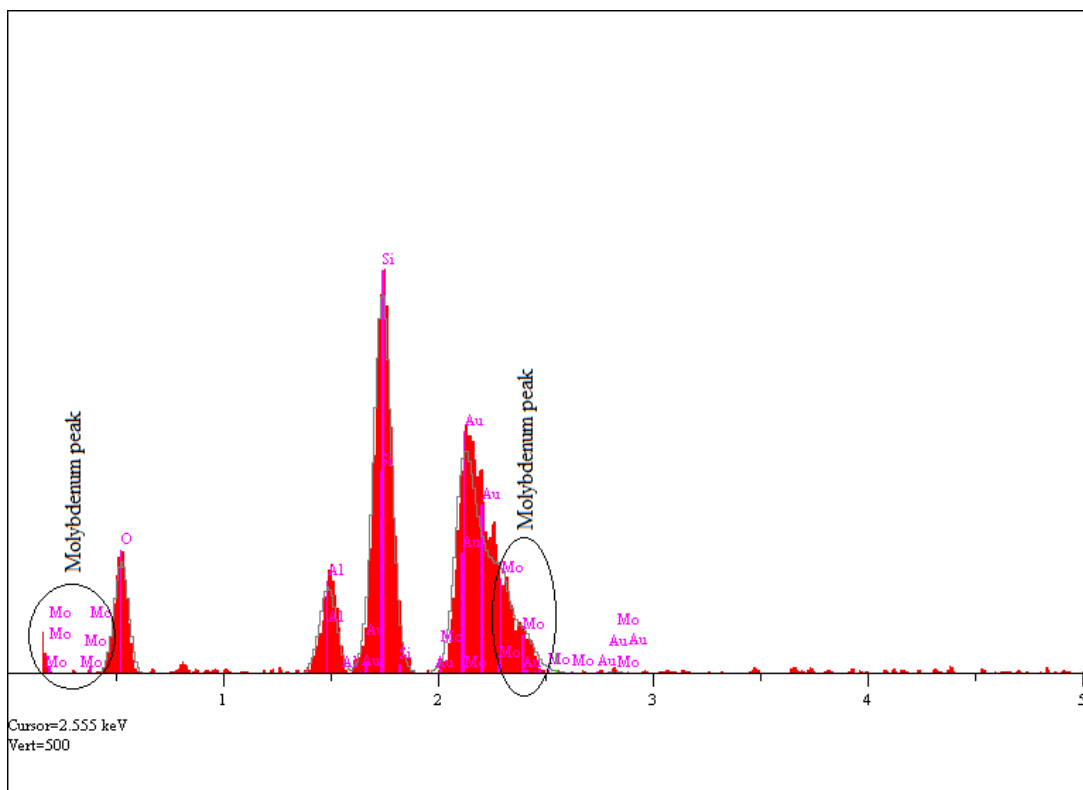


Fig 5. XRD patterns of calcined γ -Alumina, 10 wt.% Cu in γ -Alumina and 10 wt.% Mo in γ -Alumina



a)



b)

Figure 6. a) SEM and b)EDS analysis of 5 wt.% Mo on silica-alumina

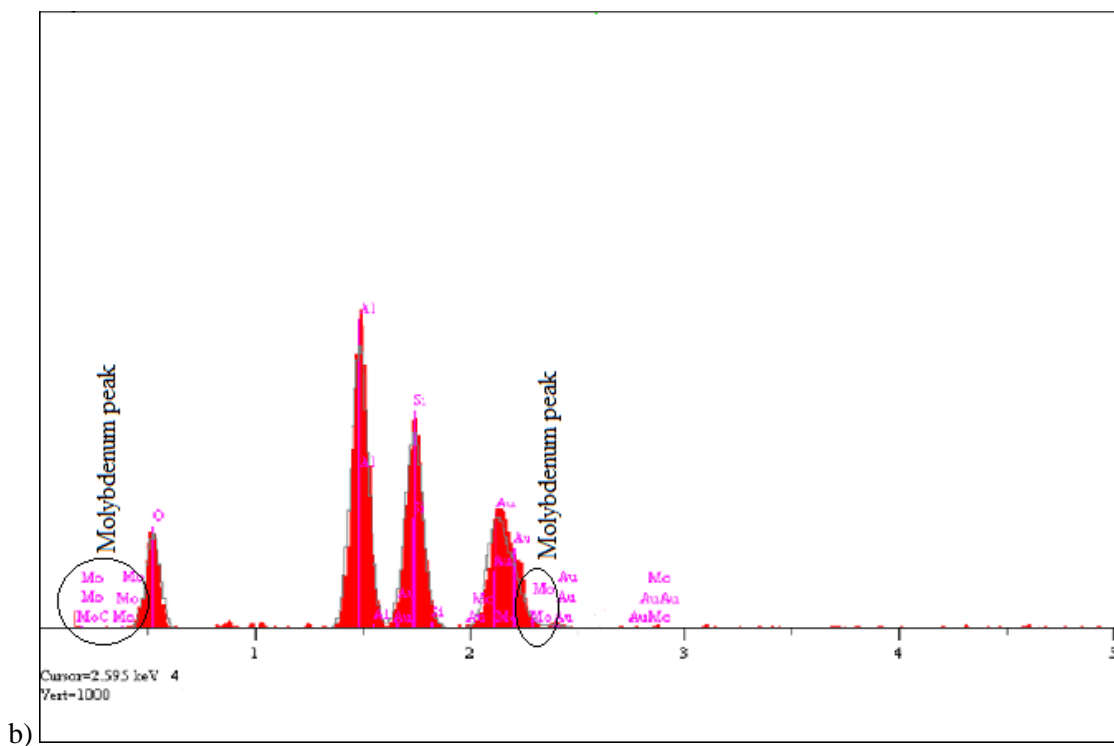
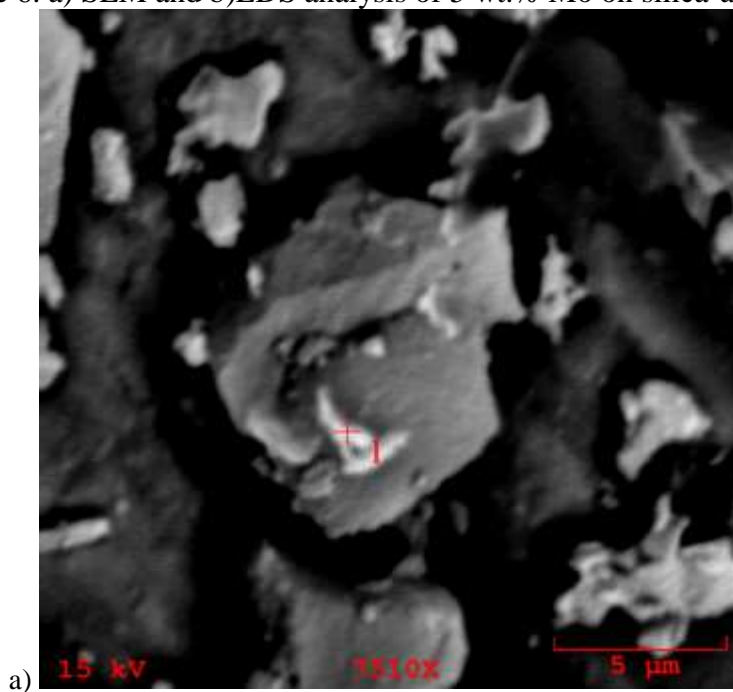


Figure 7. a) SEM and b) EDS analysis of 10 wt.% Mo in γ -alumina

MoO₃, resulting in a limited concentration of Mo doped on the support and the rest converted to molybdic acid. Even though the concentration of Mo dopant was lower than expected, the presence of molybdic acid during the calcination step, improved the acidity of the catalyst.

SEM and EDS analysis of 5 wt. % and 10 wt. % copper doped silica alumina is shown in figure 8. As can be seen, the Cu was well-dispersed on the surface of the silica-alumina catalyst and its characteristic peak is present in the EDS results. Comparison of 5 wt. % and 10 wt. % of copper-doped silica-alumina showed that at the smaller load of Cu dopant, the particles were doped as very fine particles. On the other hand, in 10 wt. % doped sample, the dopant is more in the form of Cu coagulates which may clog the pores of the catalyst support and limit the access of phenolic dimers to the active acid sites. This phenomenon explains the lower concentration of GC-detectable compounds in samples with 10 wt. % Cu.

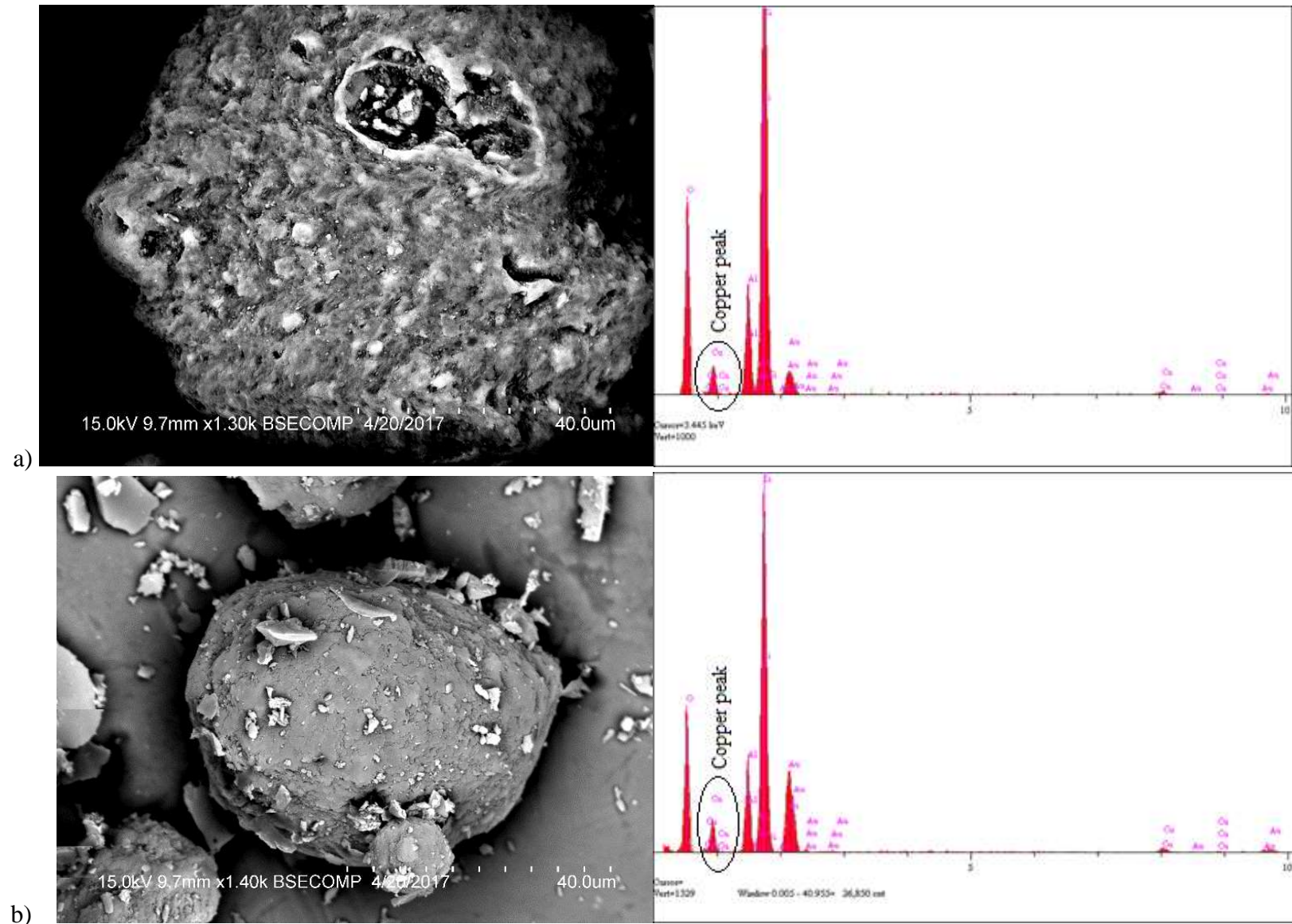


Fig 8. SEM and EDS analysis of a) 5 wt. % Cu in $\text{SiO}_2/\text{Al}_2\text{O}_3$, b) 10 wt. % Cu in $\text{SiO}_2/\text{Al}_2\text{O}_3$

2.5.2. Temperature bounding studies

Lignin has a very complex structure with strong bonds that require elevated temperature to break them. The required energy to break lignin bonds depends on the experimental conditions and is not consistent [61]. Moreover, it is well established that low temperature and a low heating rate process will increase the formation of bio-char [62], which can foul the catalyst.

Screening study results showed that 5wt.% copper doped silica-alumina facilitates the formation of monomeric compounds. Therefore, the effect of temperature on degradation of lignin was examined in more detail using the best condition from the initial screening study. The reaction conditions for this temperature study are summarized in table 7. Each experiment was conducted in triplicate.

Table 7. Reaction condition for temperature bounding studies

Reaction temperature	300, 320, 350 °C
Lignin concentration in water	1.2 wt.%
Catalyst	5 wt.% Cu in SiO ₂ -Al ₂ O ₃
Stirring rate	400 rpm
Reaction time	30 min

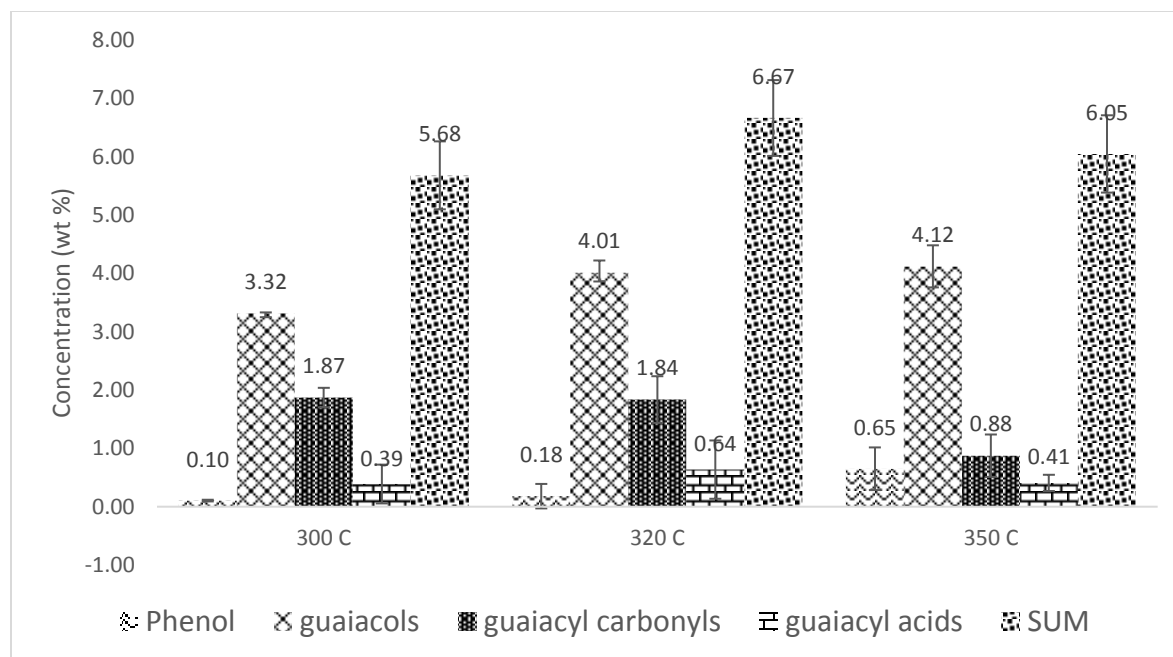


Fig 9. Temperature bounding experimental results in terms of concentration of products per gram of lignin

Figure 9 shows the results obtained from GC-MS analysis of the extracted samples in DCM. The overall recovery of liquid phase products was bounded by the temperature region. By increasing the temperature, the concentration of guaiacols and phenol were increased while guaiacyl carbonyls were decreased. Guaiacyl acids as well as total GC elutable compounds had a bell shape profile with temperature increase where at 320 °C was near its maximum.

The solid residue obtained from the temperature bounding experiments was crushed into a fine powder and analyzed with TGA. TG curves and mass loss at different thermal steps are summarized in figure 11 and table 8.

As can be seen, the total mass loss decreases with increase in experimental reaction temperature. The weight loss at 25-200 °C can be attributed to monomeric compounds and physically adsorbed water while thermal decomposition of oligomers take place at 600-900 °C. In theory, since catalytic decomposition of lignin at 350 °C had the lowest mass in the TG

analysis, lignin degradation should be more efficient at higher reaction temperatures. However, GC-MS analysis results showed that 320 °C is more suitable for formation of lower molecular weight compounds. This suggests that at 350 °C a greater degree of re-polymerization occurs.

SEM analysis of solid residues are presented in figure 10. The morphology of the particles showed differences since the catalyst particles are covered with char. EDS analysis of each sample shows a significantly large peak of carbon in all samples. Comparison of the particles shows a trend where at 300 °C the char covered catalyst particle is very porous and has a beehive structure where dimeric compounds can still access the active surface of the catalyst. At 320°C, the particles are not as porous but yet the spherical shape of the catalyst particle is still visible. At 350°C, char extensively cover the particles and no spherical structure is visible. Comparing these observations with GC-MS analysis of the liquid phase products suggests that at 320 °C the density of char around the silica-alumina particles are so high that further increasing the temperature does not facilitate the catalytic degradation since the access to the active sites on the surface of the catalyst is extremely limited. Therefore, the maximum potential of Cu doped silica-alumina catalyst can be obtained at 320°C.

Moreover, all of the reactions in this research were conducted in a 500 ml batch vessel. On average, it takes 2 hours for the vessel to reach to 300 °C and 3 hours to reach 350°C . It also takes 1 to 2 hours for the vessel to cool down to room temperature, which gives time for the produced monomers and dimers to re-polymerize. It is postulated that a significant amount of char was generated during the cooling down phase. Since this phase is longer at higher temperatures, it is reasonable to assume that at higher temperatures, the risk of formation of char is higher.

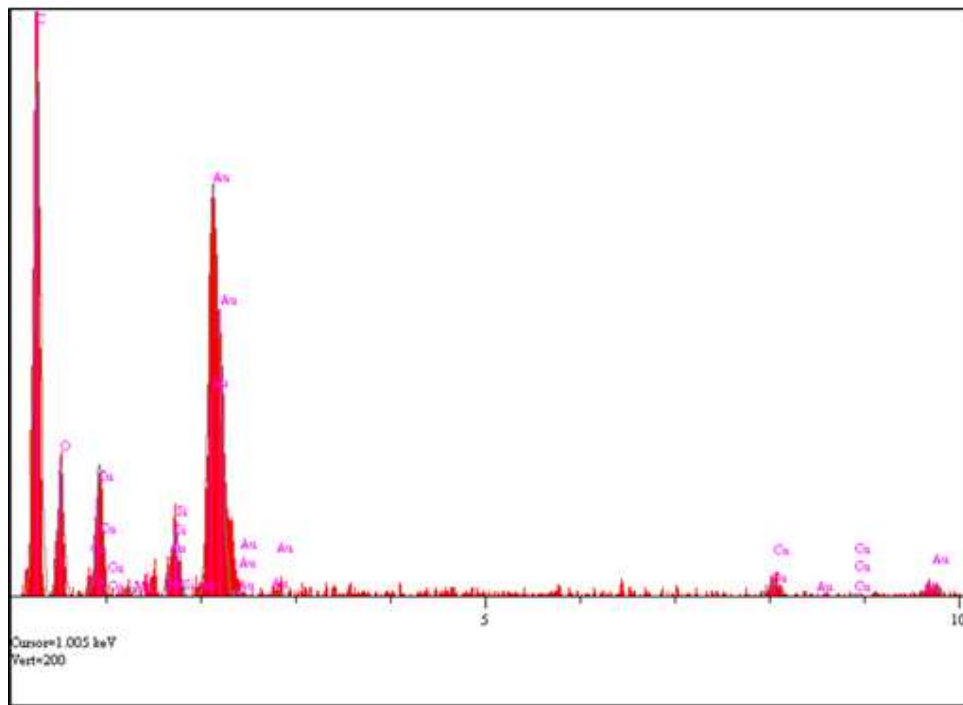
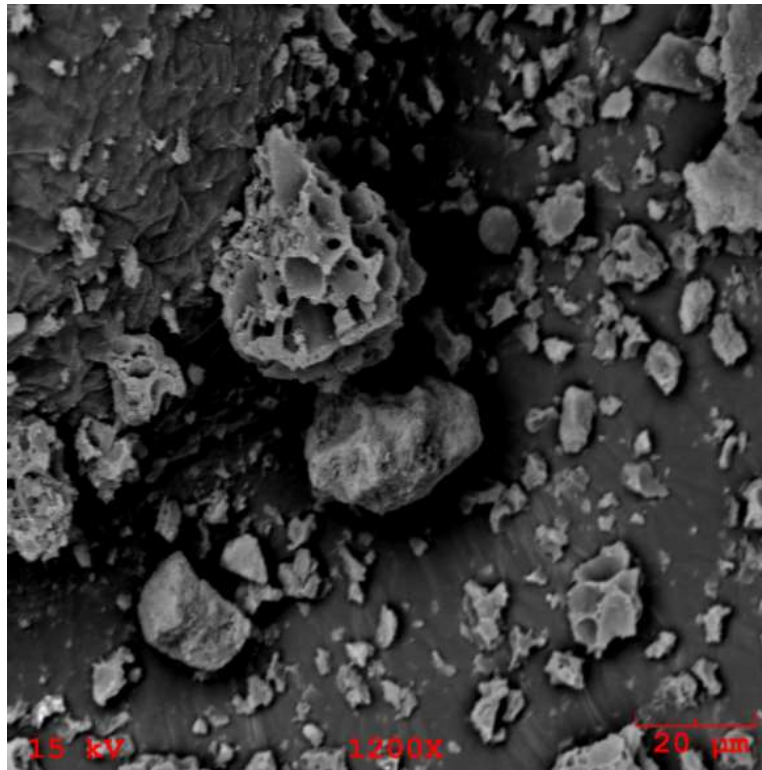
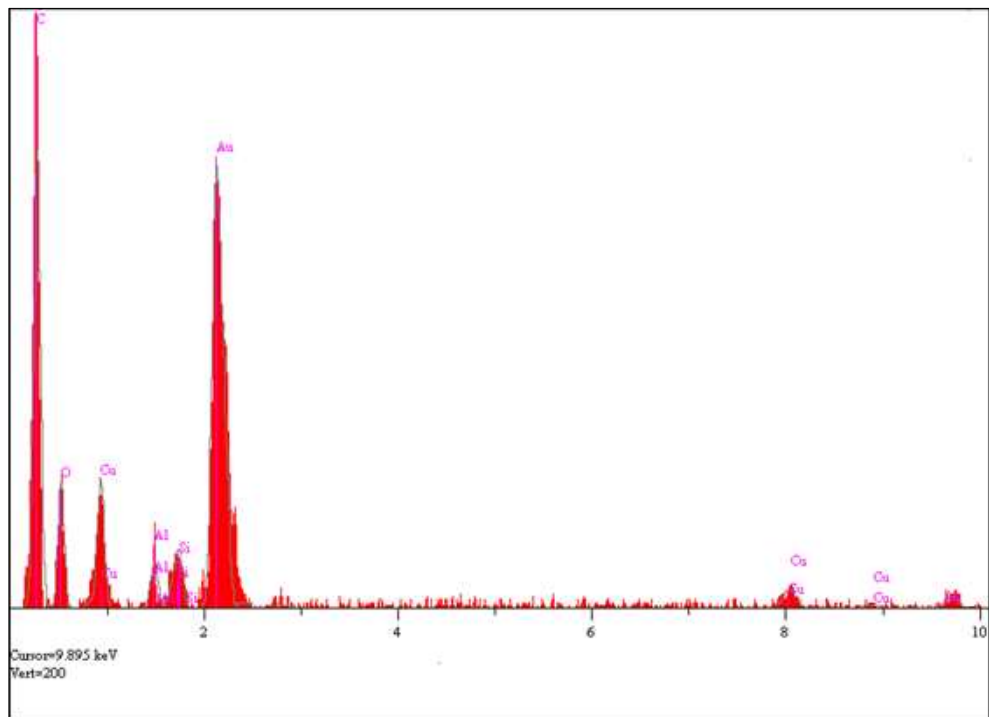
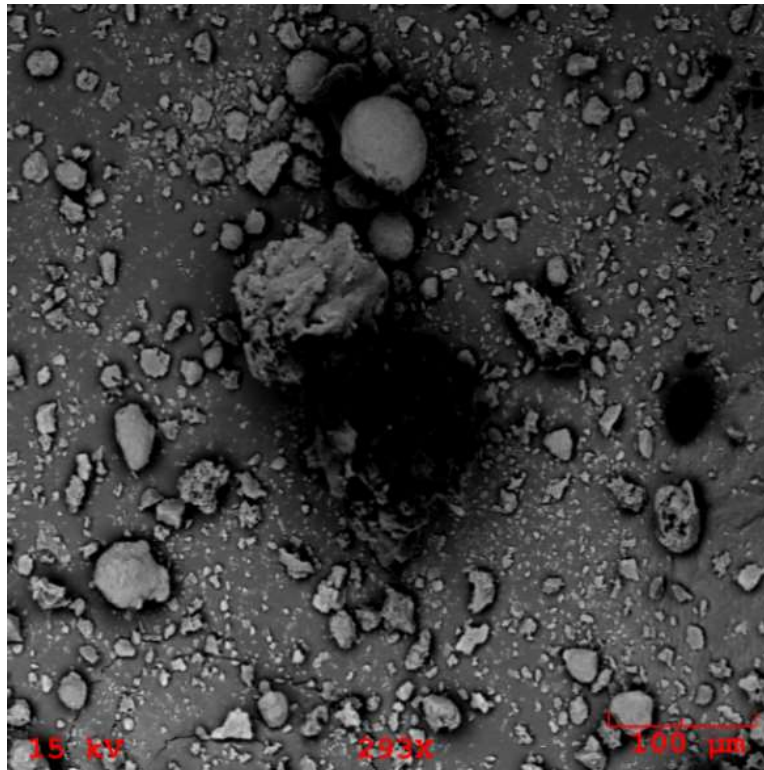


Fig 10. Solid residues collected from reactor at reaction temperatures of a) 300°C b) 320°C c) 350°C



b)

Figure 10. Continued

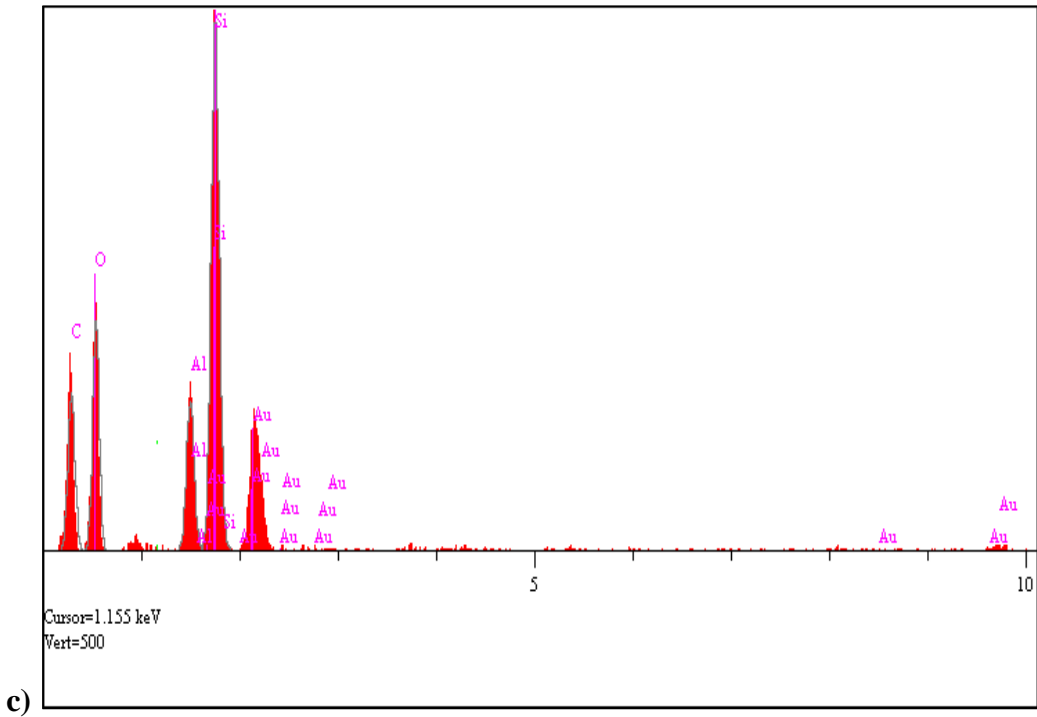
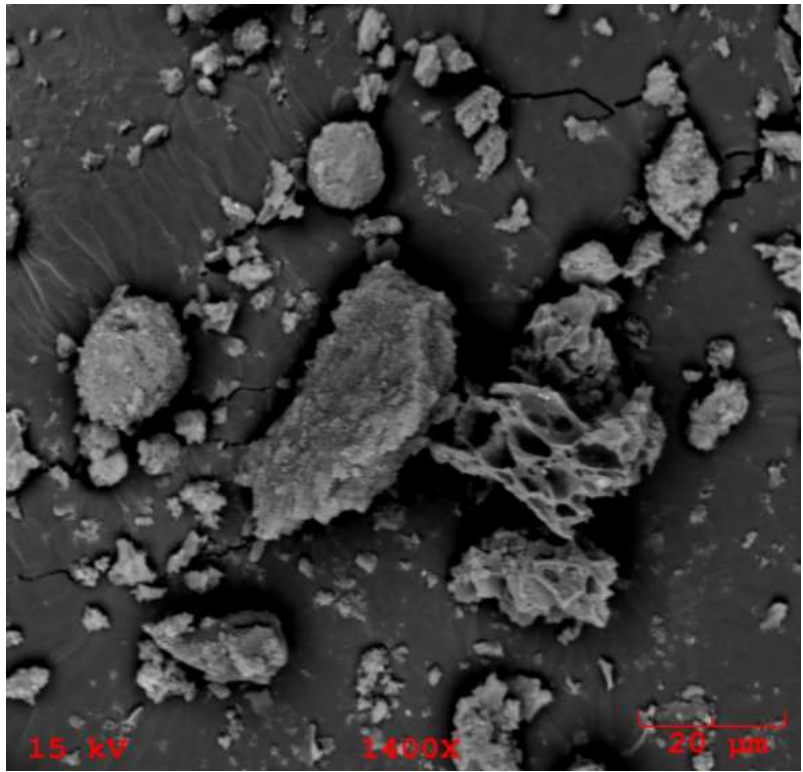


Figure 10. Continued

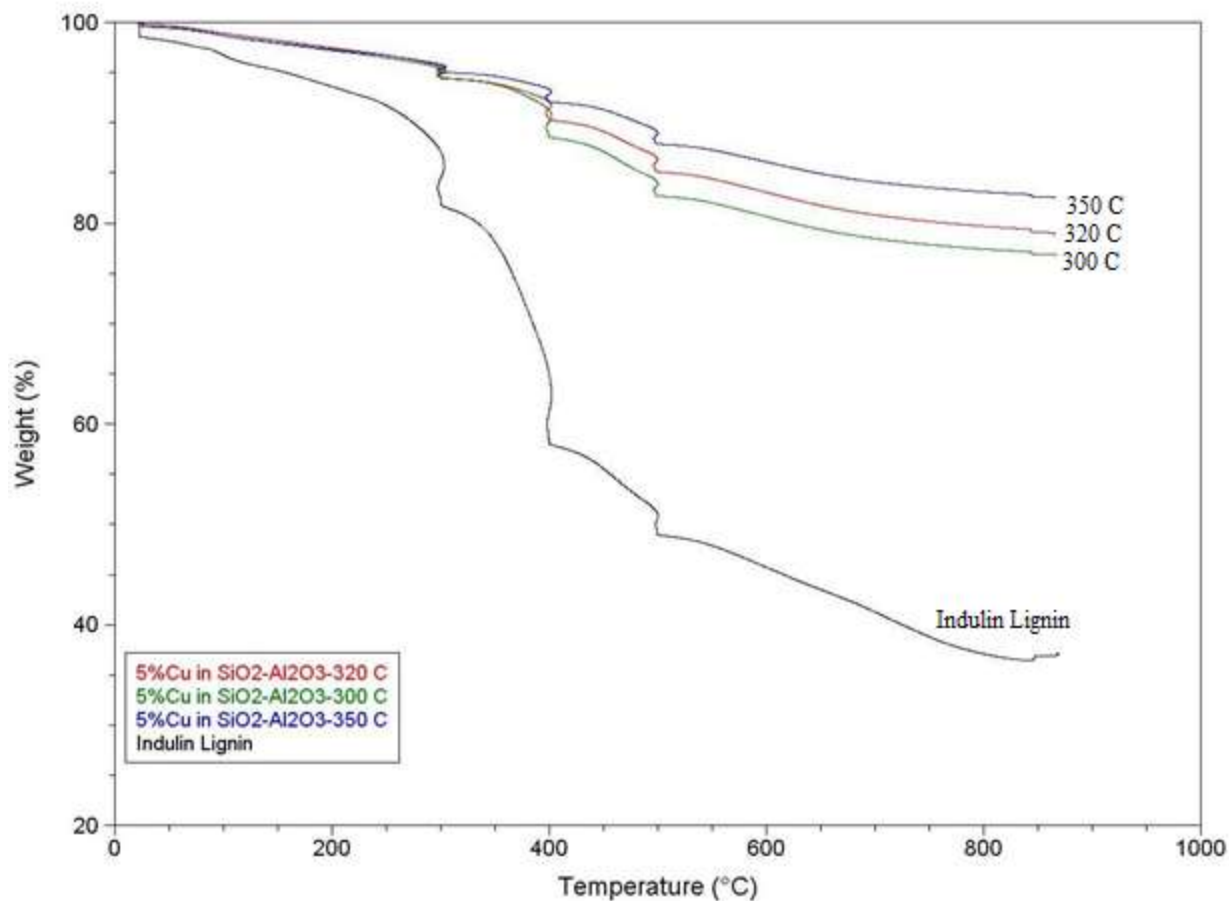


Fig 11. TG curves of reactor residues from temperature study with 5 wt.% Cu in SiO₂/Al₂O₃ at 300, 320 and 350 °C

Table 8. Mass loss during TG analysis of reactor residues collected from temperature studies (wt % loss)

Sample	25-200 °C	200-400 °C	400-600 °C	600-900 °C
Raw Indulin Lignin	6.3	28.7	19.2	8.8
5%Cu in SiO ₂ -Al ₂ O ₃ -300 °C	2.8	5.9	10.6	3.8
5%Cu in SiO ₂ -Al ₂ O ₃ -320 °C	2.5	5.4	9.0	4.0
5%Cu in SiO ₂ -Al ₂ O ₃ -350 °C	2.7	4.0	7.2	3.5

2.6. Conclusion

Silica-alumina and γ -Alumina were used as catalyst supports to prepare 5 and 10 wt. % Cu and Mo doped catalysts through a wet impregnation method. A Plackett-Burmen screening study was conducted in two replicates to examine catalyst synthesis as well as operating conditions. The DOE results showed that dopant type and dopant concentration had a significant effect on almost all groups of lignin degradation products while lignin concentration, stirring rate and reaction time had no major effect on products distribution within the parameters bound in this study. EDS and XRD analysis results showed that Cu was successfully doped in both catalyst supports. Since Mo concentration was below the XRD detection limit, it did not show any characteristic peak while quantification with EDS show small peaks of Mo. Moreover, the presence of molybdic acid in the catalyst calcination step also improved the acidity of the final catalyst.

Temperature bounding studies were conducted at three temperatures: 300, 320, 350 °C in two replicates to investigate the effect of reaction temperature on products distribution. GC-MS analysis of DCM-extracted samples along with TG analysis of reactor solid residues showed that at 320 °C the formation of monomeric compounds will be maximized while the formation of char will be minimized. Based on the results, reaction at higher temperature may lead to re-polymerization, which decreases the monomeric compounds concentration and increases the possibility of char, tar and gaseous products formation.

CHAPTER III

NON-CATALYTIC DECOMPOSITION OF LIGNIN INTO CHEMICALS AND INTERMEDIATES

3.1. Introduction

Lignin is one of the most abundant biopolymers. On average, 24 wt % of a plant's structure is composed of lignin [1]. Wood pulping processes are the main resource of commercially produced lignin where the lignin is usually burnt due to its high heating value. While only 1-2 % of the lignin is currently being used to produce other types of products, burning lignin can produce 66% of pulp and paper industries electricity needs [2, 3].

In theory, breaking lignin bonds will result in a variety of phenolic compounds such as guaiacols, cresols, vanillin etc. Lignin from softwood contains 40-50% β -O-4 bonds where deoxygenation of lignin will result in dissociation of C-O bonds to generate phenolic monomers. The significant density of ether bonds in lignin's structure has motivated many studies of degradation of lignin model compounds where β -O-4 bonds were present [4-8]. Although these types of studies explain certain degradation pathways, the overall selective transformation of lignin has yet to be defined [9].

Base catalyzed depolymerization (BCD) of lignin at elevated temperatures leads to the cleavage of mainly ether bonds. Lavoie et. al, investigated BCD of lignin at temperatures varying from 300 to 330 °C. Based on the reported results, the product distribution consisted of 10 % monomers, 60% dimers/trimers and 30 % char [10], suggesting that at basic condition and 300 °C, there is sufficient energy for dissociation of aryl-alkyl bonds.

Although higher temperature seems to favor phenolic compounds production, longer reaction time will increase the formation of unwanted solid residues due to repolymerization of intermediates [11]. Selective dealkylation and dehydroxylation of lignin remained an unsolved

challenge that limits the production of monomeric compounds that can be further processed to BTX , phenols and other oxidized products [12]. The combination of low residence time and BCD reaction is expected to result in cleavage of ether bonds and production of phenolic hydroxyl groups while minimizing the formation of char.

Very few studies have investigated lignin decomposition reaction in a continuous flow reactor where the flow rate and residence time can be controlled [13, 14]. In the present work, degradation of lignin was investigated at a temperature range of 300-400 °C using a continuous flow reactor in either sub- or supercritical water. Water properties can be manipulated by changing temperature [15]. Organic compounds and gases are soluble in super critical water [16, 17] as water's polarity changes drastically under supercritical conditions. Some of the selected properties of sub- and supercritical water are summarized in table 1. As can be seen, the dielectric constant and density of supercritical water is significantly different from subcritical water. Such changes in water's properties can potentially change the lignin degradation reaction pathway towards the formation of desired monomeric compounds.

Table 1. Properties of sub and super critical water [18, 19]

	Subcritical water	Supercritical water
Temperature (°C)	25-374	≥375
Pressure (MPa)	0.1-25	≥25
Density, ρ (g/cm ³)	1-0.6	≤0.58
Dielectric constant, ϵ (F/m)	78.5-14.07	≤13
Heat capacity, C_p (KJ/Kg.K)	4.22-10.1	13-6

3.2. Experimental

3.2.1. Materials

Kraft lignin (Indulin AT) was supplied by MeadWestvaco (Glen Allen, VA) and anhydrous pellets of sodium hydroxide ($\geq 98\%$ NaOH), analytical grade o-Terphenyl, and 4-Chloroacetophenone were purchased from Sigma-Aldrich (St. Louis, MO). Deionized water was obtained from an in-house ultrafiltration milli-Q system and was used in all experiments. High pressure nitrogen gas was supplied by Praxair (Danbury, CT). Analytical grade dichloromethane was purchased from Fisher Scientific (Hampton, NH) and was used as the extracting agent.

3.2.2. Experimental set-up and procedure

The experimental setup is illustrated in figure 1. For all experiments, lignin was dissolved in water to a concentration of 10% w/w with 5% w/w of NaOH as a base catalyst. Pressurized nitrogen was used to pressure the feed through the system. The mixture was fed to the preheater using pressurized nitrogen where it was heated to 220 °C. The solution was mixed using a stirrer set at 400 rpm. Before running the experiments, the reaction vessel was preheated to the desired temperature while filled with de-ionized water. Once the feed in the preheater reached 220 °C, the water was discharged from the reaction vessel and the lignin solution was continuously fed to the reaction vessel. The reaction vessel was a 4 m long stainless-steel tube with 0.95 cm outer diameter and 0.16 cm wall thickness. The reactor was heated with an insulated electric heater. The flowrate through the reactor was controlled using a backpressure regulator.

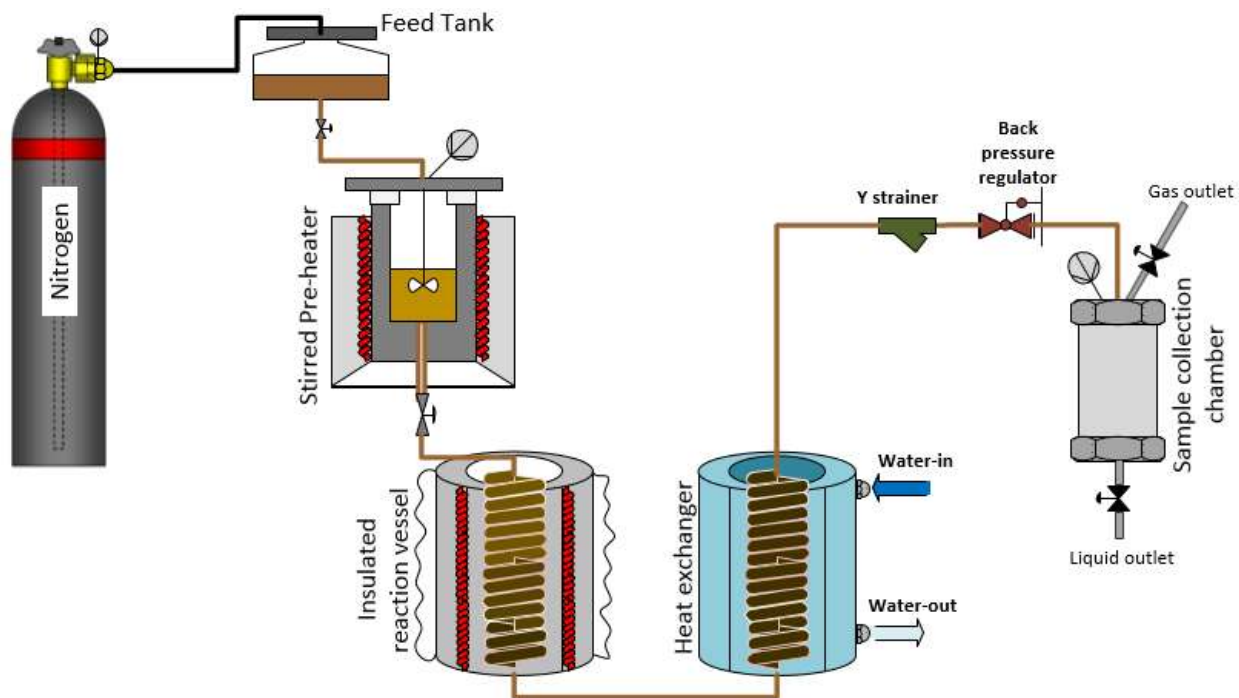


Figure 1. Schematic diagram of the continuous flow reactor

3.2.3. Engineering design and modeling

The reactor model was simulated using a developed MATLAB code. Preliminary experiments were conducted to verify the model with experimental data. Figure 2 summarizes an overview of the temperature profile along the reaction vessel. As can be seen, the temperature at the reaction vessel inlet was maintained at 220 °C for all the experiments. The temperature rises to the reaction set point temperature over time. However, it should be noted that the temperature threshold of degradation of lignin is 300 °C, which needs to be considered and evaluated in the reaction residence time. To verify the compatibility of the results with the simulated model, the temperature profile results which was collected through online monitoring of the reaction system were presented for two reaction temperatures and are presented in figure

3. As can be seen the model efficiently predicted the experimental data, which further verifies the validity of the experimental data.

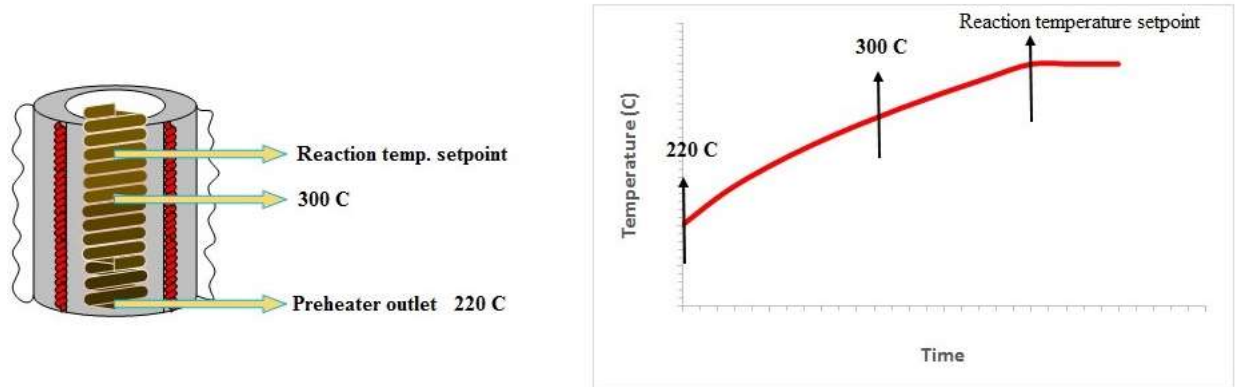
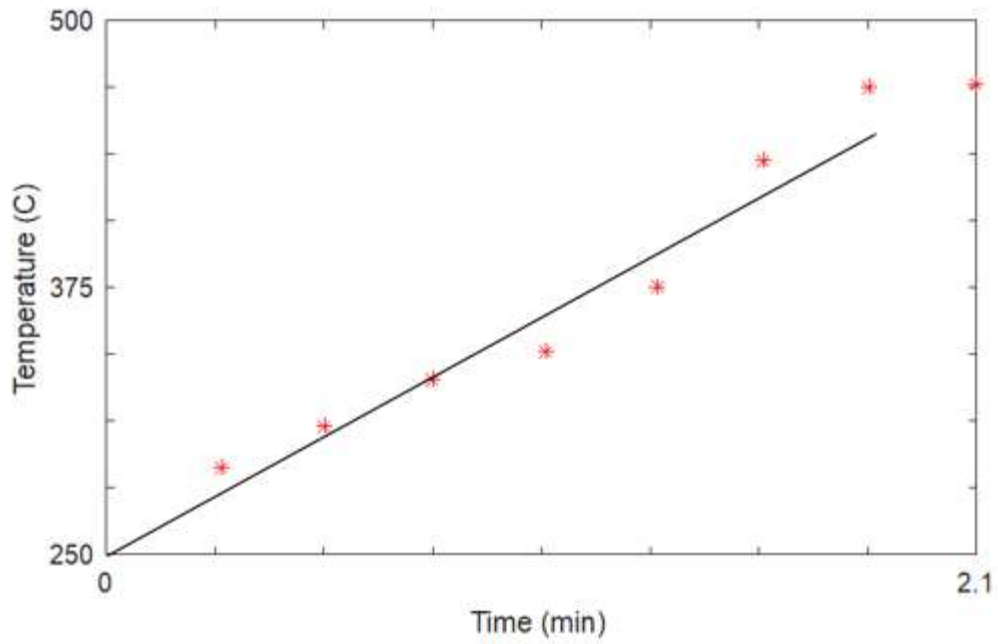
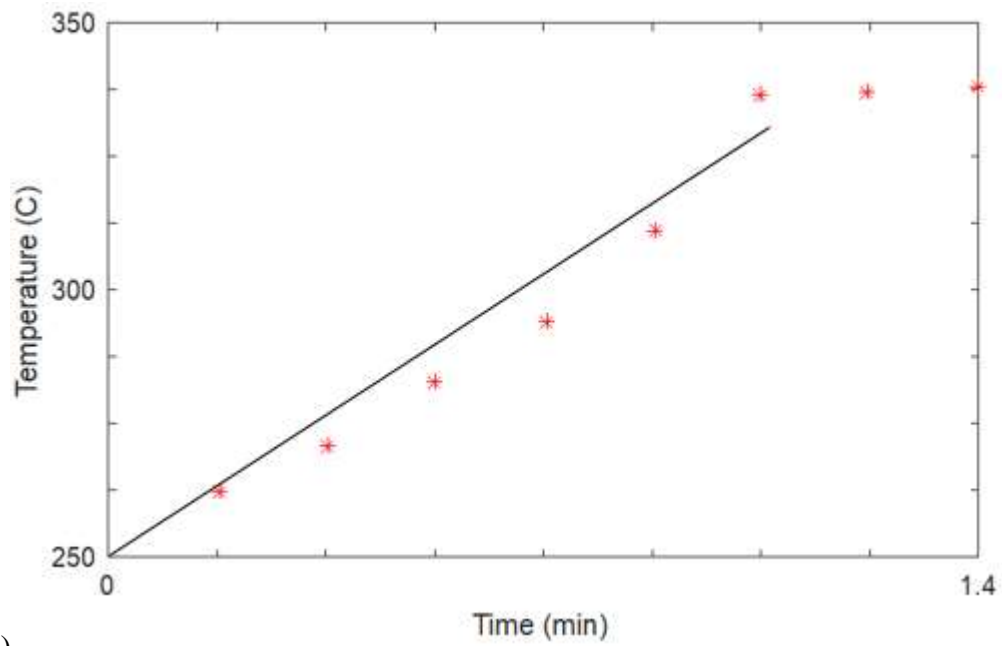


Figure 2. Illustration of temperature profile along the reaction vessel



a)



b)

Figure 3. Experimental data versus the predicted model for reaction temperature a) 480 °C, 340 °C

Table 2 summarizes the experiments that were conducted in this study. The experiments were divided in two categories: subcritical, which range from 300 to 370 °C and supercritical, which range from 380 to 480 °C. The system pressure for all experiments was set at 25 MPa, and each experiment was conducted in triplicate.

Table 2. Summary of parameter variations in the experiments

	Exp. 1	Exp. 2	Exp. 3	Exp. 4	Exp. 5	Exp. 6
Reaction temperature (°C)	335	340	350	400	420	480
Residence time at above 300 °C (min)	0.6	0.64	0.65	0.9	1.1	1.2
Residence time at reaction setpoint (min)	0.34	0.3	0.37	0.30	0.31	0.30
Total residence time (min)	1.35	1.41	1.3	1.85	1.98	2.1

Figure 4 summarizes the identification and separation procedure. The collected samples were treated with one molar hydrochloric acid to reduce the pH to below 2. The acidified samples were then placed in a hot water bath to expedite the precipitation of the solids. These solids are mostly oligomers, modified lignin, and condensed active complexes that were produced at elevated temperature [73]. The samples were filtered and solid residues were collected on filter paper. The solids were weighed and dried for further analysis with TGA. DCM was used to extract the monomers from aqueous phase and is identified as the monomer rich fraction. This fraction was subsequently analyzed with GC-FID/MS.

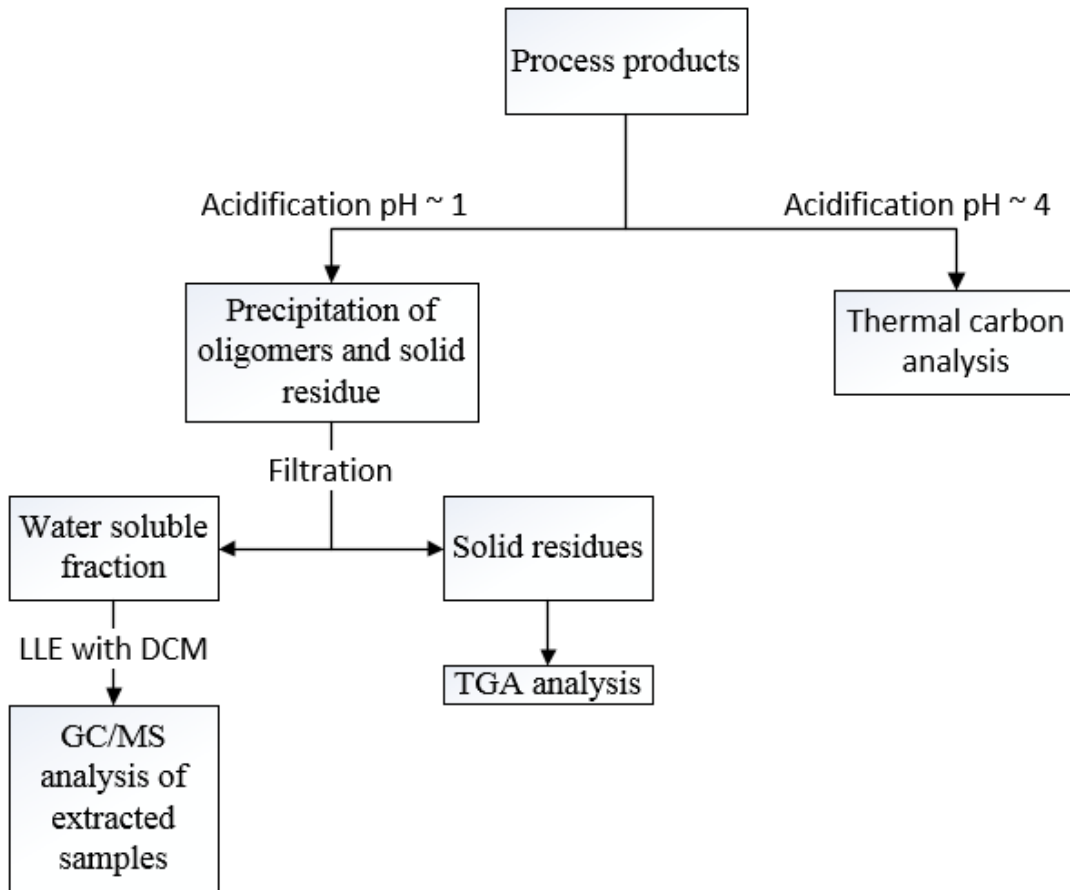


Figure 4. Separation and analysis steps of the experiments products

3.2.3. Analytical methods

After each experiment, the pH of the aqueous samples were measured using a MP220 Basic pH/mV/°C Meter (Mettler Toledo, OH, USA).

An OCEC (Organic Carbon Elemental Carbon) aerosol analyzer purchased from Sunset Laboratory Inc. (Tigard, OR, USA) was used to measure the carbon content of the acid-treated samples. The temperature was programmed from 200 to 890 °C through three general steps. The first step consists of thermal desorption at 200 and 300 °C under a flow of helium with heating rates of 5 and 2 °C/s, respectively. This represents the monomer fraction. The second step consists of heating ramps to 400, 500 and 890 with heating rates of 2, 2 and 6 °C/s, respectively under a flow of He. This step represents the oligomer fraction. At the last step which is referred as the pyrolytic step, the oven temperature was reduced to 550 °C with a cooling rate of 7 °C/s under an oxidizing agent of 90% He and 10% O₂. This was done to burn off the residual mass which was defined as the coke or char. To analyze the samples with thermal carbon analyzer, the samples pH were lowered by adding approximately 700 µl one molar HCl to 4. Before analysis, each sample was vortexed for one minute.

The aqueous phase analysis was performed using a GC–FID/MS (HP 5890 gas chromatograph) equipped with an autosampler (HP 7673 injector). For the analysis, the liquid product samples (1 ml) were derivatized with dichloromethane (3ml) at room temperature. The analyses were performed in splitless mode with an injection volume of 1 µl. The GC separation was performed using a 42 m long Agilent DB-5MS capillary column with 250 µm I.D. and 0.25 µm film thickness. Helium was used as a carrier gas at a constant flow rate of 1.2 mL/min. The GC column temperature program started at 50 °C for 1 min, followed by a 40 °C/min gradient to

80 °C and 25°C/min gradient to 320 °C and a hold for 7 min. the MS was used in the full scan mode (m/z of 33-700 amu) with the transfer line temperature of 280 °C. Figure 5 shows all the GC detectable compounds found in the aqueous phase during this study.

Thermogravimetric analysis (TGA) of solid residues was carried out using a TA instruments TGA-DSC Q-series (SDT-Q600). Thermal gravimetric curves were obtained under a dynamic atmosphere of argon at constant flow of 100 ml/min. The temperature program was as follows: isothermal at room temperature for 5 minutes, ramp with a heating rate of 25 °C per minute, then isothermal for 5 minutes at 300, 400, 500, 850 and 870 °C.

Scanning electron microscopy (SEM) (Hitachi S-3400N equipped with high TOA ports for EDS, Japan) was employed to study the surface morphology of the precipitated oligomer rich fraction that was collected during filtration of the samples. All of the samples were gold coated for twenty seconds using a Cressington 108 sputter coater (Redding, CA).

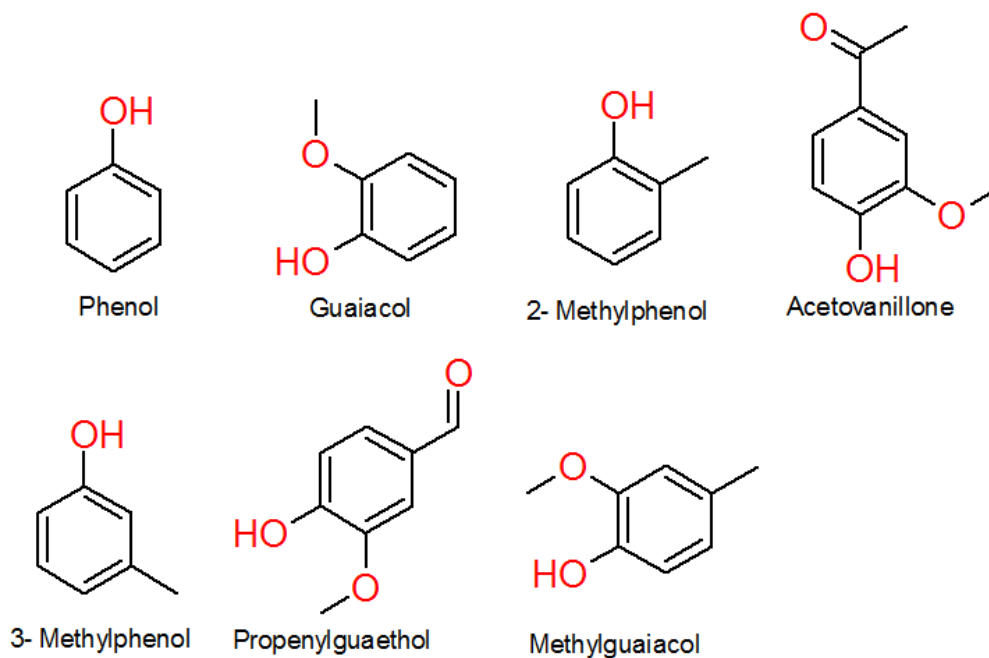


Figure 5. Identified compounds from GC-MS analysis of the DCM extracted fraction

3.4. Results and discussion

pH results from all the experiment are shown in figure 6. As can be seen, the feed has the highest pH value which is expected and the second highest pH value is for preheater outlet which verifies that no significant reaction took place at 250 °C. In the sub-critical water region, the pH reaches its minimum at 340 °C while the acidity is at its highest in the super-critical water region. During base catalyzed reactions, cleavage of aryl-aryl-ether and aryl-alkyl-ether occurs. Although the reaction pathway highly depends on the concentration of the base and the reaction temperature, BCD reactions, in general, will result in the formation of acids such as homovanillic acid and formic acid, which affects the pH of the final products [79]. During BCD reactions in supercritical condition, the number of cleaved β -O-4 ether bond within the structure of lignin will increase with temperature, which results in the formation of a higher concentration of formic, and acetic acid. It should be mentioned that the presence of acids neutralizes the base and decreases the hydrolysis reaction rate but due to the significant concentration of NaOH, this effect is negligible.

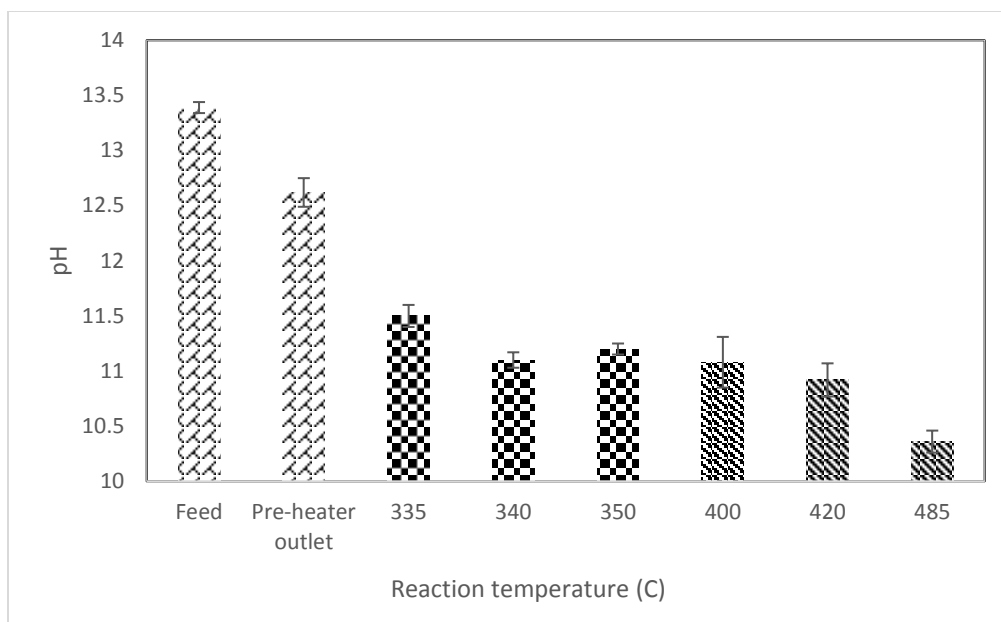


Figure 6. pH analysis of collected samples at each temperature

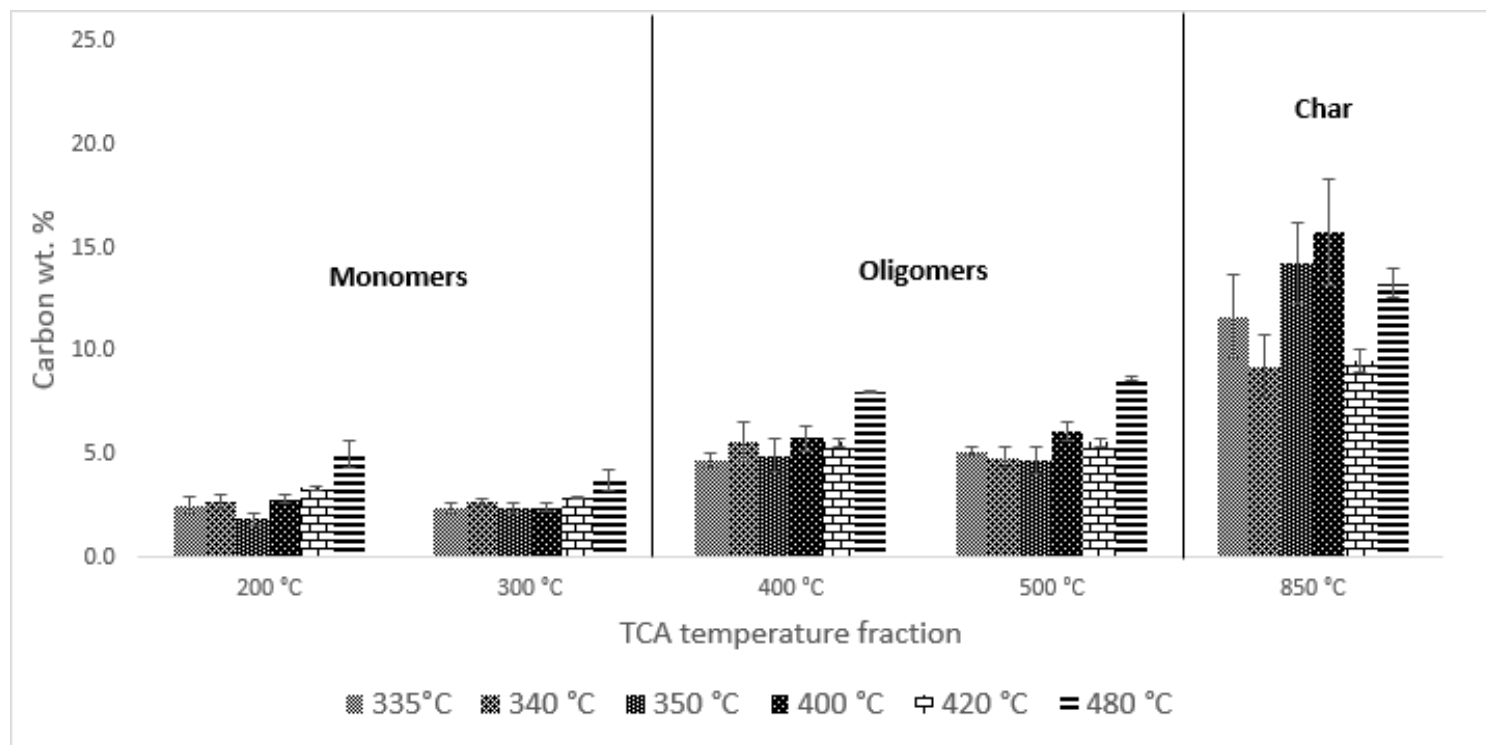


Figure 7. Thermal carbon analysis profiles at six reaction temperatures

Thermal carbon analysis of samples is shown in figure 7. The eluted carbons at 200 and 300 °C are identified as monomers. Oligomers were eluted at 400 and 500 °C. Due to the presence of oxygen at 850 °C, the eluted carbon at this temperature is identified as char. The results indicate that at subcritical conditions, the total eluted carbon in the monomeric fraction is at its maximum at a reaction temperature of 340 °C. On the other hand, the eluted monomers in supercritical condition experiments increased by temperature. This phenomenon suggests that at higher reaction temperatures additional decomposition of C-C bonds will occur, resulting in the formation of a higher concentration of monomers.

In sub critical water conditions, the concentration of monomeric compounds at 340 °C was higher than reaction temperatures of 335 and 350 °C. Even though the experiments temperatures are very close, it appears that somewhere within 340 and 350 °C in subcritical water is the threshold onset of the repolymerization phenomenon. As can be seen in figure 5, the concentration of eluted carbon at 850 °C for reaction temperature of 350 °C is higher than both 335 and 340 °C. This phenomenon is due to the possible cross-linkage of the produced monomers. It should be noted that higher concentration of monomeric compounds were formed in supercritical condition compared to subcritical condition. Since β -O-4 ether bonds have a lower dissociation energy than other C-C bonds in lignin structure [80], it is safe to assume that these bonds will cleave at lower temperature in subcritical water condition. However, at supercritical condition the dissociation of stronger C-C bonds such as α -1 and β -1 will also occur which will result in formation of higher concentration of monomeric compounds.

The results from figure 7 also showed that in supercritical water condition, higher residence time resulted in formation of higher concentration of monomeric compounds with the simultaneous formation of higher molecular weight compounds due to the repolymerization of formed active complexes at elevated temperature.

Table 3 summarizes the organic carbon, the elemental carbon (char), and the total quantified carbon concentration for all samples via thermal carbon analysis. As can be seen, eluted organic carbon concentration is higher at supercritical conditions, which indicates that lignin decomposition to small molecular weight compounds favors higher reaction temperature. In addition, more char (elemental carbon) was eluted from samples collected at supercritical condition, which is due to the significant alkaline condensation of unstable lignin fragments. To explain this phenomena, it should be noted that lignin degradation at elevated temperature will either goes toward formation of gaseous products or active complexes in gaseous phase will bond and repolymerize to form char or other high molecular weight compounds. At subcritical reaction condition, the repolymerization of monomers was not significantly active and, on average, 35 % of the initial lignin was identified as char (Table 3). Moreover, the occurrence of additional gasification processes is highly possible which would result in the formation of a higher concentration of gases. However, for supercritical conditions, the condensation of active complexes resulted in a high concentration of char. Comparing the total eluted carbon in sub- and supercritical condition shows that a higher concentration of gaseous products were formed in subcritical condition while this value reaches to near zero at 480 °C in supercritical condition.

Table 3. Total calculated concentration of recovered products out of initial lignin

	Total organic carbon wt. %	Total elemental carbon wt. %	Total wt. %	Gas wt. %
335 °C	26.4±2.29	31±0.8	57.4±3.3	42.6
340 °C	25.1±2.2	38.9±1.1	64.1±5.2	35.9
350 °C	28.2±3.6	37±1.05	65.2±0.6	34.8
400 °C	32.9±2.3	30.7±1.6	63.6±0.7	36.4
420 °C	26.9±0.8	48.3±1.1	75.2±0.3	24.8
480 °C	38.8±2.5	59.6±0.1	99.1±1.3	0.9

GC/MS analysis results of DCM extracted fraction and reaction feed is presented in figure 8. As can be seen, dissolution of lignin in sodium hydroxide at room temperature resulted in dissociation of weak α -O-4 bonds which resulted in the formation of 0.67 wt.% of guaiacols and less than 0.5 wt. % of guaiacyl carbonyls. The sodium cation will form cation adducts with lignin and polarize the ether bond which results in cleavage of β -O-4 and α -O-4 ether bonds [81]. Since the polarization of base is affected by the state of water and reaction temperature, the polarity of ether bond will increase and results in feasible cleavage of not only β -O-4 and α -O-4 but 4-O-5 bonds.

It should be noted that the GC/MS analysis shows a similar pattern as thermal carbon analysis results. Since BCD is known as a more selective process compared to other lignin degradation processes, temperature and residence time play a critical role in lignin degradation reactions. At 335 to 350 °C, the cleavage of α -O-4, β -O-4 and 4-O-5 will result in formation of hydroxyl groups while dissociation of alkyl bridges such as β -1, β - β and 5-5 take place at 400 to 480 °C .

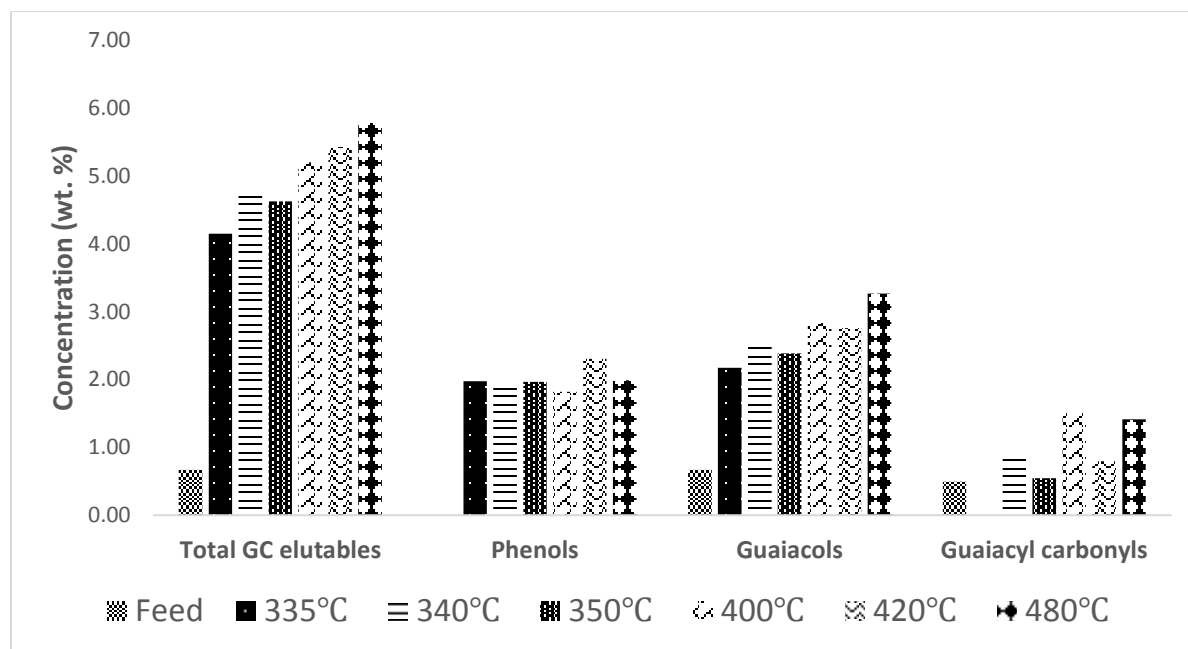


Figure 8. Monomer-rich fraction analysis results in terms of concentration of products per gram of lignin

According to Masaru et al., degradation of lignin in basic media will result in formation of formic acid as well as phenolic compounds [82]. However, these acids can easily repolymerize to form phenolic resins. This phenomenon explains the difference between the TGA carbon content at the 200 and 300 °C stages and GC/MS results since the phenolic resins will not dissolve in DCM and stays in the solid fraction.

TGA results of solid residues are summarized in table 4. Low molecular weight compounds such as monomers are eluted at 25-200 °C. As can be seen, raw lignin and solid samples from 480°C reaction temperature have the lowest monomeric concentration. This observation was expected since with lignin at this temperature range, only α -O-4 bonds will cleave and the density of this type of ether bond is limited. On the other hand, TGA and GC/MS results showed that reaction at 480 °C resulted in formation of the

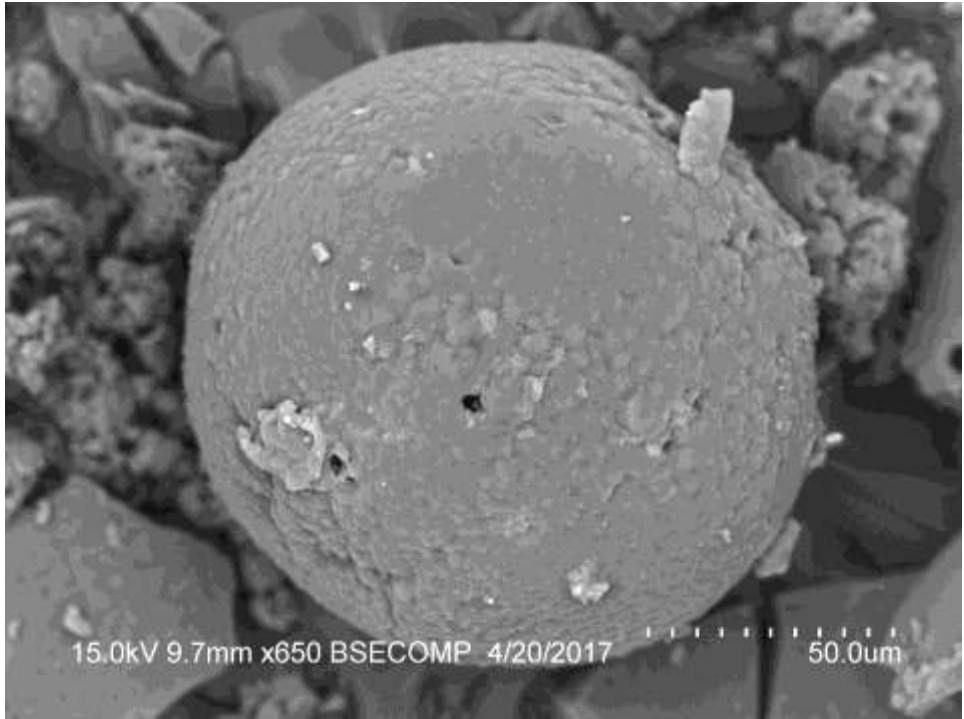
highest concentration of monomeric compounds. Since the monomers were DCM soluble, it is valid to assume that very low monomeric compounds remained in the solid phase. In general, the concentration of eluted monomeric compounds are higher in subcritical condition samples due to the presence of unstable lignin fragments that can readily break at near 200 °C. The same pattern is valid for oligomers that elute at the 200-400 °C thermal step. However, at 600-900 °C, the concentration of high molecular weight compounds are clearly higher at supercritical conditions which further proves that the reactions at supercritical conditions will result in significant alkaline condensation.

Table 4. Mass loss during TG analysis of solid residues

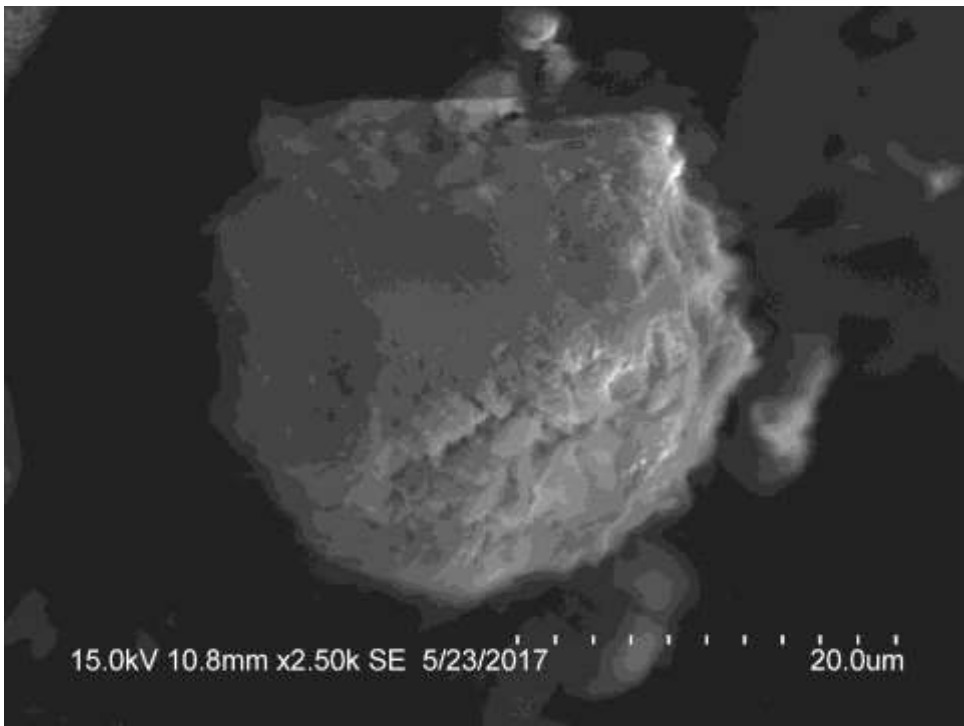
Sample	25-200 °C	200-400 °C	400-600 °C	600-900 °C
Raw lignin	6.3	28.7	19.2	8.8
Reactor feed	16.4	11.5	18.1	20.1
335 °C	15.2	17.8	30	11.1
340 °C	17.5	10.2	21.3	10
350 °C	14.52	8.9	24	20.6
400 °C	11.7	10	17	37.4
420 °C	9.79	10.8	10	23.5
480 °C	6.1	5.9	27	15

SEM analysis of the virgin lignin and NaOH treated lignin is shown in figure 9. Despite the limited reaction through dissolution of lignin in sodium hydroxide solution, the base treated lignin still has near-spherical shape as lignin. This means that the dissolution of lignin did not entirely destruct lignin structure.

Figure 10 shows SEM images of the solid residues collected from selected temperatures at sub- and supercritical conditions. In subcritical water, the reaction goes toward the formation of gases rather than strong repolymerization. Hence, the obtained solid residues are not strongly covered with coke and they have smaller size compared to the solid particles in supercritical water experiments. As can be seen in figure 8a, the size of the solid residues are significantly larger due to the strong repolymerization of active complexes and unstable lignin fraction that were formed during the dealkylation and demethoxylation of lignin at elevated temperature.

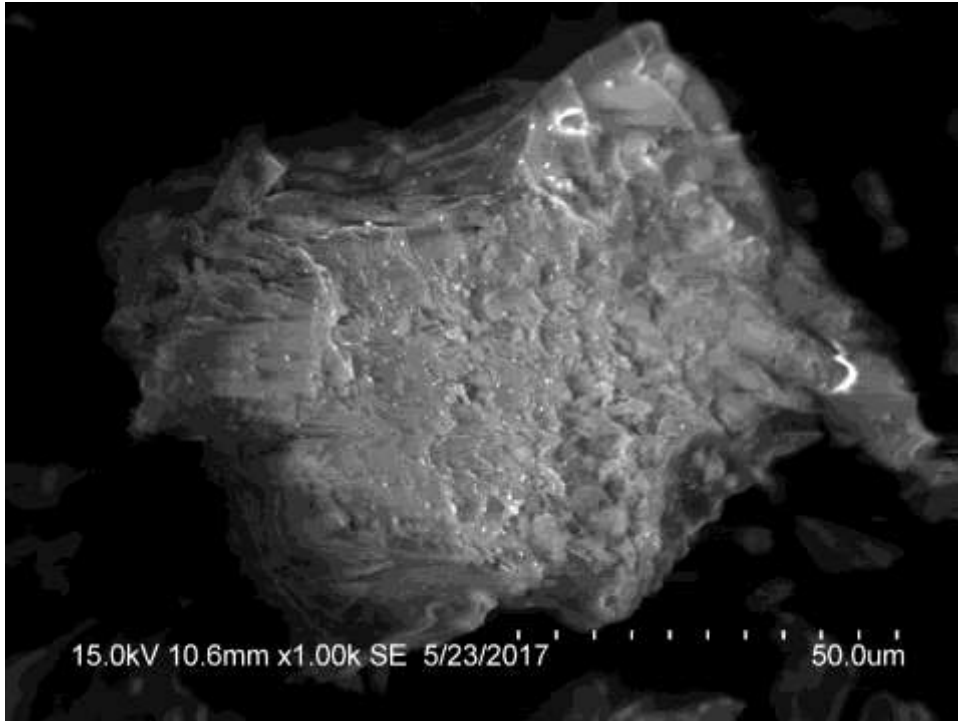


a)

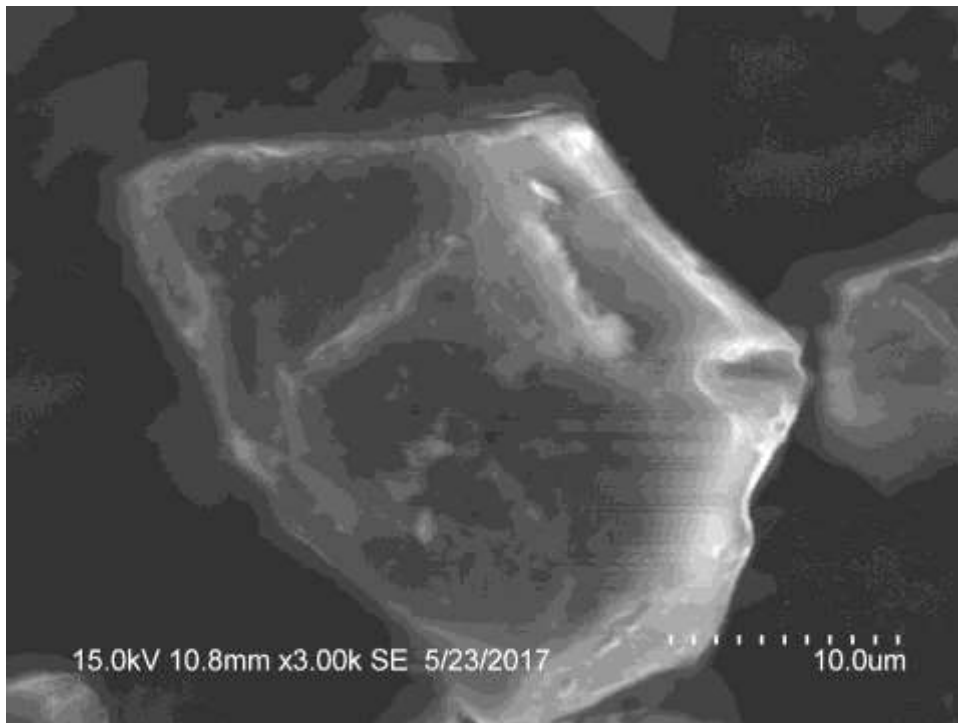


b)

Figure 9. SEM pictures of a) virgin lignin, b) sodium hydroxide treated lignin



a)



b)

Figure 10. SEM pictures of solid sample collected at a) 480 °C, b) 340 °C experimets

3.5. Conclusions

Base-catalyzed degradation of lignin was conducted in a continuous flow reactor. Sodium hydroxide was used as a catalyst to degrade lignin. Reaction temperature and water state was shown to have a significant effect on the hydrothermal degradation of lignin. The results showed that the use of a base catalyst increased the production of monomers at both sub- and supercritical water conditions. However, the polarity of the base in supercritical water played a critical role in facilitating the reaction towards formation of higher concentrations of monomeric compounds as well as char. On the other hand, degradation of lignin in subcritical water produced higher concentration of gas. Under super critical condition, water behaved as a very dense gas where the reaction happens in a single phase media while at subcritical condition both liquid and gas phases co-existed. This special behavior of water at supercritical conditions did not drastically affect the reaction pathway since the obtained monomers from GC/MS analysis remained consistent in both sub-and super critical experiments. However, the nature of the char from sub- and supercritical condition experiments were different due to the formation of highly phenolic char and phenolic resins at supercritical reaction conditions.

CHAPTER IV

CONCLUSIONS AND RECOMMENDATIONS

For the first strategy, we conducted our preliminary studies using commercially available SiO₂-Al₂O₃ and γ -alumina catalyst supports doped with six different metal ions (Fe, Ni, Cu, Mo, Zn, and Li) through a wet impregnation method. XRD analysis was conducted on all prepared catalysts to ensure that the catalyst supports were successfully doped. These experiments suggested that Cu and Mo had the best effect for monomer productions.

Experiments conducted with molybdenum and copper doped catalysts at 300 °C resulted in the formation of 4 and 5 wt % GC-MS elutable compounds, respectively. Design of experiments (DOE) was applied to investigate three experimental and four catalyst preparation related factors. GC-MS analysis results showed that 5 wt % of Cu doped on silica-alumina will result in the highest concentration of guaiacols (2.1 wt %) and guaiacyl acids (3 wt %) which are considered as the precursors for biofuel.

To investigate the effect of temperature on final products, the best conditions from the DOE analysis were tested at 300, 320, and 350 °C. The results from GC-MS analysis of the extracted liquid products and SEM analysis on morphology of the solids showed that at 300 °C, the concentration of monomeric compounds was lower due to the high concentration of unreacted lignin. On the other hand, at 350 °C, the concentration of guaiacols and guaiacyl acids were low due to the strong repolymerization of active complexes and the formation of char. Although repolymerization of active complexes at elevated temperature is inevitable, at 320 °C, the highest concentration of monomeric compounds (6.67 wt %) was obtained with lowest amount of char. However, the produced monomers concentration is too low for industrial purposes.

For the second strategy, a novel 0.01 m diameter by 4 m long tubular flow reactor was designed and built to investigate the base catalyzed decomposition of lignin in sub- and supercritical water. In previous studied experiments, base catalyzed decomposition of lignin was studied in either batch reactors or microscale flow reactors. The novelty of our system is the potential to scale up to industrial scale and the ability to tolerate tar/char formation.

A defined concentration of lignin, sodium hydroxide, and water were properly mixed to make the feed for the reaction. Three reaction temperatures at subcritical and three temperatures at super critical conditions were selected and each experiment was conducted four times.

TCA and GC-MS analysis results showed that the reaction at 340 °C, in the subcritical region yielded the highest concentration of monomeric compounds (with the lowest concentration (6 wt %) of char. Higher concentrations of monomeric compounds (7 wt %) were achieved at supercritical condition while the formation of monomeric compounds and char both increased at increased temperature. GC-MS analysis of the products also showed that the kinetics of the reactions did not change significantly under these conditions. However, the results suggest that the char that was formed at supercritical conditions was more of a phenolic nature than that produced in subcritical water. Neither of the studied conditions resulted in commercially feasible quantities of monomers or oligomers. However, the BCD study appears to have the best promise for future study, which might lead to a feasible reaction system.

APPENDIX A
CATALYST DOPING

Silica-alumina and γ -alumina were chosen as catalyst supports in this work. γ -alumina was received as 1/8" pellets. The pellets were crushed and sieved using mesh size 100. Both catalyst supports were calcined at 600 °C for 5 hours. The weight of each dopant and catalyst support is presented in table 1. The proper weight of dopant and catalyst support were added into a beaker with 150 ml of deionized water. The suspension was kept stirred overnight. The beaker was then placed in a muffle furnace for 12 hours at 120 °C for the water to evaporate. The obtained dried solids were crushed using a mortar and pestle and calcined at 500 °C for 4 hours. It should be noted that for molybdenum doped catalyst one more gram of MoO₃ was added due to the predicted loss of dopant at calcination step.

Table 1. Catalyst support and dopants weight and types used to prepare the studied catalysts

Catalyst	Dopant type	Dopant weight (g)	Doped metal ion weight (g)	Catalyst support type	Catalyst support weight (g)
5 wt.% Cu in SiO ₂ /Al ₂ O ₃	Cu(NO ₃) ₂	1.55	0.526	SiO ₂ /Al ₂ O ₃	10
10 wt.% Cu in SiO ₂ /Al ₂ O ₃	Cu(NO ₃) ₂	3.27	1.11	SiO ₂ /Al ₂ O ₃	10
5 wt.% Cu in γ -alumina	Cu(NO ₃) ₂	1.55	0.526	γ -alumina	10
10 wt.% Cu in γ -alumina	Cu(NO ₃) ₂	3.27	1.11	γ -alumina	10
5 wt.% Mo in SiO ₂ /Al ₂ O ₃	MoO ₃	1.78	0.526	SiO ₂ /Al ₂ O ₃	10
10 wt.% Mo in SiO ₂ /Al ₂ O ₃	MoO ₃	2.66	1.11	SiO ₂ /Al ₂ O ₃	10
5 wt.% Mo in γ -alumina	MoO ₃	1.78	0.526	γ -alumina	10
10 wt.% Mo in γ -alumina	MoO ₃	2.66	1.11	γ -alumina	10

APPENDIX B

BATCH EXPERIMENT SETUP

Prior to each experiment, the reaction vessel, stirrer, and cooling water coil were washed with isopropanol and rinsed with DI water in order to remove the residues from previous experiments. Depending on the experiment, a defined amount of catalyst, lignin, and water were weighed and mixed in a beaker. The beaker was covered with parafilm and placed in a sonicator for 30 minutes. Since lignin quickly precipitates in the beaker, the suspension was mixed by a spatula and poured into the reaction vessel without delay. In order to completely seal the reaction vessel and to protect the high pressure gasket from sticking to the vessel, a thin layer of vacuum grease was applied to the reaction vessel lip.

The reaction vessel was then connected to the rest of the Parr reactor. Both halves of the reactor vessel clamp were aligned and the safety clasps were connected to hold the reactor in place. A torque wrench set at 30 foot-pounds was used to tighten eight bolts that seal the vessel.

In order to remove atmospheric gases, the sealed vessel was pressurized with 2 MPa of nitrogen gas. Afterwards, the vent valve was opened to purge the gas. This procedure was repeated three times to make sure that the reaction vessel was properly purged. After purging, the reaction vessel was charged with nitrogen to 2 MPa and all the valves were tightly closed.

Depending on the experiment, the stirrer rate and reaction temperature was set at their specified values and the heating rate on the reactor controller for all experiments was set at 1 °C/s. The reaction temperature was maintained with ± 1 °C tolerance. The reaction time is defined as the time elapsed after the temperature reaches its setpoint. For example, 30 minutes reaction time at 300 °C reaction temperature means that 30 minutes should elapse after the reaction temperature reaches 300 °C.

When the reaction time was completed, the heater was turned off and lowered, the cooling water valves were opened, and a fan was placed under the reaction vessel to expedite the cooling-down step. After the reactor cooled down to room temperature, the gas vent was opened and the reaction mixture pressure reduced to atmospheric pressure by venting the gas from the reactor.

The bolts on the seal clamp were loosened in the same order as they were tightened. The clamps were removed and the reaction vessel was lowered. To collect all the char formed during the experiments, the solid residues on the stirrer shaft and cooling water coil were scraped off and added to the reaction mixture. The reaction mixture was poured through a filter paper and filtered using a vacuum pump. The filtered liquid was collected and weighed and stored in a refrigerator. The solid residues on the filter paper were dried and stored in sealed jars for future analysis.

APPENDIX C

GC-MS ANALYSIS

In order to analyze the stored aqueous products from batch reactor experiments with GC/MS, 1 ml aliquot of the sample was transferred to a 4 ml vial. 50 μ l of recovery standard, which was a solution of 10,000 ppm of 4-chloroacetophenone in DCM, was added and the pH of the obtained solution was measured and maintained at 4 with 10 μ l of acetic acid.

1 ml of DCM was added to the vial and vortexed for 1 minute. After the organic DCM and water phases separated, the DCM phase was collected from the bottom of the vial and transferred to a 7 ml test tube. This step was repeated two more times. Therefore, at the end of this step, around 3 ml of DCM phase should have been collected. 75 μ l of internal standard, which was a solution of 10,000 ppm of O-terphenyl in DCM, was added to the collected DCM samples. 1.5 ml of the final sample was transferred to an autosampler vial for GC/MS analysis.

To analyze the basic liquid samples collected from the continuous flow reactor, each sample was treated with \sim 1.7 ml (depending on the pH of the sample) of one molar hydrochloric acid. The samples were then vortexed and placed in a hot water bath for an hour to expedite the precipitation of solids. The sample was filtered using a filter paper and the liquid sample was collected and stored in the refrigerator. To analyze the aqueous sample in GC/MS, the above mentioned method was used for 1ml aliquot of the sample. The collected solid residues were analyzed using TGA and SEM.

A Calibration solution prepared in UND analytical chemistry was used. The stock mixtures for this solution are presented in table 2. 20 μ l of each mixture was transferred in to a vial where 100 μ l of recovery standard and 1.8 ml of DCM were added to reach final volume of \sim 2 ml. 400 μ l of this solution was transferred into an autosampler vial and was identified as calibration "A" with the highest concentration of analytes. 200 μ l of calibration "A" solution

was transferred to a vial and diluted with 400 μ l of DCM and the obtained solution was identified as calibration solution "B". This stepwise dilution process was repeated six more times, resulted in calibration solutions "C", "D", "E", "F", "G", and "H".

All the sample and calibration vials were placed on the 7673 HP automatic liquid sampler tray. The run order was started with the injection of neat DCM followed by three runs of a test mix. The test mix injection insured that the detector's measurements were accurate and repeatable. After injection of another neat DCM to flush the remained analytes, eight calibration runs were completed starting with the most diluted calibration solution. Then the reactor samples were injected with along a DCM blank after every three or four injections. After injection of all the samples, the sequence was ended with triplicate injection of the test mix and neat DCM.

Table 2. Analyte mixtures used to prepare calibration stock solution

	weight of flask	Total volume	weight, standard	weight, analyte	Final concentration
	g	ml	g	g	mg/ml
MIX I; HB52-1 C	10.11504				
Phenol			0.53312	0.52965	105.9
Guaiacol			0.59251	0.58658	117.3
Syringol			0.52465	0.51940	103.9
Eugenol			0.53721	0.53184	106.4
Mequinol			0.53392	0.52858	105.7
Methyl guaiacol			0.54669	0.53576	107.2
4-Propyl guaiacol			0.53232	0.52700	105.4
4-Ethylguaiacol			0.5099	0.49970	99.9
DCM			2.934		586.8
		5			
MIX II; HB46-02 D	9.92691				
Vanillin			0.5022	0.49718	99.4
Acetovanillone			0.58239	0.57074	114.1
Syringaldehyde			0.49267	0.48282	96.6
DCM			6.20899		1241.8
		5			
MIX III; HB59-09 A	9.9757				
Vanillic acid			0.09684	0.0939	18.8
Homovanillic acid			0.10088	0.0989	19.8
acetone			3.84698		769.4
		5			
MIX IV; HB46-04 C	9.94188				
bicreosol			0.20513	0.20513	41.0
TD-14			0.07963	0.07963	15.9
DMSO			6.19147		1238.3
		5			
MIX V; HB60-01 A					
methylphenol			0.51031	0.50521	102.1
ethylphenol			0.5809	0.56347	116.2
propylphenol			0.53317	0.52784	106.6
isoeugenol			0.55583	0.54972	111.2
vinylguaiacol			0.60877	0.59659	121.8
homovanillyl alcohol			0.47115	0.46644	94.2
DCM					
		5			

APPENDIX D

ADDITIONAL CATALYTIC EXPERIMENTAL DATA IN BATCH REACTOR

The investigated factors introduced in chapter 2 were selected and their values were bounded through a stepwise DOE plan, which was as follows:

1. Investigation of lignin-to-water ratio at reaction temperature of 300 °C without using a catalyst
2. Investigation of catalyst-to-lignin ratio and catalyst support type based on the best result obtained from previous step using activated SiO₂-Al₂O₃ and γ -alumina as catalyst supports
3. Investigation of catalyst dopant type based on the best obtained condition from previous steps using SiO₂-Al₂O₃ and γ -alumina as catalyst supports doped with Fe, Ni, Zn, Cu, and Mo.

Table 3. Analyte target ions and retention time

Analyte	Retention time	Target ion (1)	Target ion (2)	Target ion (3)
Phenol	4.725	94	66	65
Methylphenol	5.203	108	107	79
Guaiacol	5.217	109	81	124
Ethylphenol	5.71	107	122	77
Methylguaiacol	5.841	123	138	95
Mequinol	6.07	109	124	81
RS	6.116	139	111	75
Propylphenol	6.232	107	136	77
Ethylguaiacol	6.334	137	152	15
Vinylguaiacol	6.537	135	150	107
Syringol	6.783	154	139	93
Eugenol	7.015	164	77	149
Propylguaiacol	6.841	137	166	122
Vanillin	7.116	151	152	81
Acetovanillone	7.537	151	166	123
Homovanillyl alcohol	7.754	137	168	122
Homovanillic acid	8.3	137	182	122
Syringaldehyde	8.34	182	181	111
o-Terphenyl	9.29	230.05	229.05	215
bicreosol	11.16	274	241	227
TD-14	11.97	272	273	211

Table 4. GC/MS analysis sequence for the first step of preliminary results

	Line Type	Vial	DataFile	Method	Sample Name
1)	Blank	1	01BLANK	TMIX_SS4	DCM
2)	Blank	1	02BLANK	TMIX_SS4	DCM
3)	Sample	2	03TMIX	TMIX_SS4	TMIX_low
4)	Sample	2	04TMIX	TMIX_SS4	TMIX
5)	Sample	2	05TMIX	TMIX_SS4	TMIX
6)	Blank	1	06BLANK	HB-L02	DCM
7)	Sample	3	07CAL-G	HB-L02	CAL_G
8)	Sample	4	08CAL-F	HB-L02	CAL_F
9)	Sample	5	09CAL-E	HB-L02	CAL_E
10)	Sample	6	10CAL-D	HB-L02	CAL_D
11)	Sample	7	11CAL-C	HB-L02	CAL_C
12)	Sample	8	12CAL-B	HB-L02	CAL_FB
13)	Sample	9	13CAL-A	HB-L02	CAL_A
14)	Blank	1	14BLANK	HB-L02	DCM
15)	Sample	10	15SP83	HB-L02	SP-83-2015
16)	Sample	11	16SP85	HB-L02	SP-85-2015
17)	Sample	12	17SP86	HB-L02	SP-86-2015
18)	Sample	13	18SP87	HB-L02	SP-87-2015
19)	Sample	14	19SP88	HB-L02	SP-88-2015
20)	Blank	1	20BLANK	HB-L02	DCM
21)	Sample	15	21SP89	HB-L02	SP-89-2015
22)	Sample	16	22SP90	HB-L02	SP-90-2015
23)	Sample	17	23SP91	HB-L02	SP-91-2015
24)	Sample	6	24CAL-D	HB-L02	CAL_D
25)	Sample	18	25SP92	HB-L02	SP-92-2015
26)	Sample	19	26SP93	HB-L02	SP-93-2015
27)	Blank	1	27BLANK	HB-L02	DCM
28)	Sample	20	28SP94	HB-L02	SP-94-2015
29)	Sample	21	29SP95	HB-L02	SP-95-2015
30)	Sample	22	30SP96	HB-L02	SP-96-2015

31)	Sample	23	31SP97	HB-L02	SP-97-2015
32)	Blank	1	32BLANK	HB-L02	DCM
33)	Sample	24	32SP98	HB-L02	SP-98-2015
34)	Sample	25	33SP99	HB-L02	SP-99-2015
35)	Sample	26	34SP100	HB-L02	SP-100-2015
36)	Sample	27	35SP101	HB-L02	SP-101-2015
37)	Blank	1	36BLANK	HB-L02	DCM
38)	Sample	3	37CAL-G	HB-L02	CAL_G
39)	Sample	4	38CALF	HB-L02	CAL_F
40)	Sample	5	39CALE	HB-L02	CAL_E
41)	Sample	6	40CALD	HB-L02	CAL_D
42)	Sample	7	41CALC	HB-L02	CAL_C
43)	Sample	8	42CALB	HB-L02	CAL_B
44)	Sample	9	43CALA	HB-L02	CAL_A
45)	Blank	1	44BLANK	HB-L02	DCM
46)	Sample	2	45TMIX	TMIX_SS4	TMIX_low
47)	Sample	2	46TMIX	TMIX_SS4	TMIX_low
48)	Sample	2	47TMIX	TMIX_SS4	TMIX_low
49)	Blank	1	48BLANK	TMIX_SS4	DCM

Table 5. GC-MS analysis results of the first step of preliminary study

Samples	Lignin(g)	Water(ml)	guaiacols	guaiacyl carbonyls	guaiacyl dimers	guaiacyl acids	other	SUM
SP-83-2015	5	100	2.25	0.16	0.03	0.28	0.16	3.18
SP-85-2015	5	200	2.13	0.45	0.04	0.42	0.11	3.80
SP-86-2015	5	300	2.86	0.63	0.07	0.58	0.14	5.58
SP-87-2015	10	100	2.09	0.10	0.01	0.23	0.15	2.81
SP-88-2015	10	200	2.23	0.33	0.03	0.34	0.13	3.50
SP-89-2015	10	300	2.64	0.38	0.04	0.38	0.13	4.10
SP-90-2015	20	100	1.33	0.02	0.00	0.12	0.13	1.72
SP-91-2015	20	200	1.71	0.09	0.01	0.22	0.12	2.30
SP-92-2015	20	300	1.92	0.26	0.03	0.32	0.12	2.97
SP-93-2015	5	100	3.26	0.22	0.04	0.40	0.22	4.61
SP-94-2015	5	200	3.49	0.53	0.06	0.47	0.18	5.74
SP-95-2015	5	300	3.02	0.75	0.07	0.59	0.14	6.08
SP-96-2015	10	100	2.19	0.10	0.02	0.24	0.17	2.95
SP-97-2015	10	200	2.32	0.31	0.03	0.34	0.14	3.58
SP-98-2015	10	300	1.96	0.35	0.04	0.37	0.11	3.29
SP-99-2015	20	100	1.34	0.03	0.00	0.14	0.13	1.75
SP-100-2015	20	200	2.14	0.13	0.01	0.23	0.14	2.89
SP-101-2015	20	300	2.34	0.25	0.03	0.30	0.13	3.38

Table 6. GC/MS analysis sequence for the second step of preliminary results

	Line Type	Vial	Data File	Method	Sample Name
1)	Blank	1	01BLANK	TMIX_SS5	Blank
2)	Sample	2	02TMIX	TMIX_SS5	Test
3)	Sample	2	03TMIX	TMIX_SS5	Test
4)	Sample	2	04TMIX	TMIX_SS5	Test
5)	Blank	1	05BLANK	TMIX_SS5	Blank
6)	Sample	3	06JK3308	HB-L02	Cal G
7)	Sample	4	07JK3307	HB-L02	Cal F
8)	Sample	5	08JK3306	HB-L02	Cal E
9)	Sample	6	09JK3305	HB-L02	Cal D
10)	Sample	7	10JK3304	HB-L02	Cal C
11)	Sample	8	11JK3303	HB-L02	Cal B
12)	Sample	9	12JK3302	HB-L02	Cal A
13)	Blank	1	13BLANK	HB-L02	Blank
14)	Sample	10	14JK3002	HB-L02	SP103
15)	Sample	11	15JK3003	HB-L02	SP104
16)	Sample	12	16JK3004	HB-L02	SP105
17)	Sample	13	17JK3006	HB-L02	SP106
18)	Blank	1	18BLANK	HB-L02	DCM
19)	Sample	14	19JK3008	HB-L02	SP107
20)	Sample	15	20JK3009	HB-L02	SP108
21)	Sample	16	21JK3010	HB-L02	SP109
22)	Sample	17	22JK3012	HB-L02	SP110
23)	Blank	1	23BLANK	HB-L02	Blank
24)	Sample	18	24JK3101	HB-L02	SP111
25)	Sample	19	25JK3102	HB-L02	SP112
26)	Sample	20	26JK3103	HB-L02	SP113
27)	Sample	21	27JK3104	HB-L02	SP114
28)	Blank	1	28BLANK	HB-L02	Blank
29)	Sample	22	29JK3104	HB-L02	SP115
30)	Sample	23	30JK3105	HB-L02	SP116

31)	Sample	24	31JK3106	HB-L02	SP117
32)	Sample	25	32JK3107	HB-L02	SP118
33)	Blank	1	33BLANK	HB-L02	Blank
34)	Sample	3	34JK3308	HB-L02	Cal G
35)	Sample	4	35JK3307	HB-L02	Cal F
36)	Sample	5	36JK3306	HB-L02	Cal E
37)	Sample	6	37JK3305	HB-L02	Cal D
38)	Sample	7	38JK3304	HB-L02	Cal C
Table 6 (continued)					
39)	Sample	8	39JK3303	HB-L02	Cal B
40)	Sample	9	40JK3302	HB-L02	Cal A
41)	Blank	1	41BLANK	HB-L02	Blank
42)	Sample	2	42TMIX	TMIX_SS5	Test
43)	Sample	2	43TMIX	TMIX_SS5	Test
44)	Sample	2	44TMIX	TMIX_SS5	Test
45)	Blank	1	45BLANK	HB-L02	Blank

Table 7. GC-MS analysis results of the second step of preliminary study

Sample Name	Catalyst Type	Catalyst weight (g)	guaiacols	guaiacyl carbonyls	guaiacyl dimers	guaiacyl acids	other	SUM
SP103	SiO ₂ /Al ₂ O ₃	0.5	3.97	0.70	0.07	0.44	0.16	6.73
SP104	SiO ₂ /Al ₂ O ₃	2	3.56	0.80	0.09	0.44	0.11	6.56
SP105	SiO ₂ /Al ₂ O ₃	3.5	3.29	0.83	0.09	0.45	0.10	6.28
SP106	SiO ₂ /Al ₂ O ₃	5	2.70	0.86	0.08	0.42	0.07	5.26
SP107	Al ₂ O ₃	0.5	3.20	0.68	0.06	0.38	0.11	5.71
SP108	Al ₂ O ₃	2	2.89	0.68	0.06	0.38	0.10	5.20
SP109	Al ₂ O ₃	3.5	2.68	0.63	0.07	0.36	0.10	4.88
SP110	Al ₂ O ₃	5	2.61	0.50	0.04	0.36	0.07	4.75
SP111	SiO ₂ /Al ₂ O ₃	0.5	2.13	0.49	0.05	0.35	0.08	3.65
SP112	SiO ₂ /Al ₂ O ₃	2	2.65	0.87	0.07	0.38	0.07	5.13
SP113	SiO ₂ /Al ₂ O ₃	3.5	2.63	0.90	0.05	0.43	0.07	5.37
SP114	SiO ₂ /Al ₂ O ₃	5	2.50	0.90	0.05	0.42	0.06	5.07
SP115	Al ₂ O ₃	0.5	2.78	0.83	0.05	0.38	0.09	5.23
SP116	Al ₂ O ₃	2	2.80	0.83	0.07	0.40	0.10	5.31
SP117	Al ₂ O ₃	3.5	4.27	0.90	0.06	0.50	0.15	7.70
SP118	Al ₂ O ₃	5	4.52	0.77	0.06	0.48	0.20	7.80

Table 8. GC-MS analysis results of the third step of preliminary study

Sample name	Dopant type & concentration	Catalyst support type	guaiacols	guaiacyl carbonyls	guaiacyl dimers	guaiacyl acids	other	SUM
SP127	5% Fe	Al ₂ O ₃	0.88	1.42	0.00	3.08	2.46	7.85
SP128	5% Ni	SiO ₂ /Al ₂ O ₃	2.18	1.86	0.00	3.55	3.64	11.23
SP129	20% Fe	SiO ₂ /Al ₂ O ₃	0.70	1.13	0.00	3.87	3.37	9.08
SP130	5% Cu	SiO ₂ /Al ₂ O ₃	2.18	2.27	0.00	4.76	4.04	13.24
SP131	20% Mo	SiO ₂ /Al ₂ O ₃	1.32	1.54	0.00	4.12	3.10	10.09
SP132	20% Ni	SiO ₂ /Al ₂ O ₃	2.24	2.13	0.00	4.83	3.87	13.07
SP133	5% Mo	SiO ₂ /Al ₂ O ₃	2.18	1.66	0.00	3.78	4.50	12.13
SP 134	20% Mo	Al ₂ O ₃	1.56	2.32	0.00	4.23	5.05	13.16
SP 135	5% Cu	Al ₂ O ₃	2.42	2.93	0.00	5.51	4.38	15.24
SP 136	5% Zn	SiO ₂ /Al ₂ O ₃	2.31	1.52	0.00	3.98	2.40	10.20
SP 137	5% Ni	Al ₂ O ₃	1.20	1.40	0.00	2.67	2.40	7.67
SP 138	20% Cu	SiO ₂ /Al ₂ O ₃	0.47	1.66	0.00	2.85	1.91	6.89
SP 139	20%Fe	Al ₂ O ₃	0.88	1.42	0.00	3.08	2.46	7.85
SP 140	20% Zn	SiO ₂ /Al ₂ O ₃	1.25	1.90	0.00	3.45	2.90	9.50
SP 141	20% Zn	Al ₂ O ₃	0.99	1.31	0.00	2.48	2.40	7.19
SP 142	20% Ni	Al ₂ O ₃	0.38	1.62	0.00	3.14	3.17	8.31
SP 143	5% Mo	Al ₂ O ₃	0.58	1.79	0.00	3.53	2.25	8.15
SP 144	5% Fe	SiO ₂ /Al ₂ O ₃	0.67	1.42	0.00	3.97	2.09	8.14
SP 145	5% Zn	Al ₂ O ₃	0.65	1.72	0.00	5.12	3.95	11.44
SP 146	20% Cu	Al ₂ O ₃	0.46	1.86	0.00	3.45	2.67	8.45

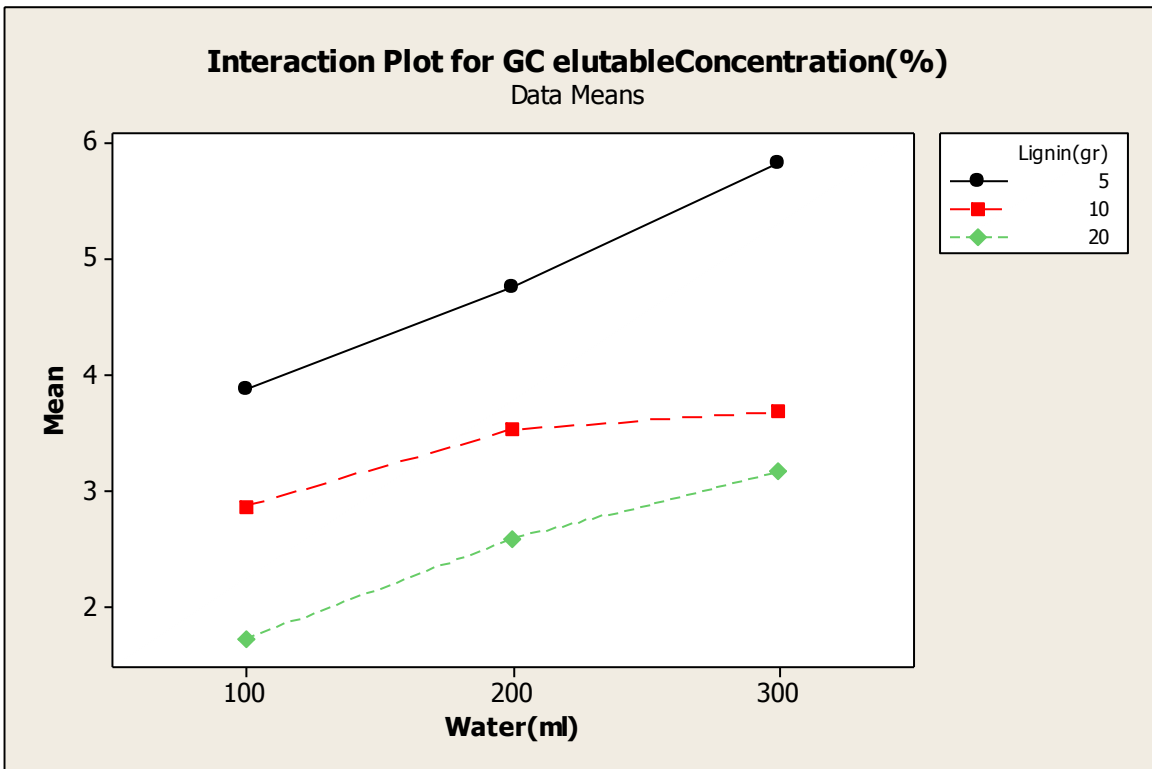
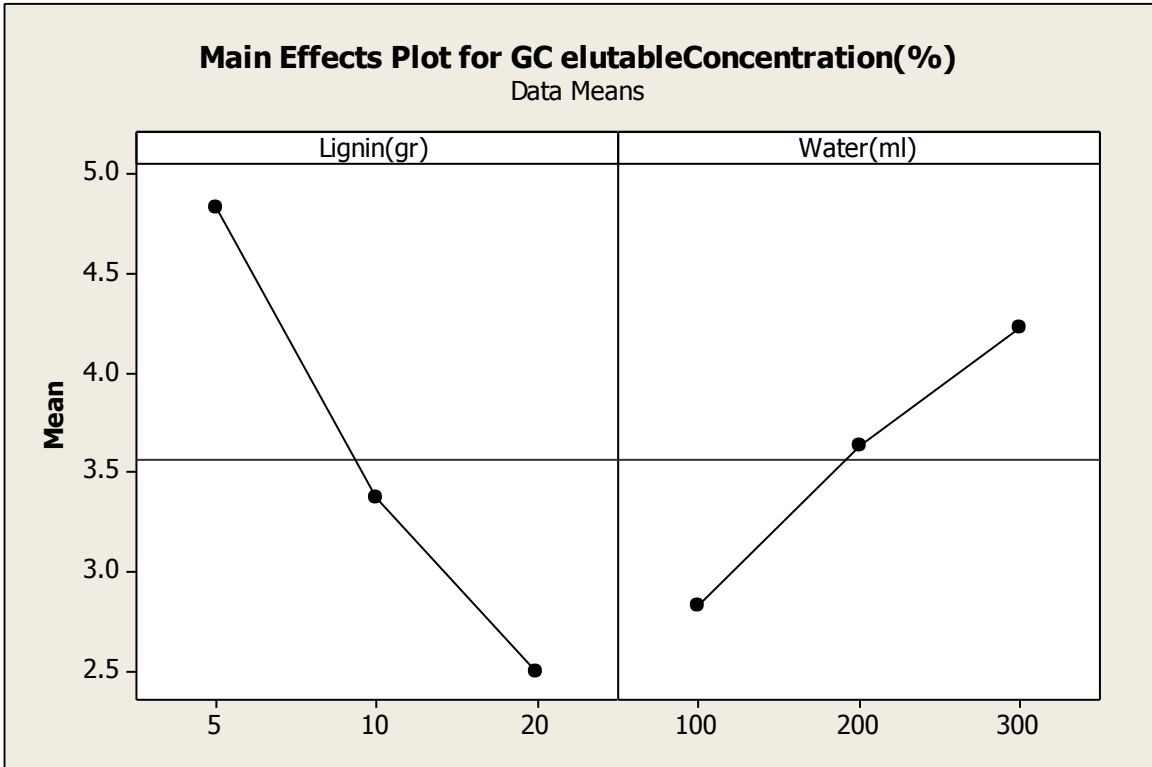
APPENDIX E:

MINITAB PLOTS

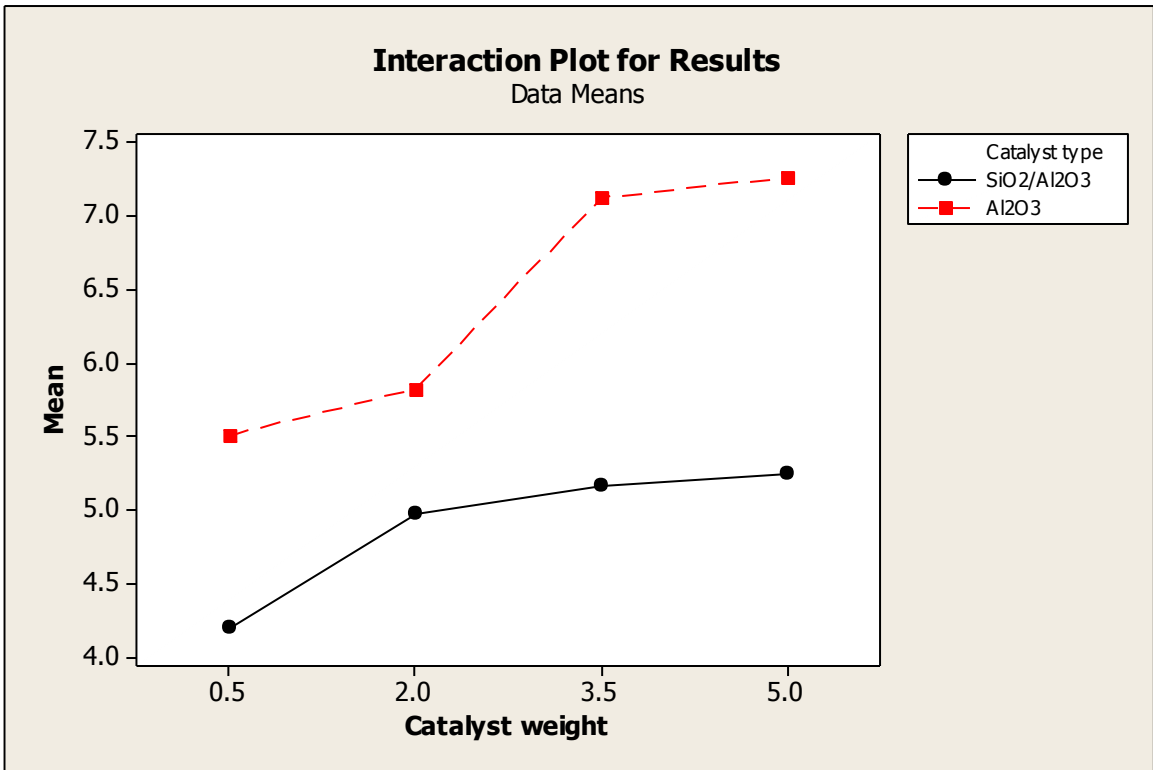
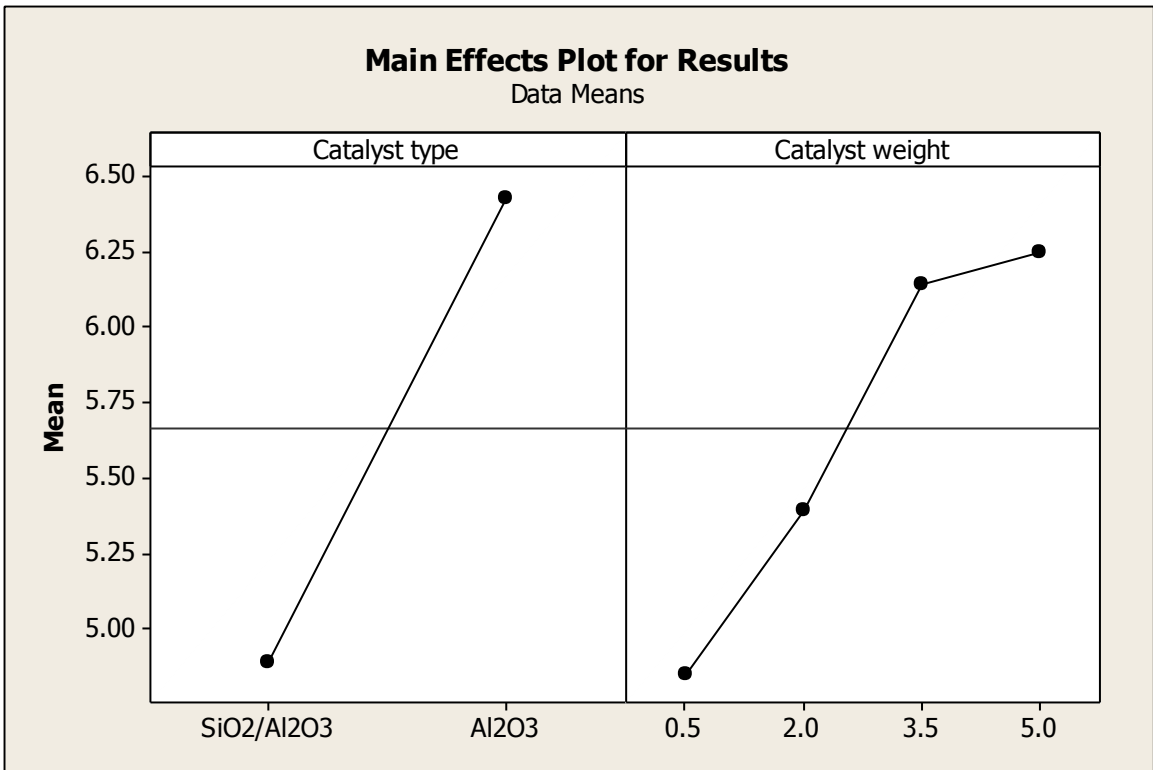
Pareto charts was used to graphically summarize and display the relative importance of the differences between groups of data. Main effect plots were used to examine differences between level means for one or more factors. There is a main effect when different levels of a factor affect the response differently. A main effects plot graphs the response mean for each factor level connected by a line. The normal probability plot is a graphical technique for assessing whether or not a data set is approximately normally distributed.

Pareto charts, main effect, and normal probability plots are individually labeled with chart title and respective target compound.

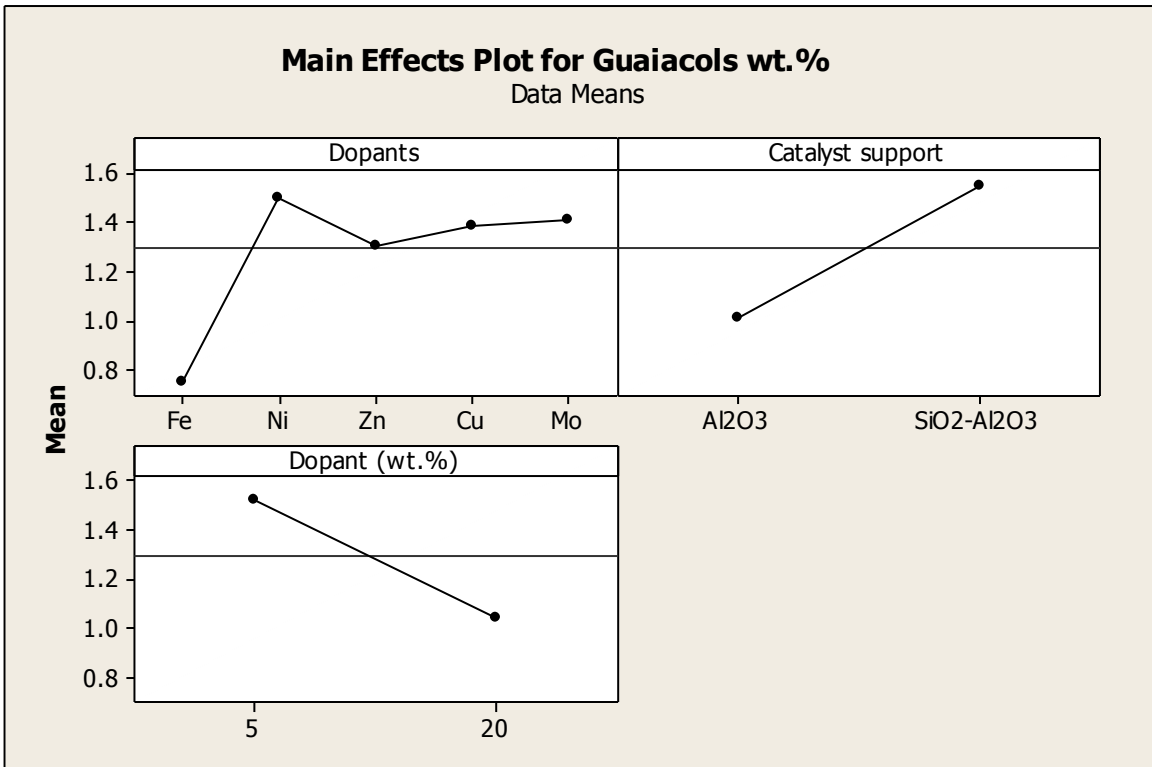
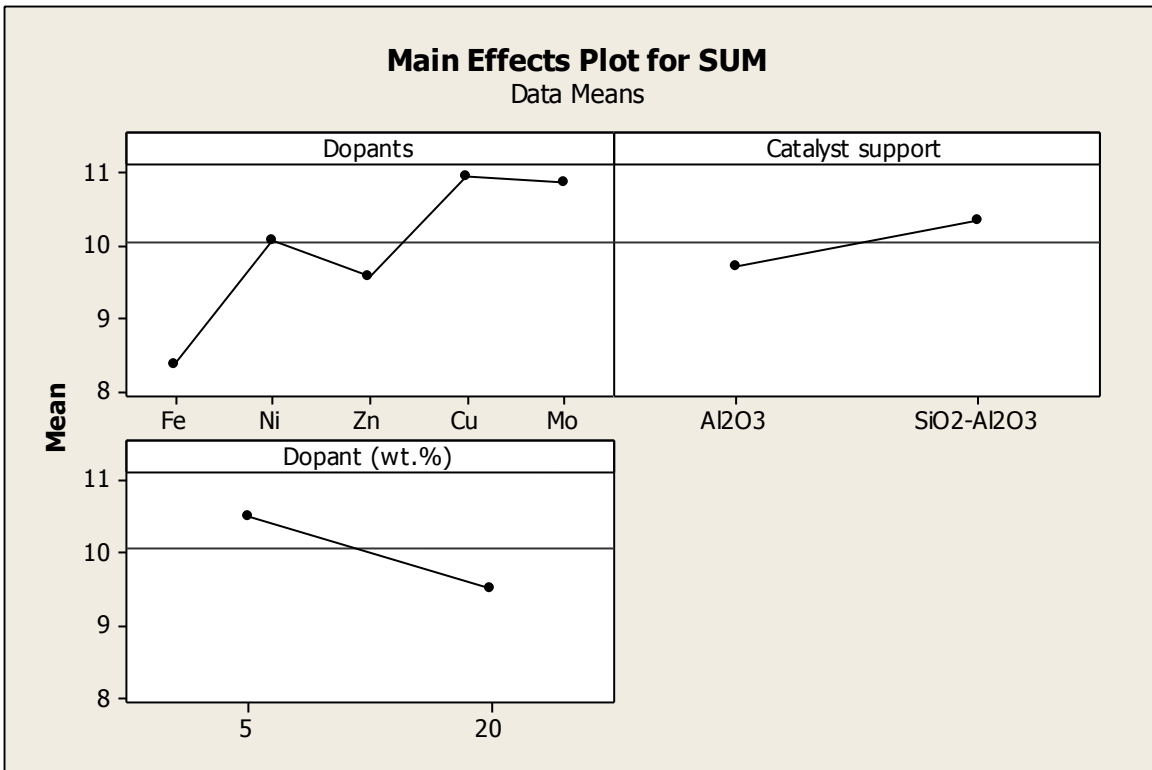
FIRST STEP OF PRELIMINARY EXPERIMENTS RESULTS



SECOND STEP OF PRELIMINARY EXPERIMENTS RESULTS

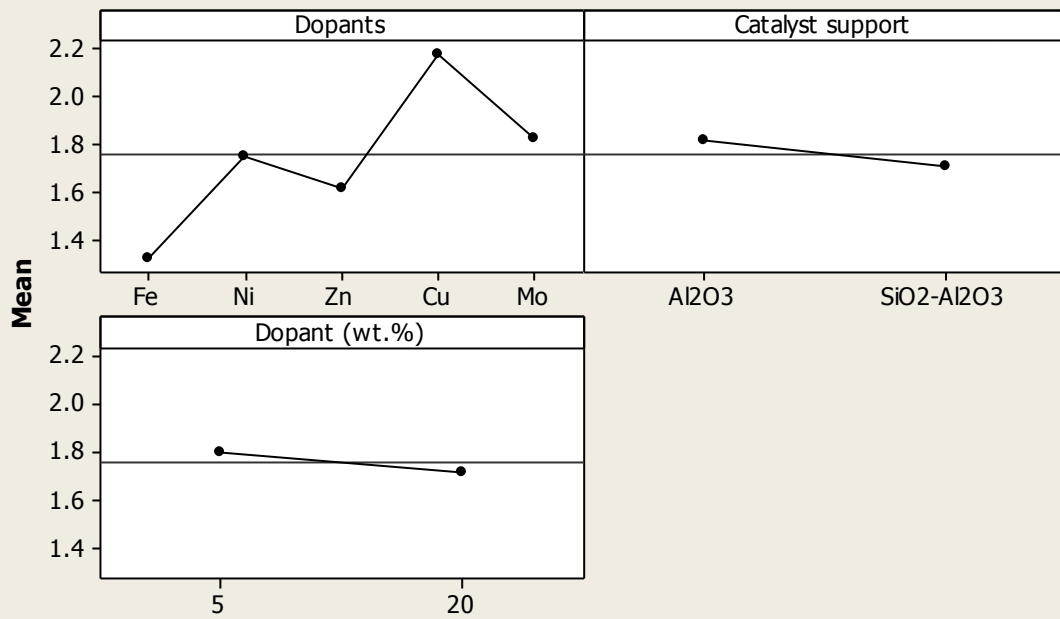


THIRD STEP OF PRELIMINARY EXPERIMENTS RESULTS



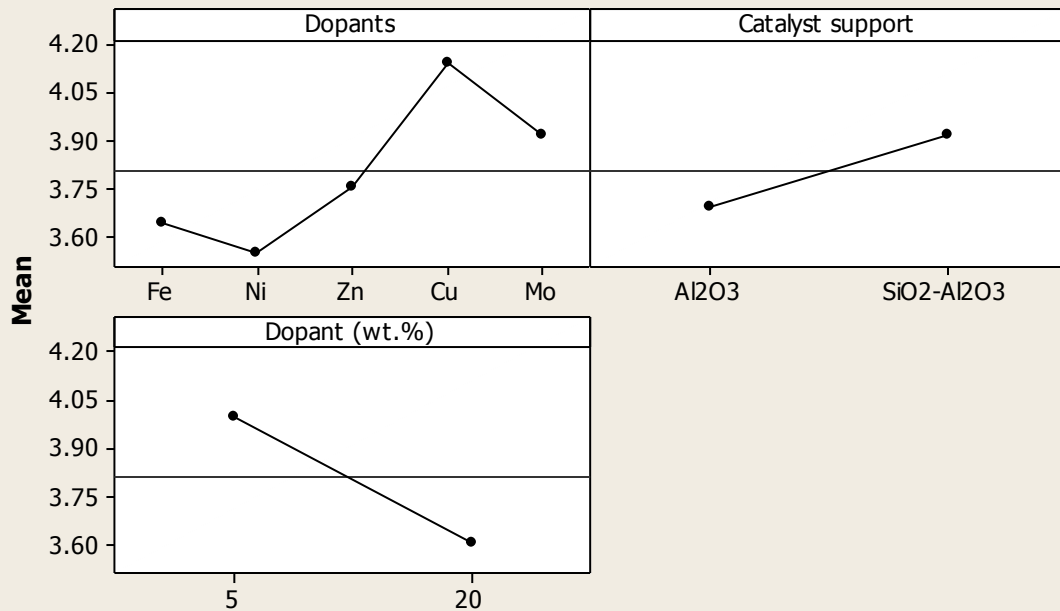
Main Effects Plot for Guaiacyl carbonyls wt.%

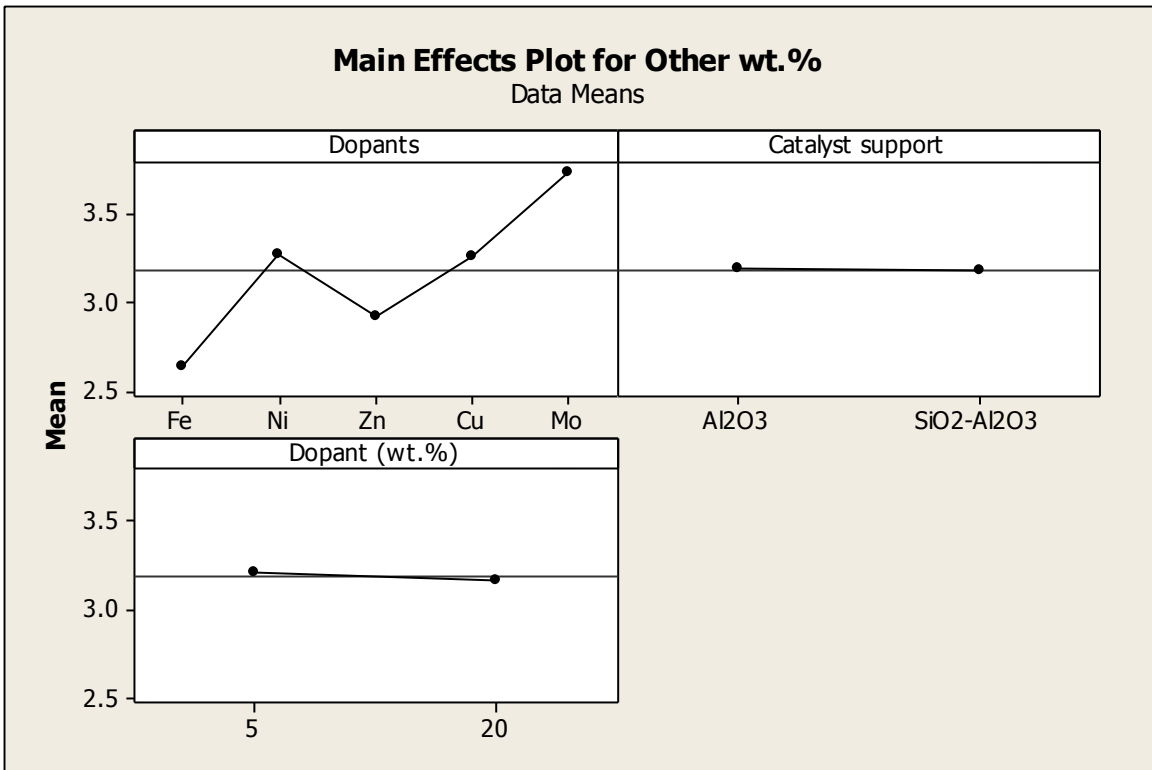
Data Means



Main Effects Plot for Guaiacyl acids wt.%

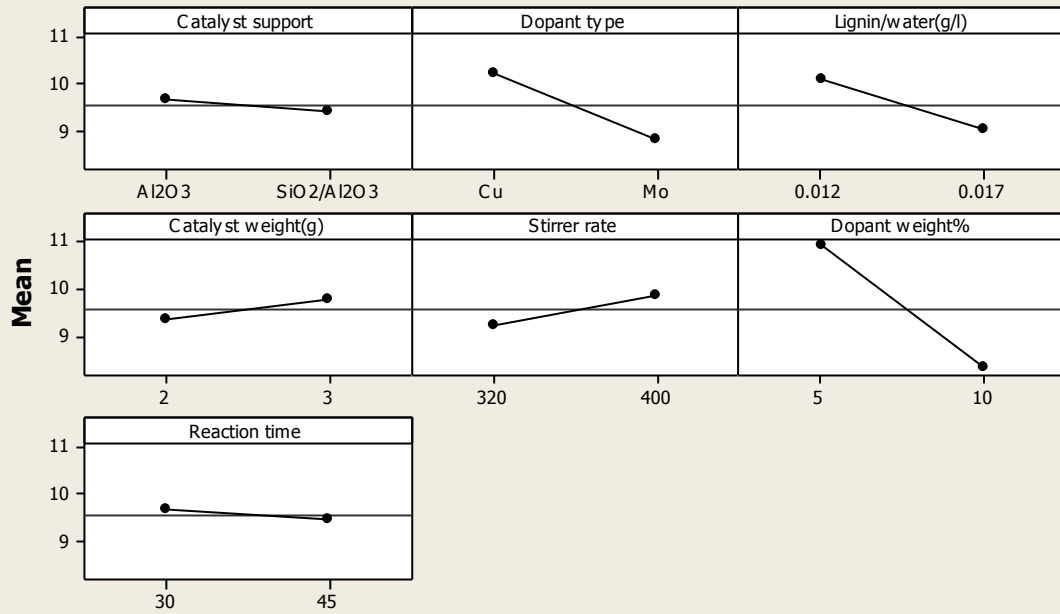
Data Means



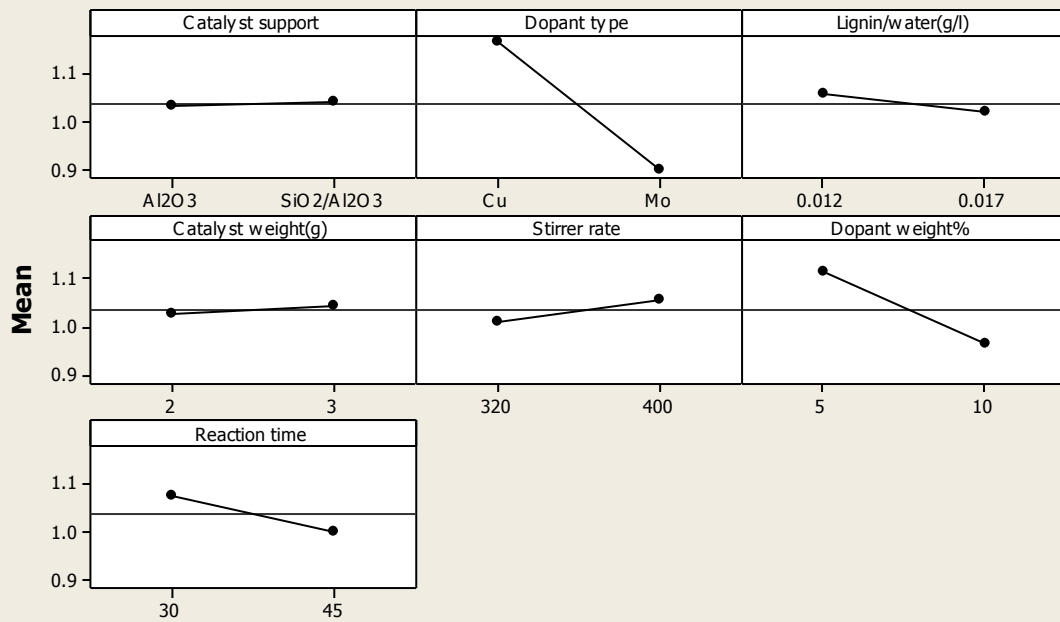


FINAL SET OF EXPERIMENTS RESULTS

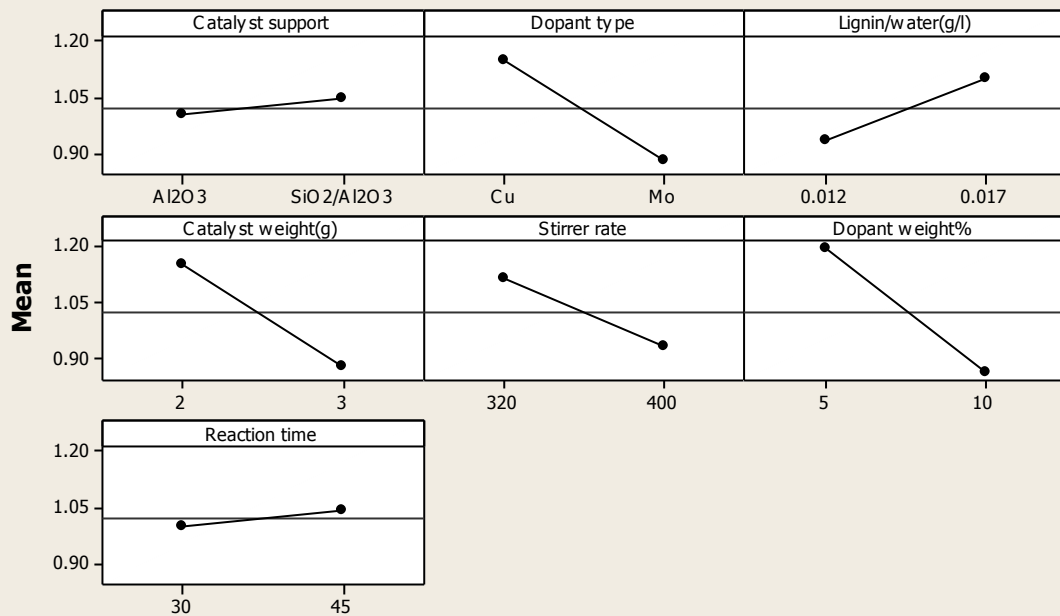
Main Effects Plot for SUM Data Means



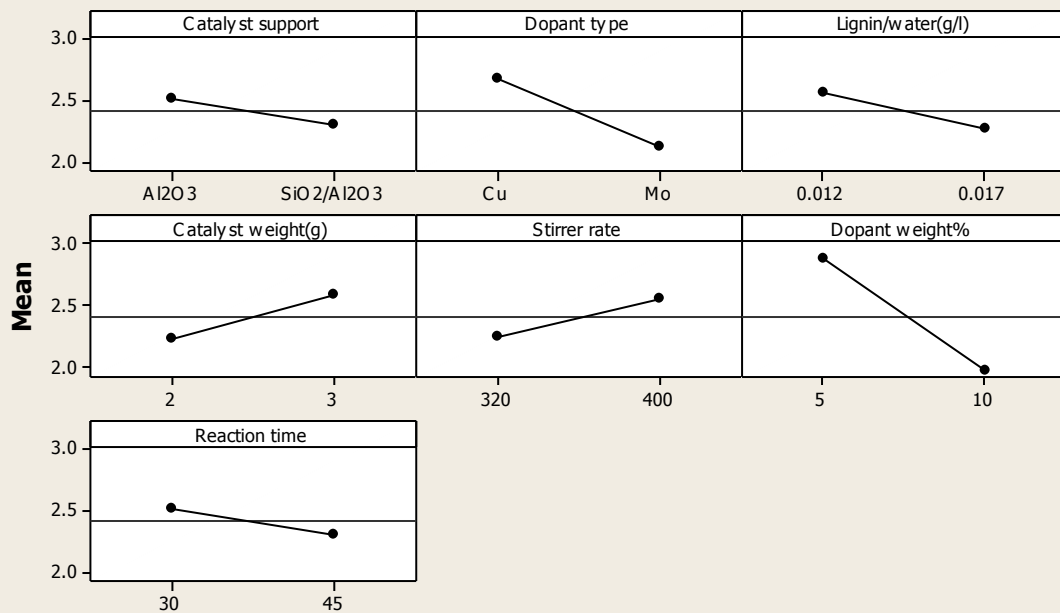
Main Effects Plot for guaiacyl carbonyls Data Means



Main Effects Plot for guaiacols Data Means

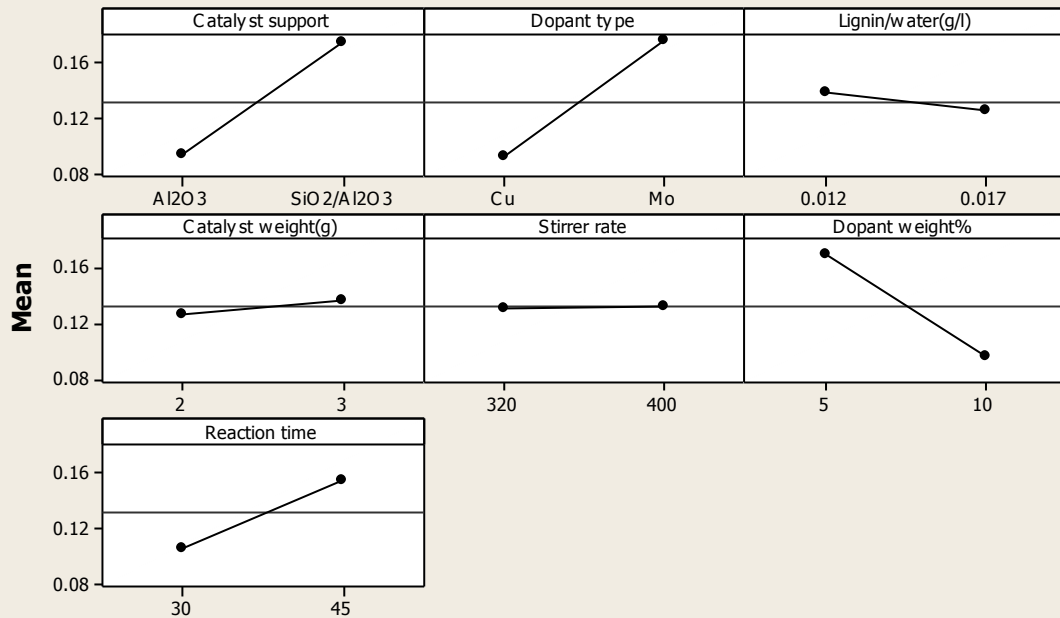


Main Effects Plot for other Data Means



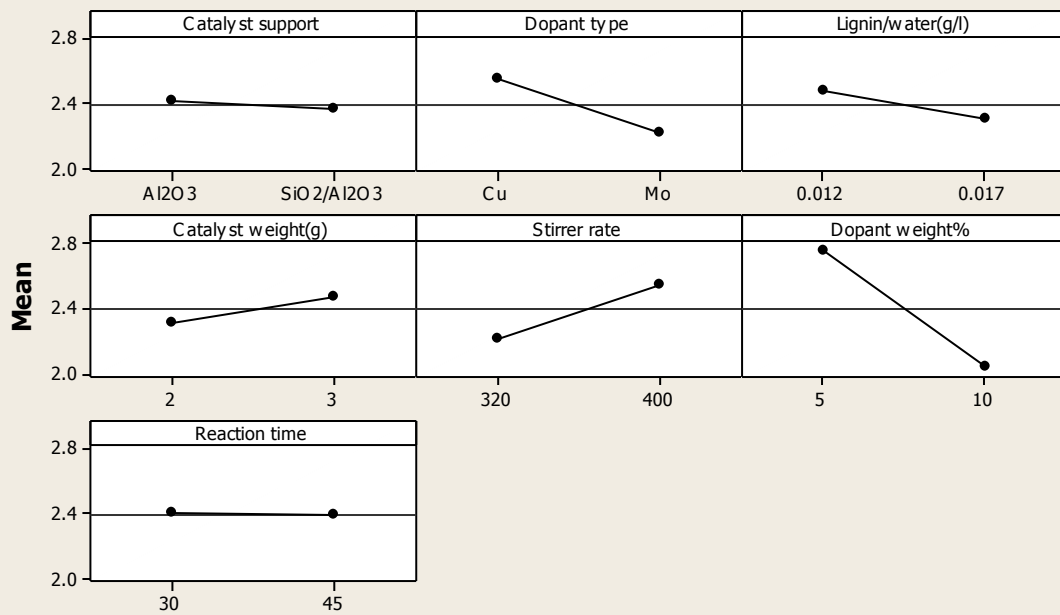
Main Effects Plot for guaiacyl dimers

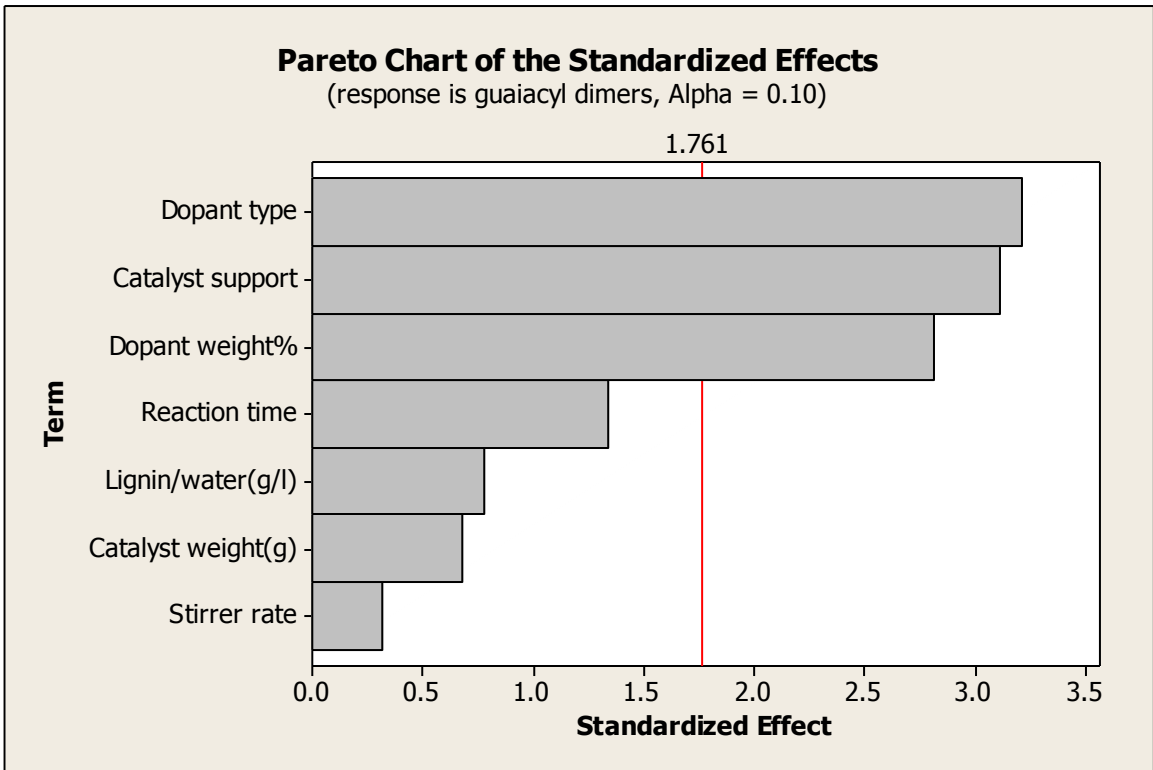
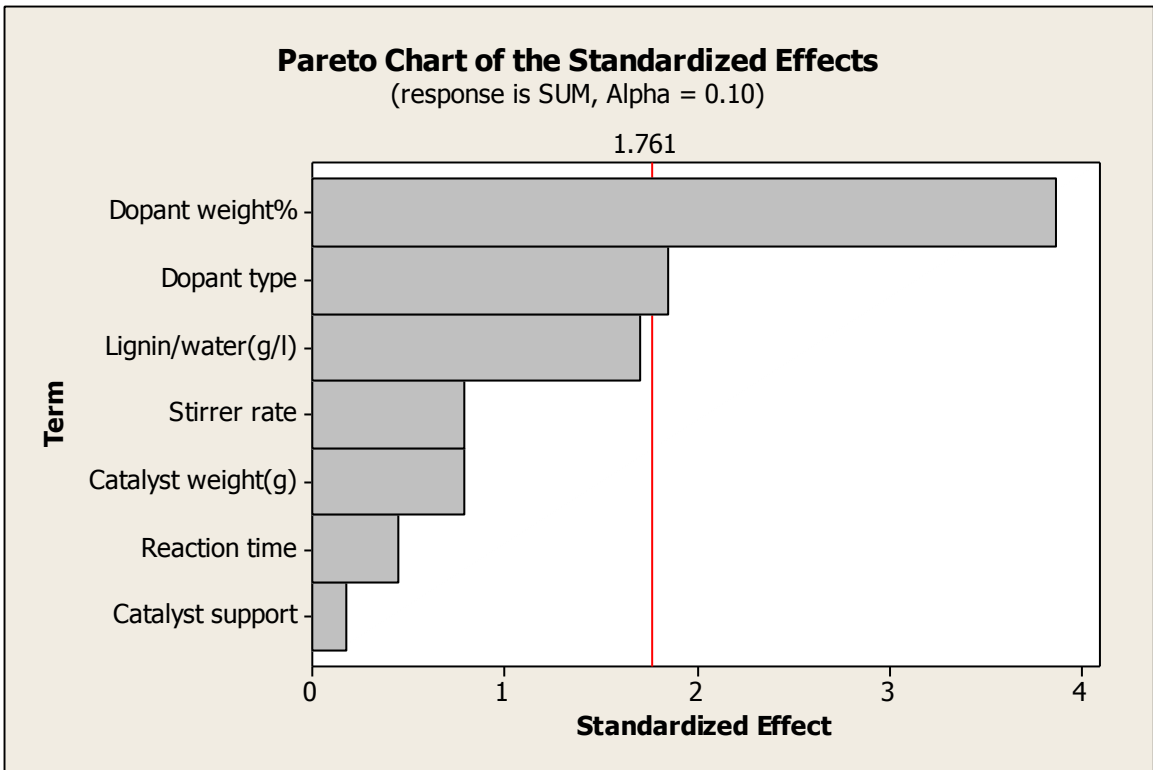
Data Means

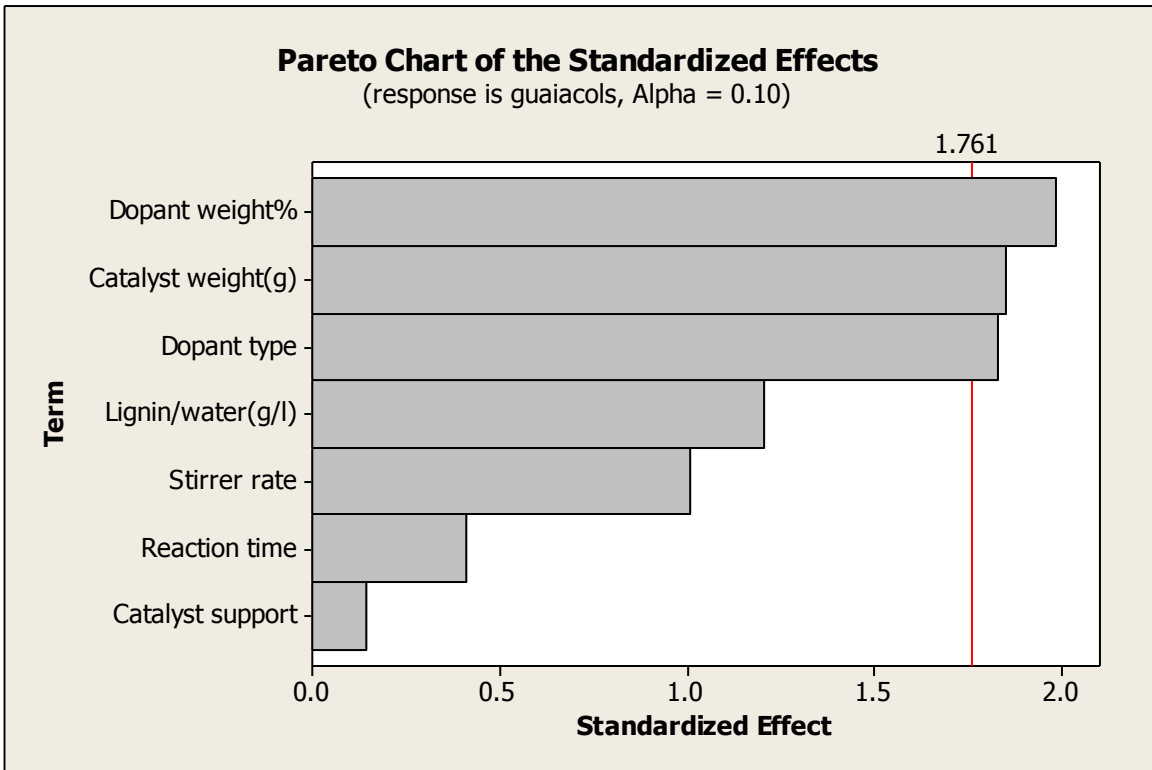
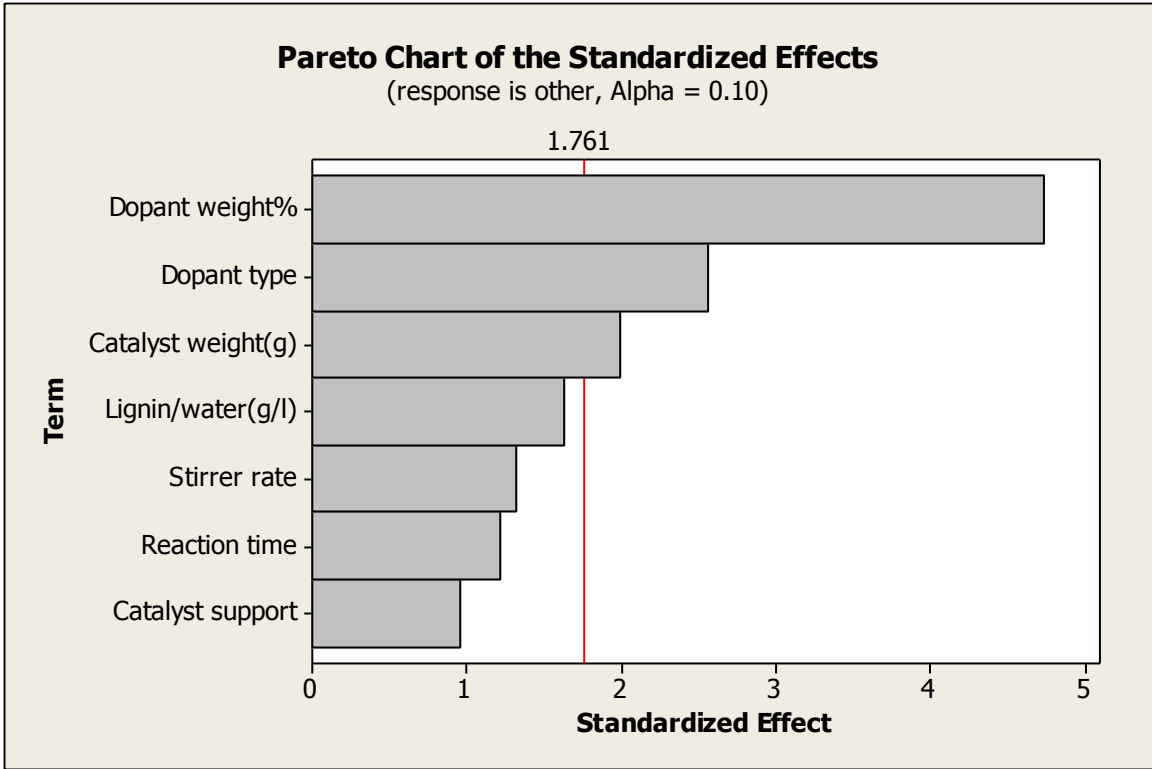


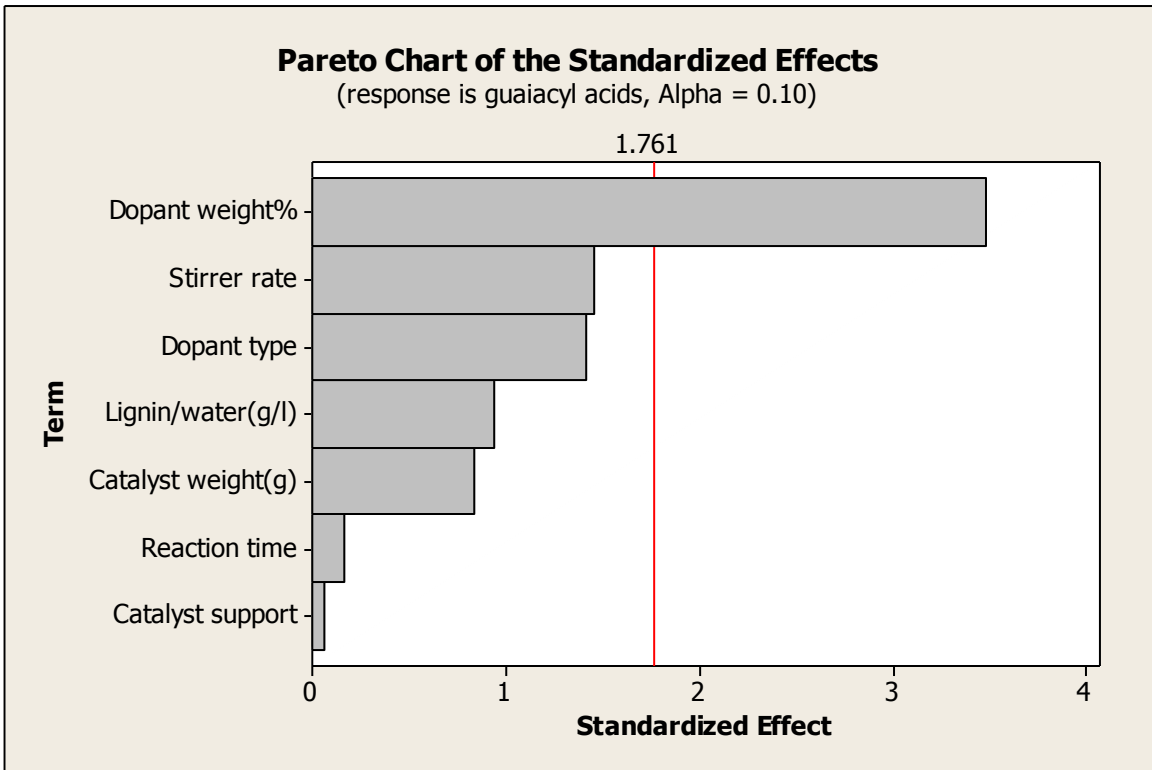
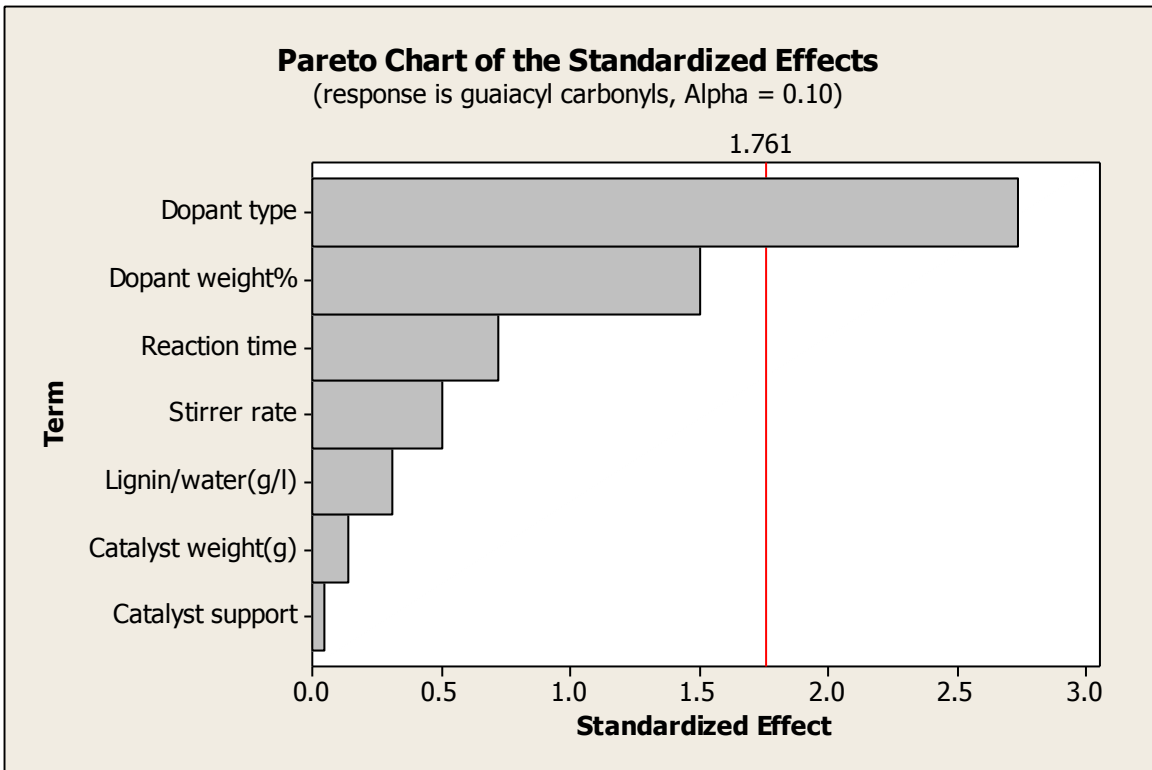
Main Effects Plot for guaiacyl acids

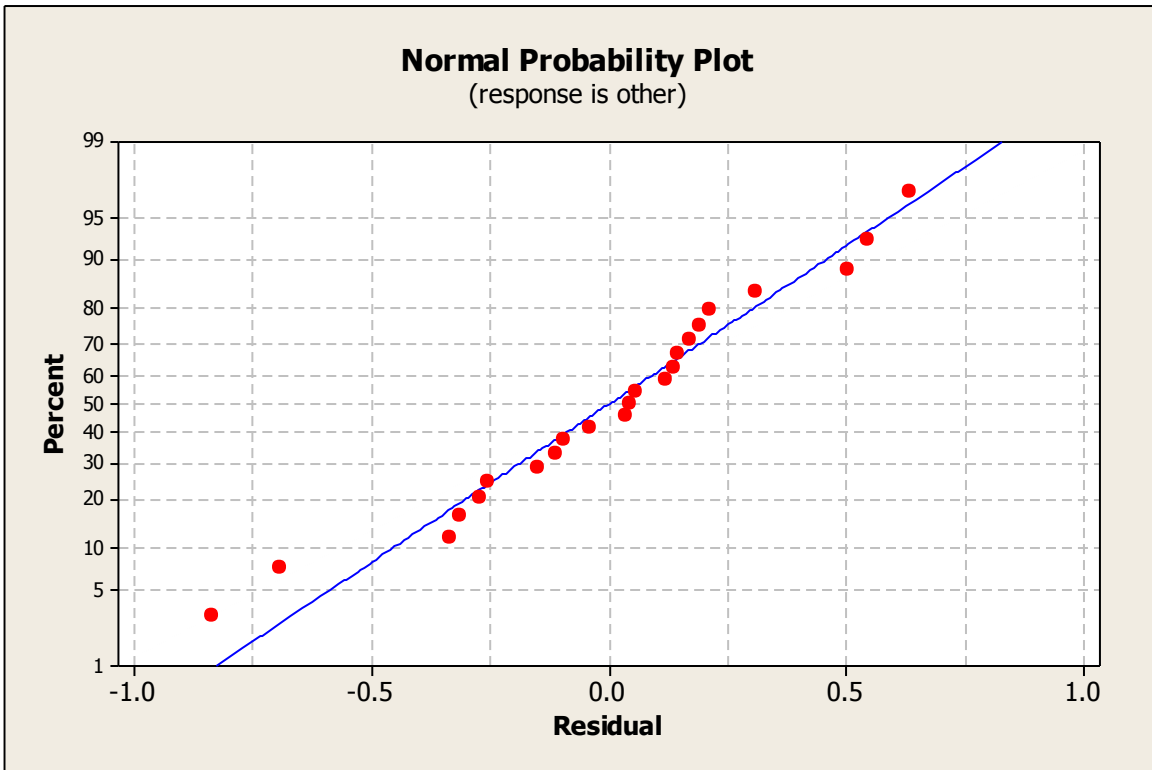
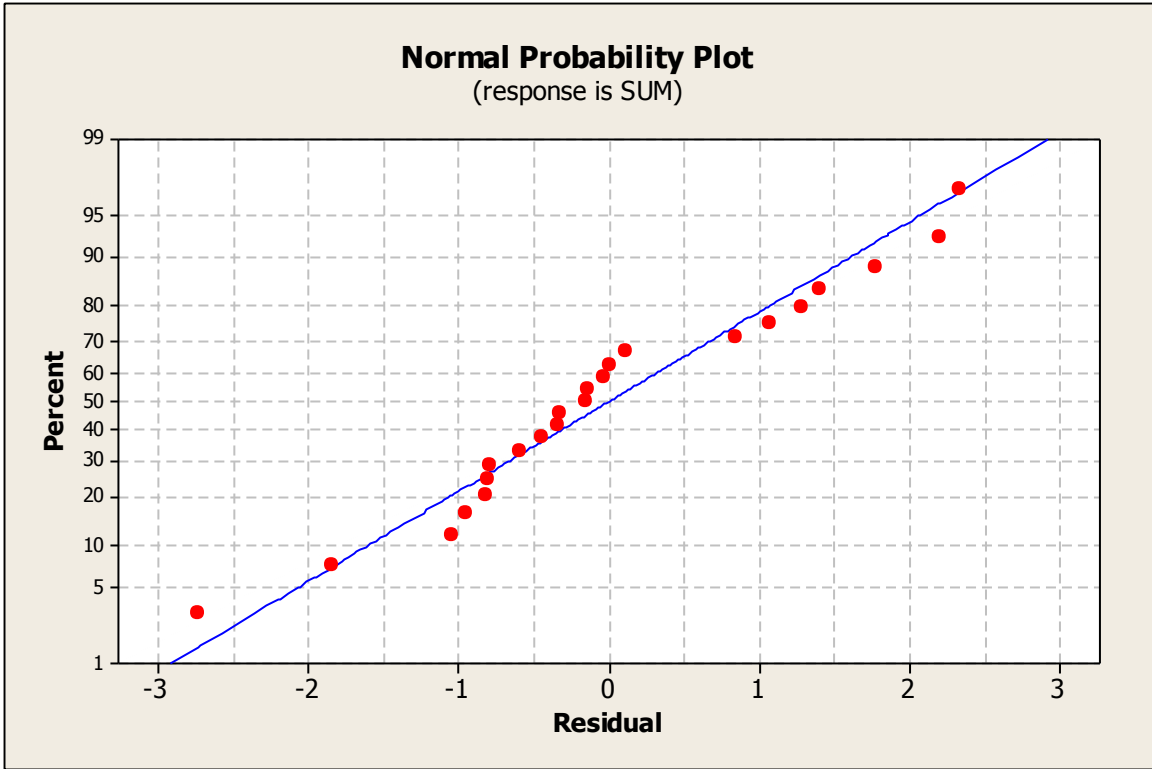
Data Means

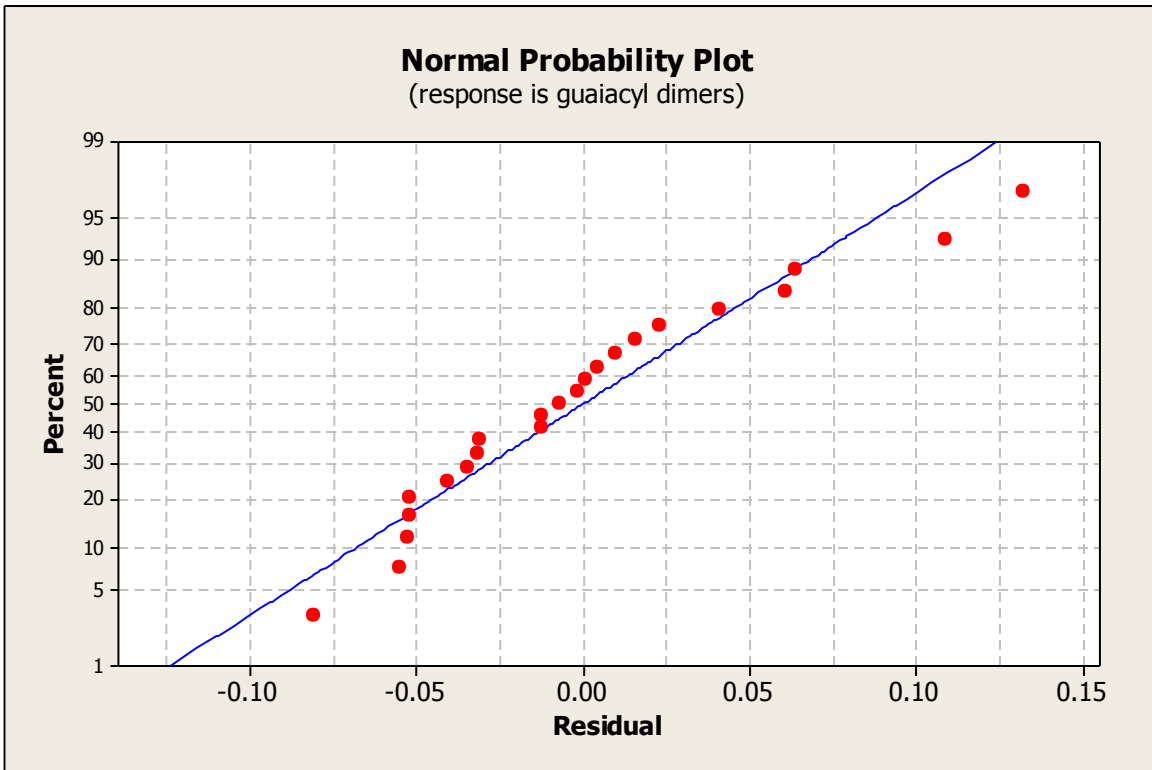
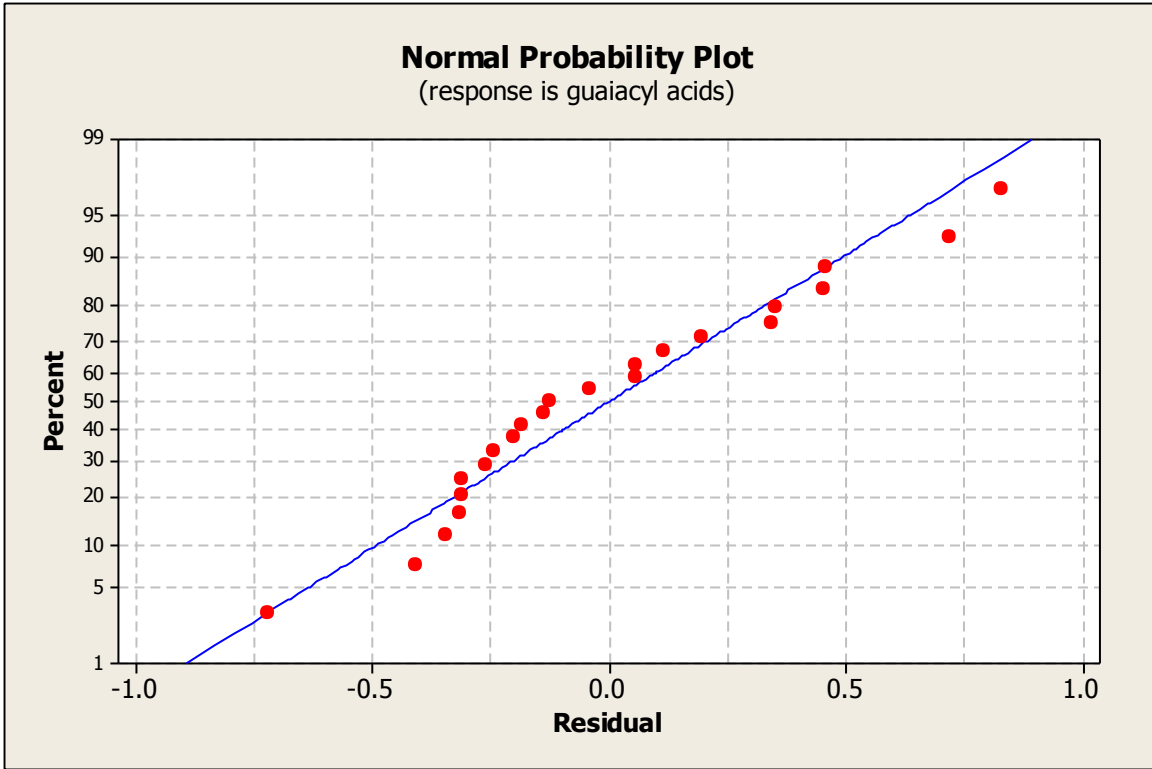


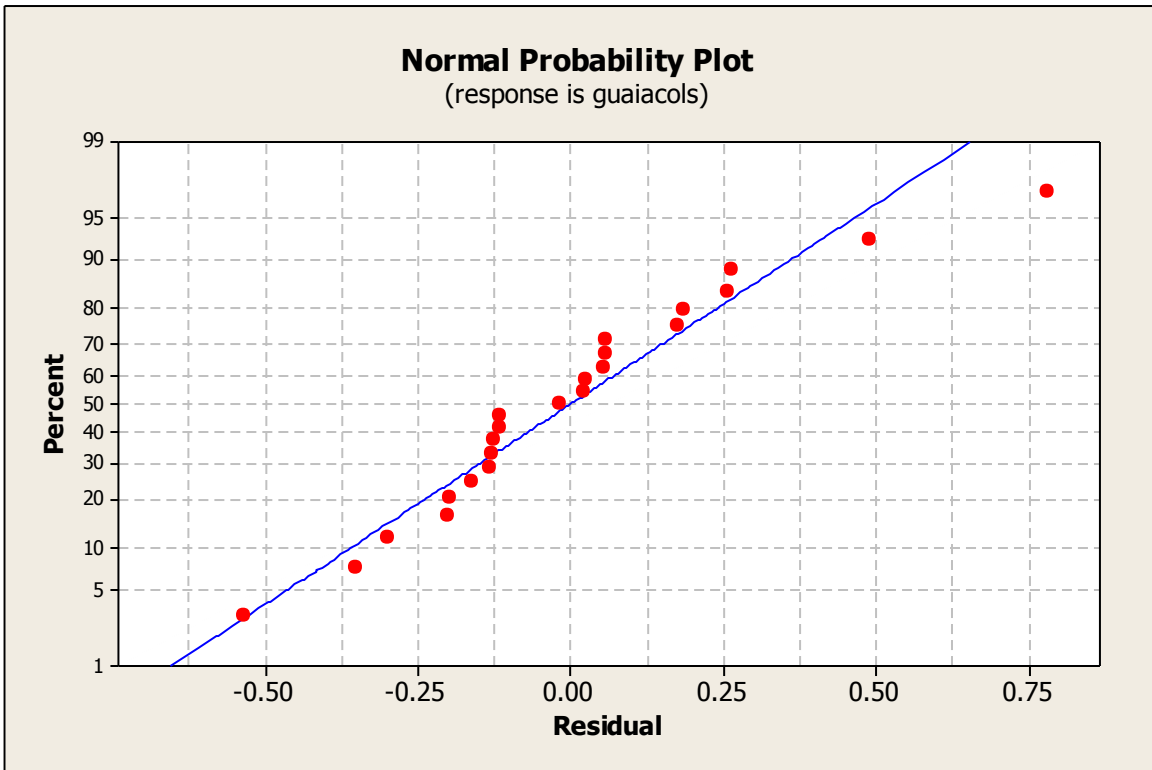
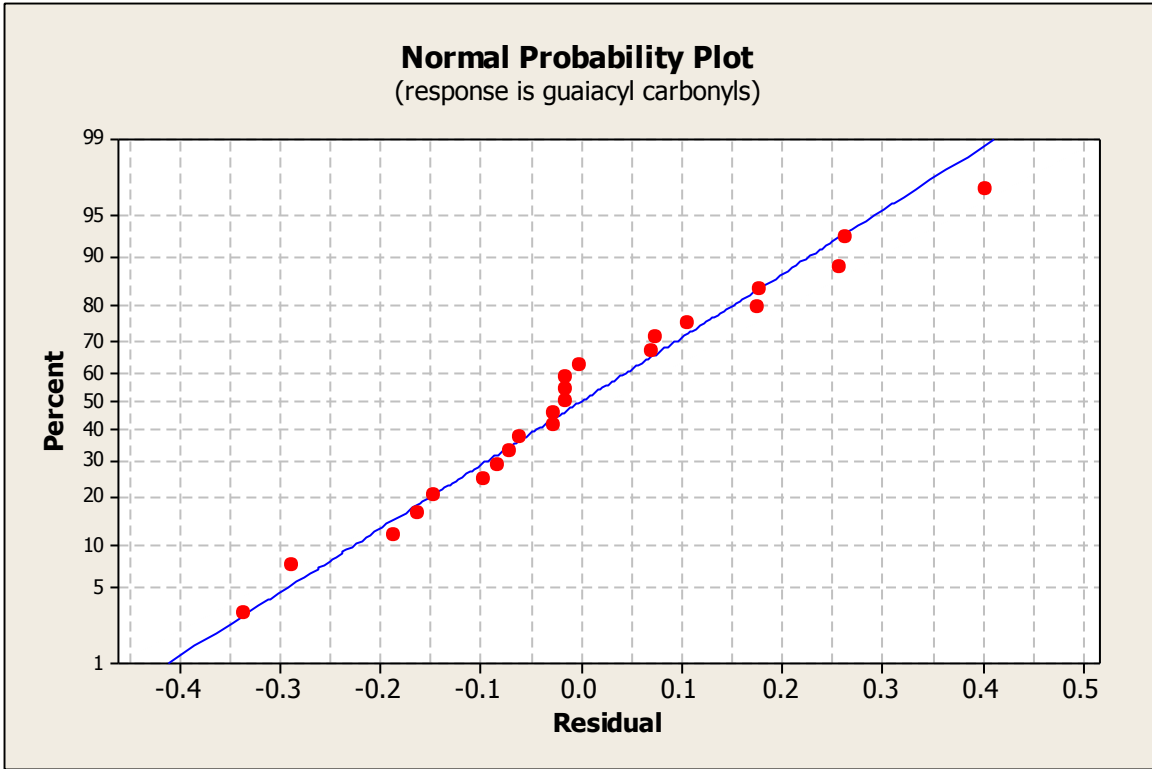












APPENDIX F

CONTINUOUS FLOW REACTOR EXPERIMENTAL PROCEDURE

The reactor setup is presented in figure 1 of chapter 3. The feed tank was filled with a well-mixed solution of water, NaOH, and lignin. The screw cap was tightened and the connection valves between the feed tank and pre-heater were completely opened. A nitrogen tank equipped with a flowmeter set at 30 ml/min was connected to the feed tank so the nitrogen could pressurize the feed to the preheating vessel. After transferring the feed to the preheating vessel, all the inlet valves were shut. In order to remove the atmospheric gases from the preheating vessel, the system was purged with nitrogen at 2 MPa for three times. After purging the vessel, the preheater was charged with 1.4 MPa nitrogen and all the valves were tightly shut. The preheater temperature was set at 220 °C and the stirrer rate was set at 400 rpm. When the preheater temperature reached 150 °C, the reactor heater was turned on and set at the selected reaction temperature. By the time the preheater reached 220 °C, the reaction vessel is also reached to the reaction temperature.

After the preheater reached to 220 °C, the nitrogen gas inlet valve was opened and the preheater was pressurized with high pressure nitrogen. While the nitrogen gas valve remained open, two isolation valves mounted between the preheater and the reaction chamber were opened and the feed was pressurized through the reactor using the nitrogen gas as the driving force. The flowrate during the reaction was controlled by a back pressure regulator, mounted at the outlet of the reactor. No sample was collected for the first 7 minutes of the reaction since the system was not yet at steady state.

When the system reached steady state, the samples were collected in a jar and the time was kept by a stopwatch to calculate the flowrate. The sample was weighed and stored in a Teflon capped vial for further analysis. For each experiment, three samples were collected in three different vials in order to verify the steady state condition by measuring the flowrate. The deviation of the flowrate should not exceed by $\pm 5\%$.

After collecting the samples, the reaction temperature was changed by manipulating the heater temperature set point. It took around 15 minutes for the system to reach the steady state condition. The same procedure was repeated for collecting the samples.

In each run, three to four reaction temperatures were tested and for each reaction temperature, at least 3 samples were collected. The pH of the samples and the reactor feed was measured immediately after the reaction was complete.

At the end of the reaction, the nitrogen inlet valve on the preheater was completely shut and all the valves placed after the preheater, including the back pressure regulator were opened. High pressure nitrogen was purged out of the reaction vessel in order to release the pressure and clean the tubes from reaction residues.

APPENDIX G

XRD ANALYSIS FOR ALL CATALYSTS

The XRD analysis of selected catalysts was conducted using a Rigaku Smartlab 3Kw instrument equipped with a D/teX detector using Cu K α radiation ($\lambda = 1.5302 \text{ \AA}$). The samples were scanned in the range of $10 < 2\theta < 80^\circ$.

All the catalysts were analyzed with XRD . The following figures are the reports generated by Rigaku Smartlab software.

Qualitative Analysis Results

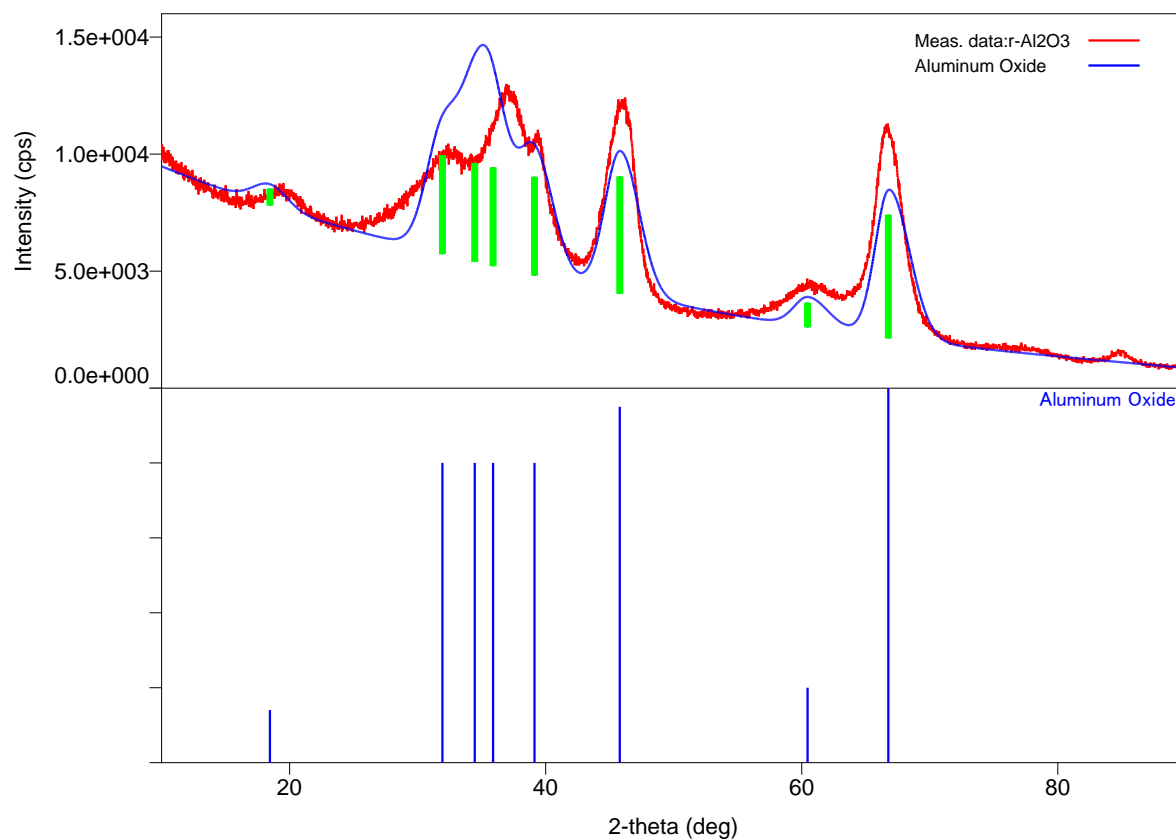
General information

Analysis date 2016/04/25 17:03:23
Sample name r-Al₂O₃ Measurement date 2016/04/25 15:54:42
File name r-Al₂O₃.ras Operator Administrator
Comment

Qualitative analysis results

Phase name	Formula	Figure of merit	Phase reg. detail	DB card number
Aluminum Oxide	Al ₂ O ₃	0.394	ICDD (PDF-	00-037-1462

Phase data pattern



Qualitative Analysis Results

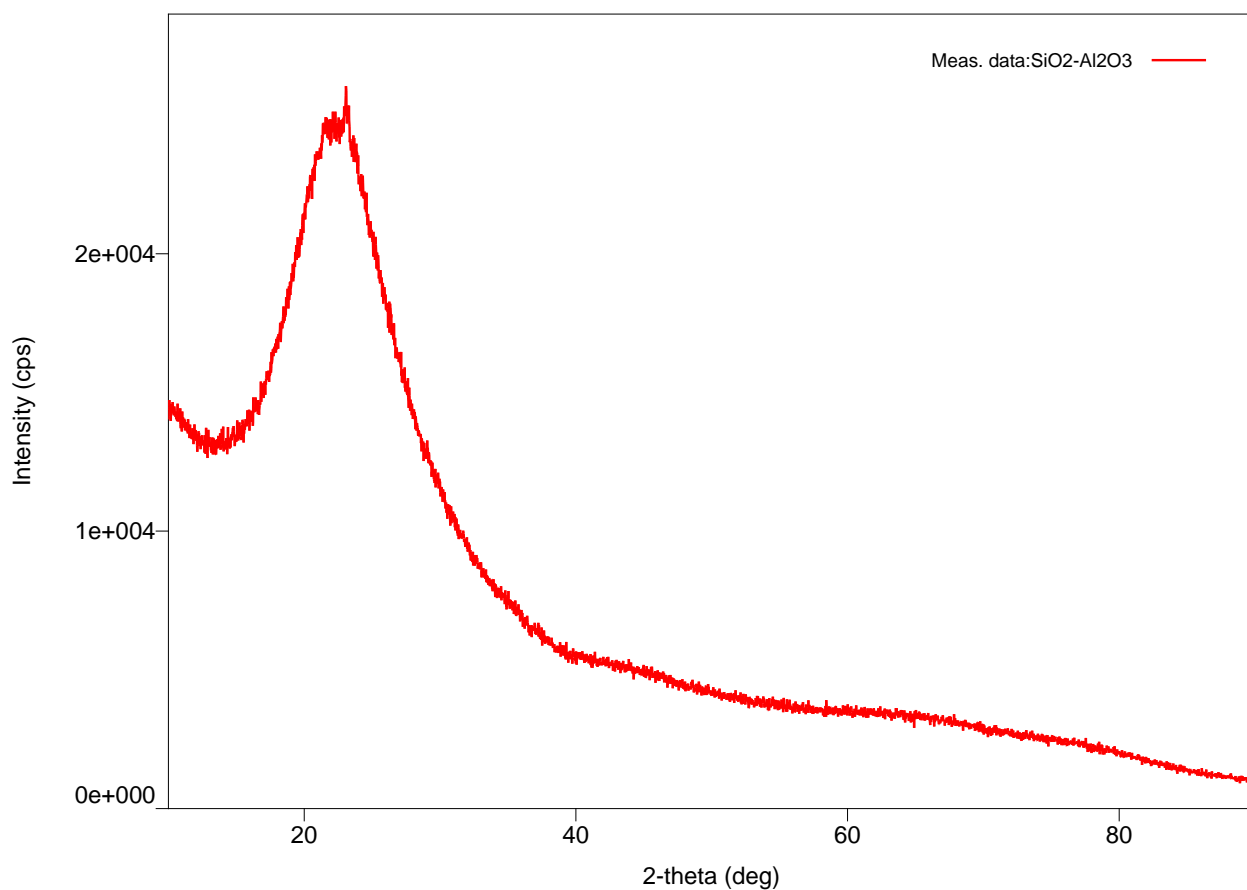
General information

Analysis date	2016/04/25 17:06:49	Measurement date	2016/04/25 15:32:37
Sample name	SiO2-Al2O3	Operator	Administrator
File name	SiO2-Al2O3.ras		
Comment			

Qualitative analysis results

Phase name	Formula	Figure of merit	Phase reg. detail	DB card number
------------	---------	-----------------	-------------------	----------------

Phase data pattern



Qualitative Analysis Results

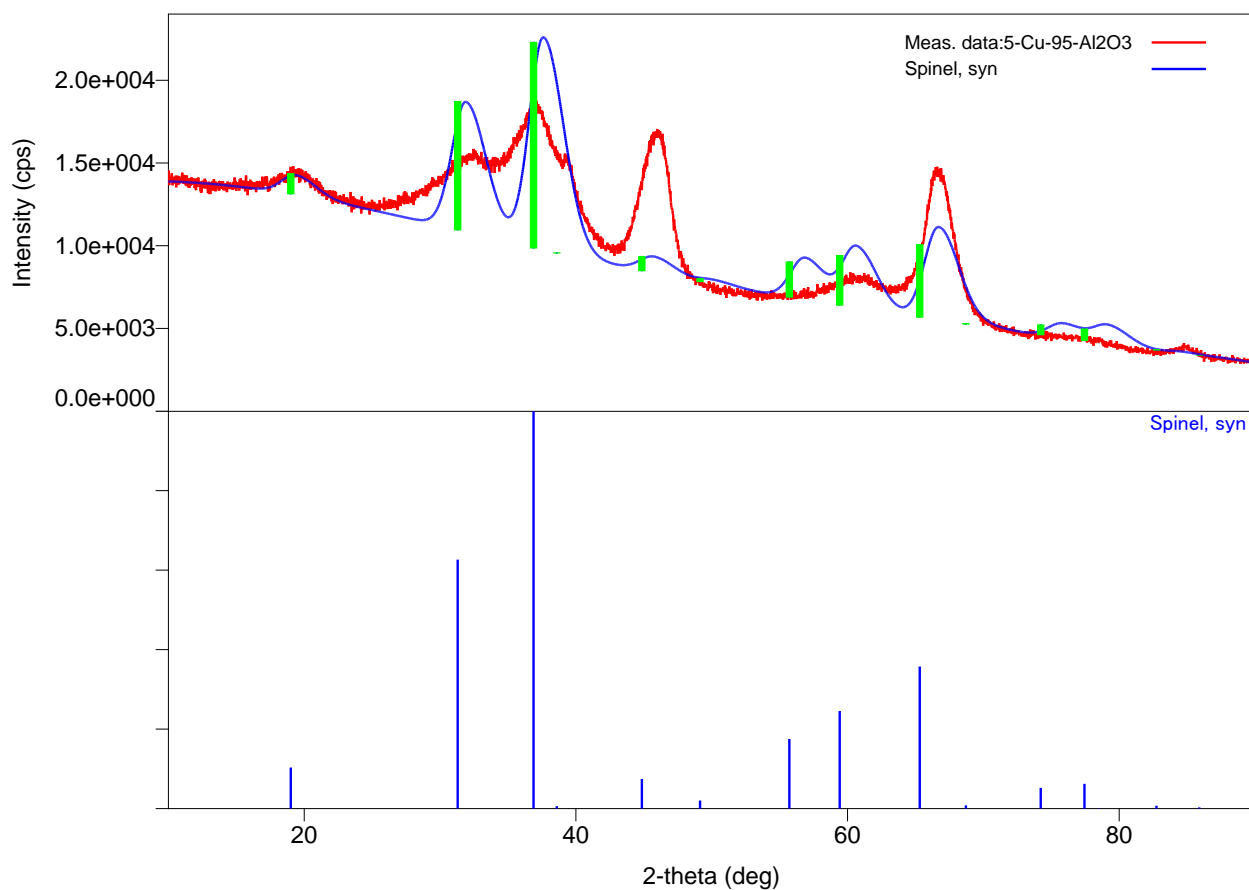
General information

Analysis date	2016/04/25 17:12:57	Measurement date	2016/04/25 13:06:41
Sample name	5-Cu-95-Al2O3	Operator	Administrator
File name	5-Cu-95-Al2O3.ras		
Comment			

Qualitative analysis results

Phase name	Formula	Figure of merit	Phase reg. detail	DB card number
Spinel, syn	Cu Al2 O4	0.880	ICDD (PDF-	01-073-1958

Phase data pattern



Qualitative Analysis Results

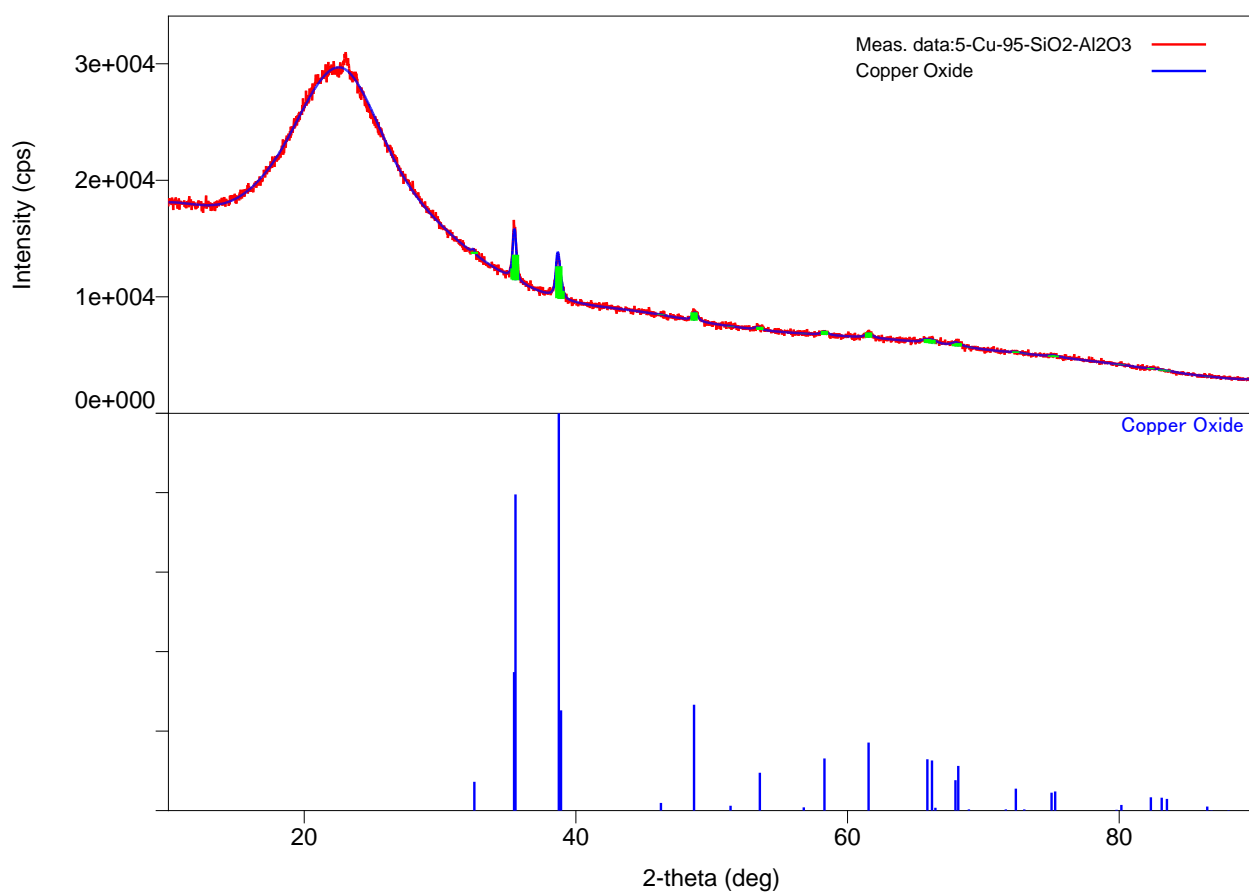
General information

Analysis date 2016/04/25 16:49:36
Sample name 5-Cu-95-SiO2-Al2O3 Measurement date 2016/04/25 12:22:35
File name 5-Cu-95-SiO2-Al2O3.ras Operator Administrator
Comment

Qualitative analysis results

Phase name	Formula	Figure of merit	Phase reg. detail	DB card number
Copper Oxide	Cu O	0.425	ICDD (PDF-	01-089-5898

Phase data pattern



Qualitative Analysis Results

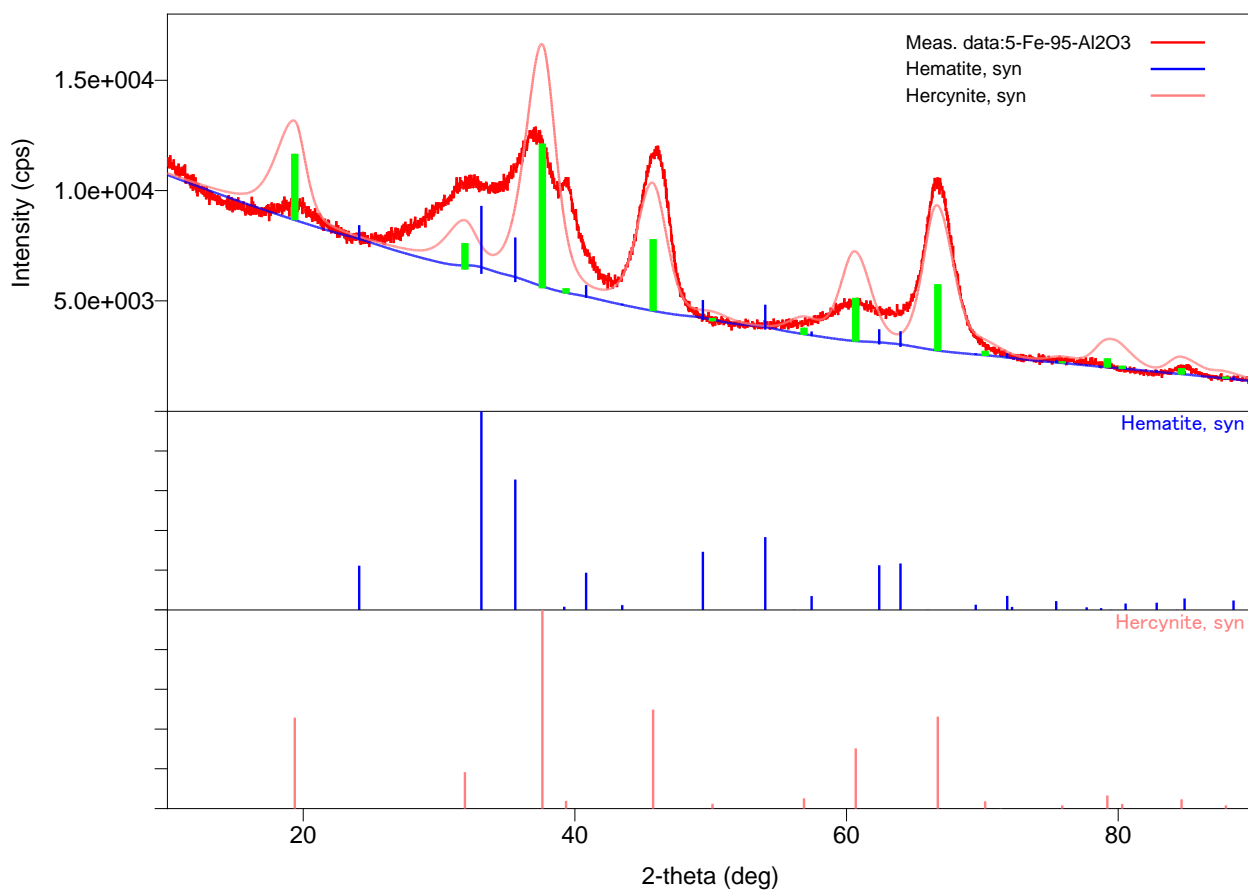
General information

Analysis date 2016/04/25 16:56:59
Sample name 5-Fe-95-Al2O3 Measurement date 2016/04/25 12:44:38
File name 5-Fe-95-Al2O3.ras Operator Administrator
Comment

Qualitative analysis results

Phase name	Formula	Figure of merit	Phase reg. detail	DB card number
Hematite, syn	Fe ₂ O ₃	0.953	ICDD (PDF-	01-089-0596
Hercynite, syn	Fe (Al ₂ O ₄)	0.670	ICDD (PDF-	01-075-9709

Phase data pattern



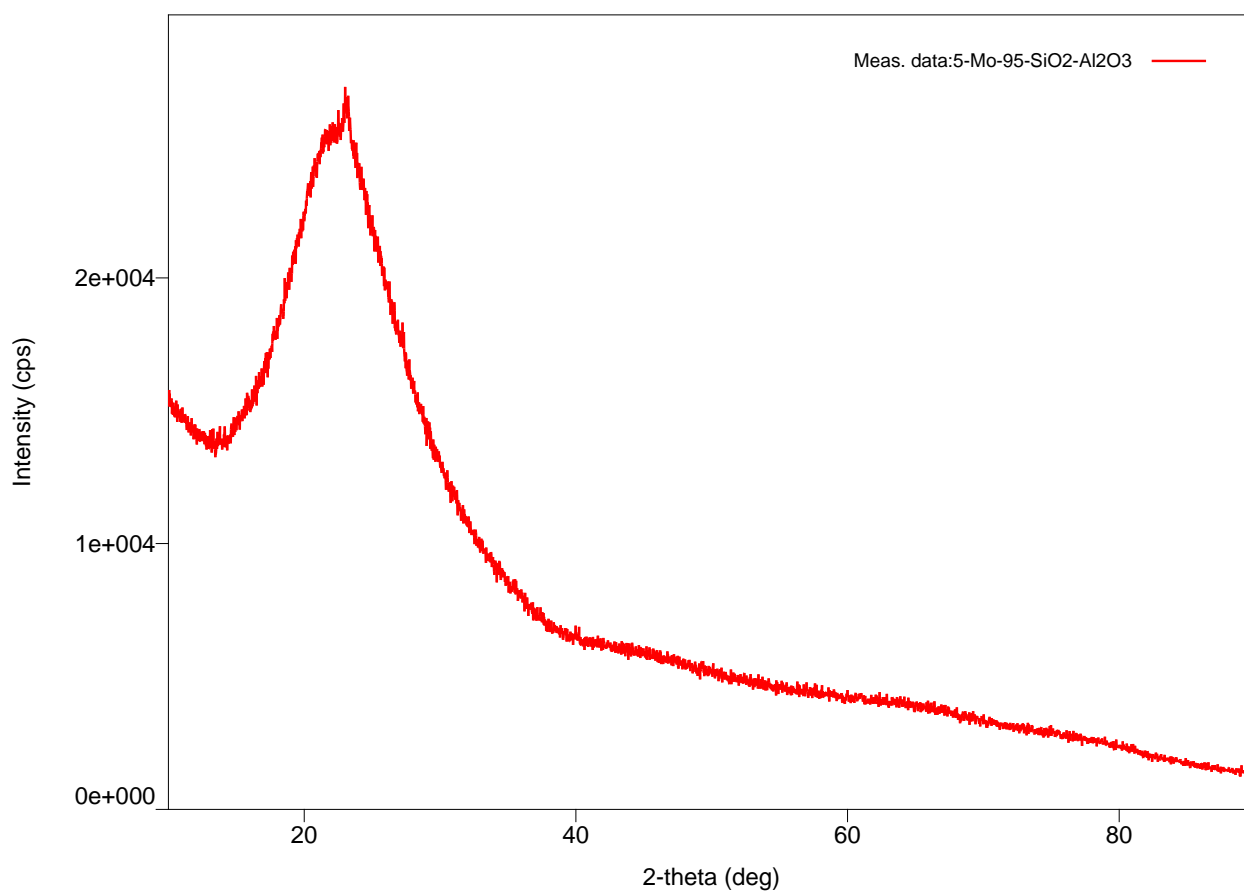
Qualitative Analysis Results

General information

Analysis date	2016/04/25 17:01:25	Measurement date	2016/04/25 13:28:45
Sample name	5-Mo-95-SiO2-Al2O3	Operator	Administrator
File name	5-Mo-95-SiO2-Al2O3.ras		
Comment			

Qualitative analysis results

Phase data pattern



Qualitative Analysis Results

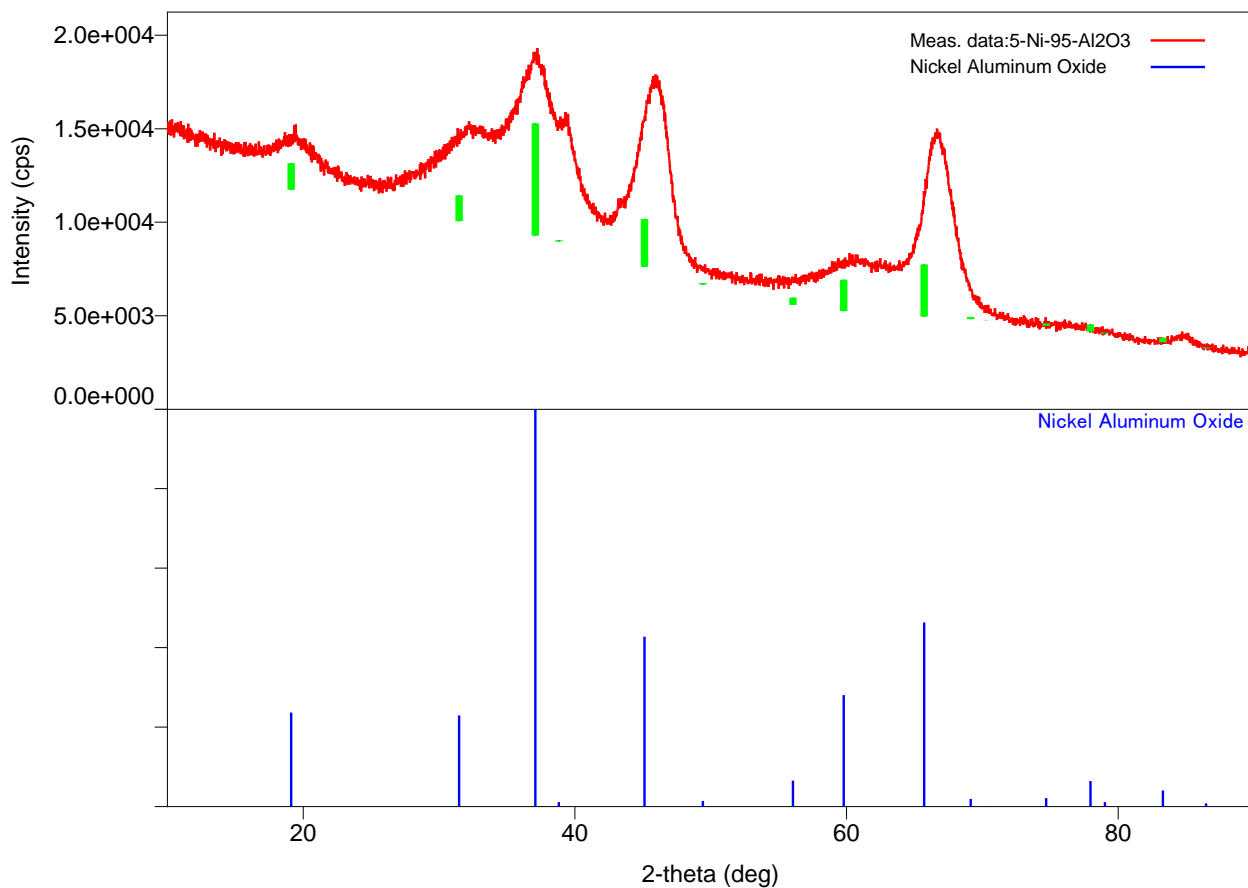
General information

Analysis date	2016/04/25 16:58:54	Measurement date	2016/04/25 13:50:48
Sample name	5-Ni-95-Al2O3	Operator	Administrator
File name	5-Ni-95-Al2O3.ras		
Comment			

Qualitative analysis results

Phase name	Formula	Figure of merit	Phase reg. detail	DB card number
------------	---------	-----------------	-------------------	----------------

Phase data pattern



Qualitative Analysis Results

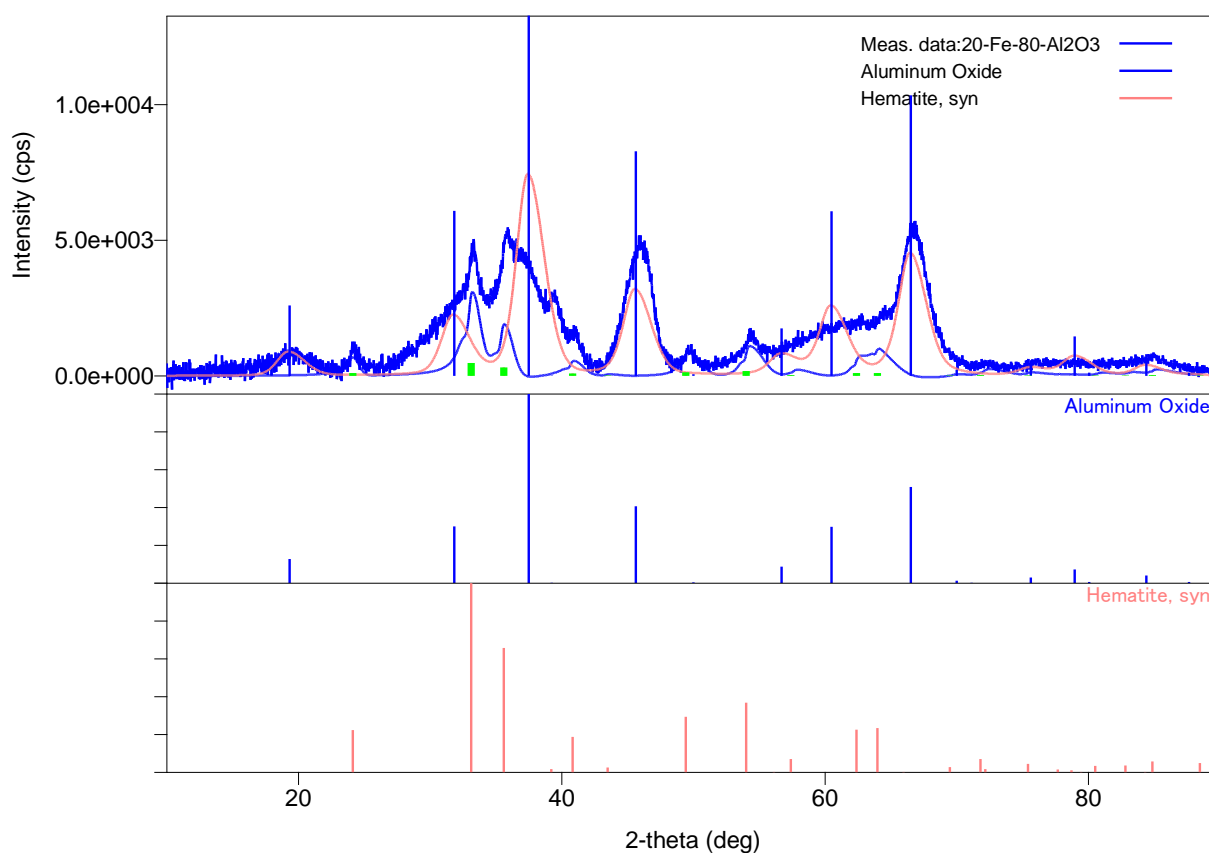
General information

Analysis date 2016/04/25 16:26:24
Sample name 20-Fe-80-Al2O3 Measurement date 2016/04/25 12:00:30
File name 20-Fe-80-Al2O3.ras Operator Administrator
Comment

Qualitative analysis results

Phase name	Formula	Figure of merit	Phase reg. detail	DB card number
Hematite, syn	Fe ₂ O ₃	2.548	ICDD (PDF-	01-089-0596
Aluminum Oxide	Al ₃ O _{3.52}	1.259	ICDD (PDF-	01-078-5518

Phase data pattern



APPENDIX H

CONTINUOUS FLOW REACTOR SIMULATION WITH MATLAB

The continuous flow reactor was initially designed using a MATLAB code. The code is able to size the reactor and estimate the temperature at specified spots of the reaction vessel based on the users reaction condition inputs. The code along with some of the simulated results are presented.


```

clc
Tin=input('fluid input temperature(celsius): ');
D=input('inner Diameter:(meter): ');
d=input('tube wall thickness:(meter): ');
M=input('fluid mass flow rate:(Kg/s): ');
P=input('working pressure(Psia): ');
Ts=input('tube outer wall temperature(celsius): ');
% A has considered to be cross sectional surface area
A=(pi.*D.^2)/4;
% body area of 0.1m part of the tube
As=pi.*D.*0.05;
% inner and outer radiuses
ri=D/2;
ro=ri+d;
% roughness value for new stainless steel
eps=2e-6;
% length Counter
L=0;
% total pressure drop counter
DPtotal=0;
% start Q
QQ=0;
% start T
TT=0;
% counter
flag=0;

Ts1=0;
Ts2=0;
Ts3=0;

% defined criteria to evaluate critical/boiling temperature
if P<3600
Tcritical=53.9832022.*(P+14.696).^0.240752055;
else
    Tcritical=374;
end;

% out stream temperature
Tout=Tcritical-15;

if (Tin<324&&Tin>24)
q=M.*(1.356212e-13.*(Tout.^7-Tin.^7)-1.392967e-10.*(Tout.^6-
Tin.^6)...
+0.58174e-7.*(Tout.^5-Tin.^5)-1.23043e-5.*(Tout.^4-Tin.^4)...
+1.44560e-3.*(Tout.^3-Tin.^3)-0.87798e-1.*(Tout.^2-
Tin.^2)+77.758660.*(Tout-Tin));
elseif (Tin<374&&Tin>324)
q=M.*(0.49666e-4.*(Tout.^5-Tin.^5)-0.83537e-1.*(Tout.^4-Tin.^4)...
+0.56207e2.*(Tout.^3-Tin.^3)-1.89096e4.*(Tout.^2-
Tin.^2)+3.1808516e6.*(Tout-Tin));
end;

```

```

% counters for total absorbed heat and residence time
Qtotal=0;
tres=0;
n=0;
% this is the counting factor

figure; hold on;

for i=1:2000
    rho=-0.000000077941.*Tin.^4 + 0.000048856*Tin.^3 -
0.012603*Tin.^2 + 0.57538.*Tin + 986.63;
    if (Tin<324&&Tin>24)
        Cp=(9.5e-13.*(Tin.^6)-8.35e-10.*(Tin.^5)+2.9e-7.*(Tin.^4)-4.9e-
5.*(Tin.^3)+4.3e-3.*(Tin.^2)-0.17.*Tin+77).*55.5;
    elseif (Tin<374&&Tin>324)
        Cp=(2.4833333e-04.*Tin.^4 - 3.3415167e-1.*Tin.^3 +
1.6862260e2.*Tin.^2 - 3.7819252e4.*Tin + 3.1808516e6).*55.5;
    end;
% viscosity
    v=1.0399203e-17.*Tin.^6 - 1.4147813e-14.*Tin.^5 + 7.7815343e-
12.*Tin.^4 - 2.2293983e-09.*Tin.^3 + 3.5764535e-07.*Tin.^2 ...
-3.2117290e-05.*Tin + 1.4968175e-03;
% thermal conductivity of the pipe
    k=-2.1592e-11.*Tin.^4 +1.7551e-08.*Tin.^3-1.0127e-
05.*Tin.^2+1.9820e-03.*Tin+5.6630e-1;
    u=M/(rho.*A);
    Re=(rho.*u.*D)/v;
    Pr=Cp.*v/k;
    u=M/(rho.*A);
    f=(0.79.*log(Re)-1.64).^2;
    DP=2.*f.*(0.05/D).*(rho.*u.^2);

    Nu=(f/8).*(Re-1000).*Pr/(1+12.7.*(f/8)^0.5.*((Pr^0.6666667)-
1));
    h=0.023.*(k/D).*Re.^0.8.*Pr.^4;
    U=1/((1/h)+(ri/k).*log(ro/ri));
    Q=U.*As.*(Ts-Tin);
    Qtotal=Q+Qtotal;
    DPtotal=DPtotal+DP;
    T=Tin+(Qtotal/(M.*Cp));

    if T>310&&flag==0
        QQ=QQ+Qtotal;
        TT=TT+T;
        LL=L+0.05;
        tt=tres+((A.*0.05)/(M/rho));
        flag=1;
    end

    if T>Tout&&T<Tcritical
        L=L+0.05;
        t=(A.*0.05)/(M/rho);
        tres=t+tres;
        hold on;
    subplot(2,2,1)
    plot(L,T,'-r*')

```

```

        title('*Fluide Temperature*')
        hold on;
subplot(2,2,2)
plot(L,tres,'b--o')
title('*Residence Time*')
hold on;
subplot(2,2,3)
plot(L,Re,'g*')
title('*Reynolds Number*')
hold on;
subplot(2,2,4)
plot(L,DP,'--gs')
title('*Pressure Drop*')
        break;
else
    Tin=T;
    L=L+0.05;
    t=(A.*0.05)/(M/rho);
    tres=t+tres;

    end;
    hold on;
subplot(2,2,1)
plot(L,T,'-.r*')
title('*Fluide Temperature*')
    hold on;
subplot(2,2,2)
plot(L,tres,'b--o')
title('*Residence Time*')
    hold on;
subplot(2,2,3)
plot(L,Re,'g*')
title('*Reynolds Number*')
    hold on;
subplot(2,2,4)
plot(L,DP,'--gs')
title('*Pressure Drop*')
end
DT=TT-Tin;
Uave=QQ/((pi.*D.*LL).*DT);

Error=((Qtotal-q)/q)*100;
figure;
hTable = uitable();
set(hTable,'ColumnWidth',{25})
rowHeaders = {'Qtotal(W)', 'T(C)', 'L(m)', 'Re', 'Res.time(s)',
'P.Drop', 'Tstart', 'Lstart', 't.start', 'Q.start', 'Ts1/6',
'Ts1/3', 'Ts1/2' };
columnHeaders =('Results');

dat=[Qtotal; T; L; Re; tres; DPtotal; TT; LL; tt; QQ; Ts1; Ts2;
Ts3;];
hTable =
uitable('columnname',columnHeaders,'rowname',rowHeaders,'Data',dat)
;

```

REFERENCES

1. British Petroleum Company, BP Statistical Review of World Energy (2016).
2. A. Demirbas, The importance of bioethanol and biodiesel from biomass, *Energy Sources, Part B* 3 (2008) 177-185.
3. J. Goldemberg, I.C. Macedo, Brazilian alcohol program: an overview, *Energy for Sustainable Development* 1 (1994) 17-22.
4. J. Hill, E. Nelson, D. Tilman, S. Polasky, D. Tiffany, Environmental, economic, and energetic costs and benefits of biodiesel and ethanol biofuels, *Proc. Natl. Acad. Sci. U. S. A.* 103 (2006) 11206-11210.
5. P. Claassen, J. Van Lier, A.L. Contreras, E. Van Niel, L. Sijtsma, A. Stams, S. De Vries, R. Weusthuis, Utilisation of biomass for the supply of energy carriers, *Appl. Microbiol. Biotechnol.* 52 (1999) 741-755.
6. Y.P. Zhang, Reviving the carbohydrate economy via multi-product lignocellulose biorefineries, *J. Ind. Microbiol. Biotechnol.* 35 (2008) 367-375.
7. C.E. Wyman, B.E. Dale, R.T. Elander, M. Holtzapple, M.R. Ladisch, Y. Lee, Comparative sugar recovery data from laboratory scale application of leading pretreatment technologies to corn stover, *Bioresour. Technol.* 96 (2005) 2026-2032.
8. Y. Sun, J. Cheng, Hydrolysis of lignocellulosic materials for ethanol production: a review, *Bioresour. Technol.* 83 (2002) 1-11.
9. N. Mosier, C. Wyman, B. Dale, R. Elander, Y. Lee, M. Holtzapple, M. Ladisch, Features of promising technologies for pretreatment of lignocellulosic biomass, *Bioresour. Technol.* 96 (2005) 673-686.

10. M. Dashtban, H. Schraft, W. Qin, Fungal bioconversion of lignocellulosic residues; opportunities & perspectives, *Int. J. Biol. Sci.* 5 (2009) 578-595.
11. A. Pandey, *Biofuels: alternative feedstocks and conversion processes*, Academic Press, 2011.
12. F. Lu, J. Ralph, Chapter 6-Lignin, *Cereal Straw as a Resource for Sustainable Biomaterials and Biofuels*, Amsterdam: Elsevier (2010) 169-207.
13. E.M. Rubin, Genomics of cellulosic biofuels, *Nature* 454 (2008) 841-845.
14. E. Sjöström, *Wood chemistry: fundamentals and applications*, Gulf Professional Publishing, 1993.
15. M. Hauteville, K. Lundquist, S. von Unge, NMR Studies of Lignins. 7. ¹H NMR Spectroscopic Investigation of the Distribution of Erythro and Threo Forms of beta-O-4 Structures in Lignins, *Acta Chem. Scand.* (1986) 31-35.
16. C.S. Lancefield, O.S. Ojo, F. Tran, N.J. Westwood, Isolation of Functionalized Phenolic Monomers through Selective Oxidation and C-O Bond Cleavage of the beta-O-4 Linkages in Lignin, *Angewandte Chemie* 127 (2015) 260-264.
17. S. Ralph, J. Ralph, L. Landucci, L. Landucci, NMR database of lignin and cell wall model compounds, US Forest Prod.Lab., Madison, WI (<http://ars.usda.gov/Services/docs.htm>) (2004).
18. T. Umezawa, T. Higuchi, Cleavages of aromatic ring and beta-O-4 bond of synthetic lignin (DHP) by lignin peroxidase, *FEBS Lett.* 242 (1989) 325-329.
19. C. Mai, O. Milstein, A. Hüttermann, Chemoenzymatical grafting of acrylamide onto lignin, *J. Biotechnol.* 79 (2000) 173-183.

20. A. Macfarlane, R. Prestidge, M. Farid, J. Chen, Dissolved air flotation: A novel approach to recovery of organosolv lignin, *Chem. Eng. J.* 148 (2009) 15-19.
21. P.A. Ciullo, *Industrial minerals and their uses: a handbook and formulary*, William Andrew, 1996.
22. P. Gallezot, Catalytic routes from renewables to fine chemicals, *Catalysis today* 121 (2007) 76-91.
23. B. Kamm, P.R. Gruber, M. Kamm, *Biorefineries—industrial processes and products*, Wiley Online Library, 2006.
24. M.P. Pandey, C.S. Kim, Lignin depolymerization and conversion: a review of thermochemical methods, *Chem. Eng. Technol.* 34 (2011) 29-41.
25. G.W. Huber, S. Iborra, A. Corma, Synthesis of transportation fuels from biomass: chemistry, catalysts, and engineering, *Chem. Rev.* 106 (2006) 4044-4098.
26. E.B. da Silva, M. Zabkova, J. Araújo, C. Cateto, M. Barreiro, M. Belgacem, A. Rodrigues, An integrated process to produce vanillin and lignin-based polyurethanes from Kraft lignin, *Chem. Eng. Res. Design* 87 (2009) 1276-1292.
27. R.B. Gupta, A. Demirbas, *Gasoline, diesel, and ethanol biofuels from grasses and plants*, Cambridge University Press, 2010.
28. D.J. Nowakowski, A.V. Bridgwater, D.C. Elliott, D. Meier, P. de Wild, Lignin fast pyrolysis: results from an international collaboration, *J. Anal. Appl. Pyrolysis* 88 (2010) 53-72.
29. H. Chang, G. Allan, *Oxidation, Lignins: Occurrence, formation and reactions*. Wiley (1971) 433-485.

30. C. Xu, R.A.D. Arancon, J. Labidi, R. Luque, Lignin depolymerisation strategies: towards valuable chemicals and fuels, *Chem. Soc. Rev.* 43 (2014) 7485-7500.
31. J. Barbier, N. Charon, N. Dupassieux, A. Loppinet-Serani, L. Mahé, J. Ponthus, M. Courtiade, A. Ducrozet, A. Quoineaud, F. Cansell, Hydrothermal conversion of lignin compounds. A detailed study of fragmentation and condensation reaction pathways, *Biomass Bioenergy* 46 (2012) 479-491.
32. A. Kruse, A. Funke, M. Titirici, Hydrothermal conversion of biomass to fuels and energetic materials, *Curr. Opin. Chem. Biol.* 17 (2013) 515-521.
33. R. Katahira, A. Mittal, K. McKinney, X. Chen, M.P. Tucker, D.K. Johnson, G.T. Beckham, Base-catalyzed depolymerization of biorefinery lignins, *ACS Sustainable Chemistry & Engineering* 4 (2016) 1474-1486.
34. A. Vigneault, D.K. Johnson, E. Chornet, Base-Catalyzed Depolymerization of Lignin: Separation of Monomers, *The Canadian Journal of Chemical Engineering* 85 (2007) 906-916.
35. A. Toledano, L. Serrano, J. Labidi, Organosolv lignin depolymerization with different base catalysts, *Journal of Chemical Technology and Biotechnology* 87 (2012) 1593-1599.
36. A. Toledano, L. Serrano, J. Labidi, Improving base catalyzed lignin depolymerization by avoiding lignin repolymerization, *Fuel* 116 (2014) 617-624.
37. G.S. Macala, T.D. Matson, C.L. Johnson, R.S. Lewis, A.V. Iretskii, P.C. Ford, Hydrogen transfer from supercritical methanol over a solid base catalyst: a model for lignin depolymerization, *ChemSusChem* 2 (2009) 215-217.

38. J. Miller, L. Evans, A. Littlewolf, D. Trudell, Batch microreactor studies of lignin and lignin model compound depolymerization by bases in alcohol solvents, *Fuel* 78 (1999) 1363-1366.
39. X. Erdocia, R. Prado, M.Á Corcuera, J. Labidi, Base catalyzed depolymerization of lignin: Influence of organosolv lignin nature, *Biomass Bioenergy* 66 (2014) 379-386.
40. J. Long, Y. Xu, T. Wang, Z. Yuan, R. Shu, Q. Zhang, L. Ma, Efficient base-catalyzed decomposition and in situ hydrogenolysis process for lignin depolymerization and char elimination, *Appl. Energy* 141 (2015) 70-79.
41. M.V. Olarte, Base-catalyzed depolymerization of lignin and hydrodeoxygenation of lignin model compounds for alternative fuel production (2011).
42. R. Beauchet, F. Monteil-Rivera, J.M. Lavoie, Conversion of lignin to aromatic-based chemicals (L-chems) and biofuels (L-fuels), *Bioresour. Technol.* 121 (2012) 328-334.
43. J. Lavoie, W. Baré, M. Bilodeau, Depolymerization of steam-treated lignin for the production of green chemicals, *Bioresour. Technol.* 102 (2011) 4917-4920.
44. Z. Yuan, S. Cheng, M. Leitch, C. Xu, Hydrolytic degradation of alkaline lignin in hot-compressed water and ethanol, *Bioresour. Technol.* 101 (2010) 9308-9313.
45. V. Roberts, V. Stein, T. Reiner, A. Lemonidou, X. Li, J.A. Lercher, Towards quantitative catalytic lignin depolymerization, *Chemistry—A European Journal* 17 (2011) 5939-5948.

46. T. Yoshikawa, T. Yagi, S. Shinohara, T. Fukunaga, Y. Nakasaka, T. Tago, T. Masuda, Production of phenols from lignin via depolymerization and catalytic cracking, *Fuel Process Technol* 108 (2013) 69-75.
47. Y. Yu, X. Li, L. Su, Y. Zhang, Y. Wang, H. Zhang, The role of shape selectivity in catalytic fast pyrolysis of lignin with zeolite catalysts, *Applied Catalysis A: General* 447–448 (2012) 115-123.
48. Y. Zheng, D. Chen, X. Zhu, Aromatic hydrocarbon production by the online catalytic cracking of lignin fast pyrolysis vapors using Mo₂N/γ-Al₂O₃, *J. Anal. Appl. Pyrolysis* 104 (2013) 514-520.
49. X. Li, L. Su, Y. Wang, Y. Yu, C. Wang, X. Li, Z. Wang, Catalytic fast pyrolysis of Kraft lignin with HZSM-5 zeolite for producing aromatic hydrocarbons, *Frontiers of Environmental Science & Engineering* 6 (2012) 295-303.
50. L. Liguori, T. Barth, Palladium-Nafion SAC-13 catalysed depolymerisation of lignin to phenols in formic acid and water, *J. Anal. Appl. Pyrolysis* 92 (2011) 477-484.
51. T.D.H. Nguyen, M. Maschietti, T. Belkheiri, L. Åmand, H. Theliander, L. Vamling, L. Olausson, S. Andersson, Catalytic depolymerisation and conversion of Kraft lignin into liquid products using near-critical water, *The Journal of Supercritical Fluids* 86 (2014) 67-75.
52. B. Joffres, C. Lorentz, M. Vidalie, D. Laurenti, A.-. Quoineaud, N. Charon, A. Daudin, A. Quignard, C. Geantet, Catalytic hydroconversion of a wheat straw soda lignin: Characterization of the products and the lignin residue, *Applied Catalysis B: Environmental* 145 (2014) 167-176.

53. A. Oasmaa, A. Johansson, Catalytic hydrotreating of lignin with water-soluble molybdenum catalyst, *Energy Fuels* 7 (1993) 426-429.
54. Q. Wua, L. Maa, J. Longb, R. Shub, Q. Zhangb, T. Wangb, Y. Xub, Depolymerization of Organosolv Lignin over Silica-alumina Catalysts, *Chinese Journal of Chemical Physics* 29 (2016) 474-480.
55. R. Van Borm, A. Aerts, M. Reyniers, J.A. Martens, G.B. Marin, Catalytic cracking of 2, 2, 4-trimethylpentane on FAU, MFI, and bimodal porous materials: influence of acid properties and pore topology, *Ind Eng Chem Res* 49 (2010) 6815-6823.
56. J. Scherzer, A.J. Gruia, *Hydrocracking science and technology*, CRC Press, 1996.
57. E.J. Hensen, D.G. Poduval, V. Degirmenci, D.J.M. Ligthart, W. Chen, F. Maugé, M.S. Rigutto, J.R.v. Veen, Acidity characterization of amorphous silica–alumina, *The Journal of Physical Chemistry C* 116 (2012) 21416-21429.
58. Z. Strassberger, A.H. Alberts, M.J. Louwse, S. Tanase, G. Rothenberg, Catalytic cleavage of lignin β -O-4 link mimics using copper on alumina and magnesia–alumina, *Green Chem.* 15 (2013) 768-774.
59. C. Crestini, F. Melone, M. Sette, R. Saladino, Milled wood lignin: a linear oligomer, *Biomacromolecules* 12 (2011) 3928-3935.
60. E. Sjöström, R. Alén, *Analytical methods in wood chemistry, pulping, and papermaking*, Springer Science & Business Media, 2013.
61. M. Liu, J. Yang, Z. Liu, W. He, Q. Liu, Y. Li, Y. Yang, Cleavage of covalent bonds in the pyrolysis of lignin, cellulose, and hemicellulose, *Energy Fuels* 29 (2015) 5773-5780.

62. A. Demirbas, Effects of temperature and particle size on bio-char yield from pyrolysis of agricultural residues, *J. Anal. Appl. Pyrolysis* 72 (2004) 243-248.
63. A. Enoki, M.H. Gold, Degradation of the diarylpropane lignin model compound 1-(3', 4'-diethoxyphenyl)-1, 3-dihydroxy-2-(4"-methoxyphenyl)-propane and derivatives by the basidiomycete *Phanerochaete chrysosporium*, *Arch. Microbiol.* 132 (1982) 123-130.
64. S. Kawai, T. Umezawa, T. Higuchi, Degradation mechanisms of phenolic β -1 lignin substructure model compounds by laccase of *Coriolus versicolor*, *Arch. Biochem. Biophys.* 262 (1988) 99-110.
65. K. Li, F. Xu, K.E. Eriksson, Comparison of fungal laccases and redox mediators in oxidation of a nonphenolic lignin model compound, *Appl. Environ. Microbiol.* 65 (1999) 2654-2660.
66. P. Raja, A. Bozzi, H. Mansilla, J. Kiwi, Evidence for superoxide-radical anion, singlet oxygen and OH-radical intervention during the degradation of the lignin model compound (3-methoxy-4-hydroxyphenylmethylcarbinol), *J. Photochem. Photobiol. A.* 169 (2005) 271-278.
67. S. Son, F.D. Toste, Non-Oxidative Vanadium-Catalyzed C–O Bond Cleavage: Application to Degradation of Lignin Model Compounds, *Angewandte Chemie International Edition* 49 (2010) 3791-3794.
68. J.J. Bozell, Approaches to the selective catalytic conversion of lignin: A grand challenge for biorefinery development, in: *Selective Catalysis for Renewable Feedstocks and Chemicals*, Springer, 2014, pp. 229-255.

69. J. Lavoie, W. Baré, M. Bilodeau, Depolymerization of steam-treated lignin for the production of green chemicals, *Bioresour. Technol.* 102 (2011) 4917-4920.
70. Z. Yuan, S. Cheng, M. Leitch, C. Xu, Hydrolytic degradation of alkaline lignin in hot-compressed water and ethanol, *Bioresour. Technol.* 101 (2010) 9308-9313.
71. T. Werpy, G. Petersen, A. Aden, J. Bozell, J. Holladay, J. White, A. Manheim, D. Eliot, L. Lasure, S. Jones, Top value added chemicals from biomass. Volume 1-Results of screening for potential candidates from sugars and synthesis gas, No. DOE/GO-102004-1992 (2004).
72. T.L. Yong, Y. Matsumura, Reaction kinetics of the lignin conversion in supercritical water, *Ind Eng Chem Res* 51 (2012) 11975-11988.
73. R. Beauchet, F. Monteil-Rivera, J. Lavoie, Conversion of lignin to aromatic-based chemicals (L-chems) and biofuels (L-fuels), *Bioresour. Technol.* 121 (2012) 328-334.
74. J. Kronholm, J. Kalpala, K. Hartonen, M. Riekkola, Pressurized hot water extraction coupled with supercritical water oxidation in remediation of sand and soil containing PAHs, *The Journal of supercritical fluids* 23 (2002) 123-134.
75. S. Yesodharan, Supercritical water oxidation: an environmentally safe method for the disposal of organic wastes, *CURRENT SCIENCE-BANGALORE*- 82 (2002) 1112-1122.
76. M.S. Wahyudiono, M. Goto, Decomposition of lignin alkaline and chemicals recovery in sub-and supercritical water, *ISASF* (2004).
77. P. Krammer, H. Vogel, Hydrolysis of esters in subcritical and supercritical water, *The Journal of Supercritical Fluids* 16 (2000) 189-206.

78. A. Kruse, E. Dinjus, Hot compressed water as reaction medium and reactant: properties and synthesis reactions, *The Journal of supercritical fluids* 39 (2007) 362-380.
79. D. Schmiedl, E. Pindel, S. Reinhardt, R. Schweppe, Base Catalyzed Degradation of Lignin for the Generation of oxy-Aromatic Compounds Possibilities and Challenges, *ERDOL ERDGAS KOHLE* 128 (2012) 357-363.
80. R. Parthasarathi, R.A. Romero, A. Redondo, S. Gnanakaran, Theoretical study of the remarkably diverse linkages in lignin, *The Journal of Physical Chemistry Letters* 2 (2011) 2660-2666.
81. V.M. Roberts, Homogeneous and heterogeneous catalyzed hydrolysis of lignin (2008).
82. M. Watanabe, H. Inomata, M. Osada, T. Sato, T. Adschiri, K. Arai, Catalytic effects of NaOH and ZrO₂ for partial oxidative gasification of n-hexadecane and lignin in supercritical water☆, *Fuel* 82 (2003) 545-552.